CENTRAL RESEARCH LIBRARY

ORNL-TM-3845

LOCKHEED MARTIN ENERGY RESEARCH LIBRARIES

3 4456 0514925 6

cy. 81

HIGH-TEMPERATURE STRUCTURAL DESIGN METHODS FOR LMFBR COMPONENTS

Quarterly Progress Report
Period Ending March 31, 1972

W. L. Greenstreet

J. M. Corum

C. E. Pugh

OAK RIDGE NATIONAL LABORATORY
CENTRAL RESEARCH LIBRARY
DOCUMENT COLLECTION
LIBRARY LOAN COPY
DO NOT TRANSFER TO ANOTHER PERSON
If you wish someone else to see this document, send in name with document and the library will arrange a loan.
UCN-7969
(3 3-67)

OAK RIDGE NATIONAL LABORATORY
OPERATED BY UNION CARBIDE CORPORATION • FOR THE U.S. ATOMIC ENERGY COMMISSION

This report was prepared as an account of work sponsored by the United States Government. Neither the United States nor the United States Atomic Energy Commission, nor any of their employees, nor any of their contractors, subcontractors, or their employees, makes any warranty, express or implied, or assumes any legal liability or responsibility for the accuracy, completeness or usefulness of any information, apparatus, product or process disclosed, or represents that its use would not infringe privately owned rights.

ORNL-TM-3845

Contract No. W-7405-eng-26

HIGH-TEMPERATURE STRUCTURAL DESIGN METHODS FOR LMFBR COMPONENTS

QUARTERLY PROGRESS REPORT
FOR PERIOD ENDING MARCH 31, 1972

W. L. Greenstreet
J. M. Corum
C. E. Pugh

JUNE 1972

NOTICE

This document contains information of a preliminary nature and was prepared primarily for internal use at the Oak Ridge National Laboratory. It is subject to revision or correction and therefore does not represent a final report.

OAK RIDGE NATIONAL LABORATORY
Oak Ridge, Tennessee 37830
operated by
UNION CARBIDE CORPORATION
for the
U.S. ATOMIC ENERGY COMMISSION

LOCKHEED MARTIN ENERGY RESEARCH LIBRARIES
3 4456 0514925 6

CONTENTS

	Page
ABSTRACT	v
SUMMARY AND STATUS	v
1. INTRODUCTION	1
2. ELASTIC-PLASTIC BEHAVIOR STUDIES	2
2.1. Experimental Tests	2
2.2. Theoretical Studies	15
3. TIME-DEPENDENT BEHAVIOR STUDIES	23
3.1. Representation of Time-Dependent Behavior of Structural Materials — An Interpretive Report	23
3.2. Multiaxial Creep Studies	23
3.3. Activities Associated with Investigations of Creep Failure Under Uniaxial and Multiaxial Conditions	26
3.4. ORNL Studies of Time-Dependent Behavior	27
4. STRUCTURAL ANALYSIS	31
4.1. Development of Elastic-Plastic-Creep Finite Element Computer Programs	31
4.2. Elastic-Plastic-Creep Analyses of Beam B3	36
4.3. Elastic-Plastic-Creep Analyses of First Proposed ORNL Pipe Thermal Ratchetting Test	39
4.4. A Preliminary Analysis of Three Uniaxial Ratchetting Tests — PVRC Sponsored Testing at Mar-Test, Inc.	47
5. STRUCTURAL TESTS	51
5.1. Elastic-Plastic-Creep Beam Tests	51
5.2. Pipe Thermal Ratchetting Tests	66
5.3. Weldment Creep-Rupture Studies	69
6. MATERIAL INVESTIGATIONS	75
6.1. Material Characterization	75
6.2. Creep Testing	87
6.3. Relaxation Testing	97
6.4. Cyclic Testing	97
7. ANALYTIC RATCHETTING STUDIES	97
7.1. Analysis	100
7.2. Results	106

CONTENTS (continued)

Page

7.3. Conclusions 111

8. HIGH-TEMPERATURE CREEP COLLAPSE TESTS OF PIPING ELBOWS 113

8.1. Test Conditions 113

8.2. Test Data 113

8.3. Test Assembly Design 114

9. DEVELOPMENT OF A SIMPLIFIED INELASTIC DESIGN ANALYSIS FOR PIPING SYSTEMS 116

9.1. Progress During January 1972 116

9.2. Progress During February 1972 117

9.3. Progress During March 1972 119

10. REFERENCES 124

ABSTRACT

This is the second of a series of quarterly progress report summarizing accomplishments in the ORNL program to develop high-temperature structural design methods for LMFBR vessels, components, and core structures. The first quarterly report covered the period from August through December 1971, while this report covers the period of January through March 31, 1972. The program has as its goal the development of a verified high-temperature design technology applicable to the long-term operating conditions expected for LMFBR systems. Although the ultimate objective is to develop verified methods and criteria for reliably designing for high temperatures and long life, near-term efforts are largely concentrated on establishing and validating methods and criteria to be used, on an interim basis, for FFTF and which are based on the current, largely unverified, state-of-the-art. The overall program is divided into a number of tasks which are being carried out with the participation and cooperation of industrial groups, universities, and design code bodies. Progress on these tasks is described herein.

SUMMARY AND STATUS

J. M. Corum

Management and coordination activities continue to represent a significant part of the overall High-Temperature Structural Design Methods Program. During this report period ORNL staff members participated, along with RDT, HEDL, and WARD personnel, in an audit of inelastic stress analysis activities at selected FFTF component vendors. The vendors visited were Foster Wheeler (IHX), Westinghouse EMD (pump), Combustion Engineering (vessel), Westinghouse ARD (core structures), and Bechtel (piping). The purpose of the audit activity was to assess the general capabilities, experience, and problems associated with inelastic analysis efforts so that a definite plan of action could be formulated for expediting inelastic structural analyses throughout the FFTF project. A particular goal

was a unified plan for computer program verification. Significant advances have been made in high-temperature design technology development, and we believe that the audit meetings have indicated that the technology can be applied on a rational, consistent basis throughout the FFTF project. Deficiencies exist and are recognized, but bases for overcoming them will not, in the main, become available in the near future. Rather, the deficiencies must be minimized by using inelastic analysis tools coupled with engineering judgement in a manner commensurate with the present state-of-the-art. On these bases, ORNL has recommended that steps be taken to carry out the necessary inelastic analyses of FFTF components with minimum delay. To this end we have also recommended specific actions to be taken. As one such action we are arranging a working group meeting between those FFTF designers currently performing inelastic analyses and computer program developers. This meeting will be held April 17, 1972, at ORNL. Depending on the outcome of this initial working meeting, additional meetings with wider participation may be held. Also, we have arranged with J. A. Swanson (ANSYS), P. V. Marcal (MARC), Y. R. Rashid (CREEP-PLAST), and Z. Zudans (EPACA) to have the inelastic analysis requirements of RDT standard F9-1T (reported in the previous quarterly report) put into their respective computer programs for use on the FFTF project. Finally, as an aid to computer program validation, we are providing the results of our high-temperature elastic-plastic-creep beam tests for inclusion in a compilation of benchmark problems aimed at the validation of analytical options contained in the computer programs used for inelastic structural analyses on the FFTF project. The catalog is being assembled by WARD, and they are performing analyses using the ANSYS and MARC programs. ORNL will perform similar validation analyses using CREEP-PLAST and EPACA. We are contributing to a similar benchmark problem compilation being undertaken by the ASME Subcommittee on Computer Program Verification and Validation.

We are working closely with WARD to develop a mutually acceptable plan for work to be performed under their program entitled Validation of High-Temperature Design Methods and Criteria (189a 08619). This effort is to supplement the ORNL High-Temperature Structural Design Methods Program by providing additional experimental data for validating high-temperature design methods. Two meetings between ORNL and WARD personnel were held

during this reporting period. On January 11, essential agreement was reached on the work plan, and on March 10 the progress was reviewed. The near-term Westinghouse effort consists of (1) basic specimen tests to determine strain limits under biaxial conditions in base metal and weldments, (2) tests of tubular type specimens under multiaxial creep conditions, (3) tests of complex structural configurations, (4) analytical work, using CREEP-PLAST and EPACA primarily, for comparison with test results, and finally (5) preparation of a design methods and criteria document for core structures. This latter document will be used by ORNL, together with similar information from Atomics International and General Electric, to compile an industry-recommended design criteria for core structures. We are assisting the WARD validation program in meeting its needs for type 304 stainless steel reference heat material from the available stockpile. Also, we are procuring piping components (straight pipe, tees, elbows, and reducers) to be tested by WARD, and we are coordinating their needs for type 316 stainless steel reference heat material with the recently initiated procurement activity.

We have prepared and submitted to RDT a letter containing recommendations for additional high-temperature experimental work in support of the high-temperature structural design methods program. Most of the recommended test work will eventually be carried out by ORNL, WARD, and ORNL subcontractors. There is an urgent need, however, for as much data as possible on a near-term basis.

As another coordination effort, we have assisted in planning materials properties tests to be carried out under the ORNL program entitled Mechanical Properties of Structural Materials (189a 10567). This program is to obtain data previously identified (and discussed in the previous quarterly progress report) as needed in support of interim structural design criteria and design technology. Some applicable data are also being obtained at other installations, and these will be factored into the overall program.

A revised and updated draft version of USAEC report ORNL-TM-3602, "Currently Recommended Constitutive Equations for Inelastic Design Analysis of FFTF Components," has been completed and will be distributed during the coming quarter to the recipients of this progress report. That

document contains the basis and background material for the inelastic analysis recommendations in RDT standard F9-1T.

The LMFBR Program Office has recently assigned ORNL the responsibility for updating the LMFBR Program Plan in the area of high-temperature systems design, Task 2-000-2. This task will be addressed during the coming quarter by personnel associated with the High-Temperature Structural Design Methods Program.

The three interpretive reports that were being prepared in the areas of mathematical representations of creep behavior, computational methods for high-temperature structural design, and the behavior of welded joints at elevated temperature have been completed, reviewed, and modified by the authors and are presently in various stages of the ORNL report preparation process. All will be published as ORNL reports in the next quarter or early in the first quarter of FY-1973. The specific report titles and numbers are:

1. E. T. Onat and F. Fardshisheh, "Representation of Creep of Metals," USAEC report ORNL-4783.
2. R. H. Gallagher, "Computational Methods in Nuclear Reactor Structural Design for High-Temperature Applications — An Interpretive Report," USAEC report ORNL-4756.
3. R. G. Gilliland, "The Behavior of Welded Joints in Stainless and Alloy Steels at Elevated Temperatures — An Interpretive Report," USAEC report ORNL-4781.

A fourth, somewhat related, report:

4. E. P. Esztergar, "Creep-Fatigue Interaction and Cumulative Damage Evaluations for Type 304 Stainless Steel — Hold-Time Fatigue Test Program and Review of Multiaxial Fatigue," USAEC report ORNL-4757,

is presently being reproduced. All of these reports will be distributed to recipients of this progress report.

Additional subcontracts have been initiated during this reporting period and negotiations were completed for another. Work began under the following subcontracts:

1. Atomics International — creep collapse tests of 16-in. piping elbows.
2. A. J. Durelli, Catholic University — high-temperature Moire strain analysis of a finite width plate with a circular hole.

3. Babcock and Wilcox Co. — study of failure under multiaxial creep conditions.
4. Battelle-Columbus Laboratories — development of a simplified inelastic piping system analysis.

In addition, the decision was made to proceed with a subcontract with The Boeing Company, Aerospace Group, to conduct a high-temperature test of a shear-lag specimen using Boeing capacitive strain gages. Technical agreement has been reached, and this effort is expected to begin June 1.

The subcontracts with General Electric and Teledyne Materials Research are being extended to reflect additions to the original work scope. General Electric is developing a transient heat conduction finite element analysis which will become an integral part of the two-dimensional elastic-plastic-creep computer program CREEP-PLAST. Teledyne, as an extension to their analytical parametric studies of ratchetting in straight pipe, will carry out a ratchetting investigation of a nozzle-to-sphere configuration. The purchase order to Southern Research Institute to conduct 15 cyclic uniaxial stress-strain tests at 1200°F on our preliminary heat of 304 stainless steel has been extended to include tests at 800, 950, and 1100°F on the reference heat of type 304 stainless steel. These data are to be used in inelastic analyses of structural tests.

A number of multiaxial (tension-compression-torsion) elastic-plastic tests has been carried out at room temperature to evaluate some of the features of the kinematic hardening model, which is recommended for FFTF analyses. Results from cyclic-torsion tests and cyclic-torsion with a constant superimposed axial load each support the kinematic hardening assumption. Interestingly, the latter type of test results in a progressive axial growth, as would be predicted by the kinematic hardening model. In preparation for high-temperature multiaxial testing, we have continued our evaluation studies of Microdot weldable strain gages at temperatures up to 1200°F. We believe that with proper procedures either the Microdot gage or the BLH high-temperature gage can provide useful information up to 1200°F, provided the maximum strain capabilities are not exceeded. Unfortunately, these maximum strain limitations restrict use of the gages in some practical applications.

Preparations for multiaxial creep testing are continuing at Brown University. Equipment and specimens are being fabricated. Particular emphasis during this period was placed on the development of a DCDT system for radial deformation measurements and on the evaluation of special infrared heat lamps. These lamps are ideally suited to the test needs, provided a lamp life of at least 1000 hr can be obtained. If this life cannot be realized, it may be necessary to use less desirable carbon-silicon heater rods instead. Multiaxial creep-rupture studies are to be carried out at Babcock and Wilcox. Emphasis under that subcontract is on failure and the evaluation of methods for defining and predicting failure. The B&W effort is planned as a 3-year investigation with selected tests that may extend beyond. At ORNL, we are continuing to develop and improve creep laws describing the uniaxial creep behavior of the preliminary and reference heats of type 304 stainless steel that are being used in the program. These creep laws are necessary ingredients in inelastic analyses of the structural tests that are being carried out.

The CREEP-PLAST computer program for elastic-plastic-creep analyses of two-dimensional bodies is essentially complete and almost ready for distribution to the public. The program, which was written to take advantage of UNIVAC software, is somewhat "input/output bound" on our IBM 360 system. This means that the total running time for a problem is disproportionately large in relation to the actual computational time, and we hope to remedy this situation before the program is distributed. The program will be distributed by ORNL to the public, but each recipient must sign an agreement stating that any corrections, changes, or modifications that are made to the program will, for a period of at least a year, be provided to ORNL. In this way, we hope to maintain an up-to-date master version of the program at ORNL, and this updated version will always be available to program users. We have used the CREEP-PLAST program on several relatively simple problems, generally with good results. We have performed elastic-plastic-creep analyses of our beam tests, and considering the fact that we have not yet developed an equation for describing the uniaxial creep data over the full range of stress levels of interest, the results from the program appear to be computed correctly. We have

checked them both with test results and with other analytical predictions obtained with our small in-house finite element programs.

The EPACA program for elastic-plastic-creep analysis of general thick shells is still being debugged at the Franklin Institute. They now estimate that the program, complete with finished user's guide, will be delivered to ORNL in May or June. However, the EPACA program is complex, and we foresee the need for considerable evaluation before it can be made available for design analyses.

We have performed, at ORNL, a number of inelastic pipe ratchetting design analyses in conjunction with our pipe thermal ratchetting test plans, and we have also had Teledyne Materials Research perform a design analysis using the ANSYS program. The ORNL studies were sensitivity analyses to assess the effects of deviations from the reference test conditions on the ratchetting strains. The Teledyne analysis was carried out to obtain an independent prediction of the behavior of the first pipe ratchetting test specimen.

We have performed a series of inelastic analyses of the Mar-Test two-bar ratchetting tests, which are being sponsored by PVRC, and we have also performed a series of Bree-type analyses to examine elastic-plastic shakedown and ratchetting. Rather than the elastic-ideally plastic material assumed by Bree, we used a bilinear stress-strain curve with kinematic hardening. The resulting Bree-type diagrams indicate that, at least for elastic-plastic behavior, the current ASME Code Case 1331-5 rules are conservative. Finally, we have agreed to perform a series of "rigorous" inelastic analyses of the LMEC beam ratchetting tests, and these analyses are under way.

At ORNL, we are continuing our high-temperature elastic-plastic creep tests of beams and of tubular weldment creep-rupture specimens, and preparations are continuing for the simple plate tests and for the pipe thermal ratchetting tests. The fourth of the planned series of four beams, made from the preliminary heat of 304 stainless steel, has been tested. This beam is a companion to the one reported in the previous quarterly, and the two together allow the examination of the effects of prior plasticity on subsequent creep and prior creep on subsequent plasticity. These results, along with appropriate materials behavior representations

are being furnished as benchmark problems as previously discussed. The next beam test will begin in May, following several improvements to the beam test facility, and will utilize the reference heat of 304 stainless steel.

We have performed one additional weldment creep-rupture test to complete the original series of tests, and we are currently machining a second-generation set of specimens. The decision has been made to again use the standard 308 stainless steel bare-wire, TIG weld process for these second-generation specimens. Extra weld rod has been obtained from the same lot for future fabrication of additional specimens and for weld characterization studies.

Design of the pipe ratchetting facility is nearing completion. To protect the main sodium valve from the thermal downshocks, we have decided to include a thermal capacitance tank just downstream from the ratchetting test specimen. This capacitance tank will absorb the thermal shock and thus increase the life of the valve. Plans for procuring the special stainless steel materials required for the facility have been completed. Also the Boeing capacitive strain gages and special signal conditioning units have been ordered for the tests. Finally, we have decided to weld the 30-in.-long test section to adjacent sections of pipe using the special F21 stick electrode process developed and being used for the FFTF vessel. Most weld characterization data to be obtained in the near future will be for this process, and hopefully we can eventually consider the weld behavior in our evaluations of the ratchetting results. We plan to use a 1/8-in.-diam electrode which will match the weld process used on a few 1/2-in.-thick plates being evaluated at ORNL. Most data for the F21 process are being obtained from 2-in.-thick plates welded with a 1/4-in.-diam electrode.

Our basic uniaxial materials investigations at ORNL continue to emphasize characterization studies, creep tests, relaxation tests, and cyclic stress-strain tests. Our characterization studies have examined 5/8-in.-diam bar versus 1-in. plate from the reference heat of type 304 stainless steel. The properties are similar after both product forms have been fully annealed. The bar characteristically has a fine-grain structure in the as-received condition but a coarse-grain structure, more nearly

matching that of the plate, after annealing. We are currently examining the structural stability of these product forms after long-term high-temperature exposure. Our creep tests continue to emphasize the reference heat, both plate and bar. Preliminary compressive creep results seem to agree with tensile creep data up to a certain strain level, after which specimen instabilities affect the compressive results. Cyclic stress-strain tests at room temperature, 800°F, and 1100°F indicate that the degree of cyclic hardening increases significantly from room temperature to 1100°F. Although the initial yield strength at room temperature is much higher than at 1100°F, the stress amplitude after a number of constant-strain-range cycles is almost as high at 1100°F as it is at room temperature.

The initial analytical pipe ratchetting parametric studies have been completed at Teledyne Materials Research, and, as previously mentioned, they are now analyzing a nozzle-to-sphere configuration for comparison with the simpler straight pipe results. In the initial effort on straight pipes, design curves were developed for ratchetting strain as a function of elastic primary and secondary stress intensities and temperature. The results indicate that existing design rules are very conservative. An exception is one of the rules in the proposed LMEC supplement to Code Case 1331-5 (to be used in the design of LMEC facilities). When compared to the results of the TMR study, this one LMEC rule is consistently and reasonably conservative for all loadings and temperatures studied.

Finally, the multiaxial creep-fatigue tests (tension-compression-torsion) at Pennsylvania State University will begin early next quarter. Previous testing has been to obtain uniaxial baseline creep-fatigue and cumulative damage data on the reference heat of 304 stainless steel in the fully annealed condition.

1. INTRODUCTION

This is one of a continuing series of progress reports describing work under the LMFBR program task to develop a structural design technology and associated design criteria applicable to LMFBR vessels, components, and core structurals. This is the second quarterly progress report (previously reports were issued on a monthly or bimonthly basis) and it covers the period January through March 1972.

The high-temperature structural design methods program includes development of analytical methods for predicting structural behaviors of components whose geometries range from relatively simple to complex. These components may be subjected to a variety of environmental conditions (including temperature to about 1200°F, temperature changes, and sodium atmosphere) and to various types of loadings and loading and temperature histories. In the case of core structurals, irradiation effects must be considered in addition to the above-named items. The work is being performed with the participation and cooperation of industrial groups and code bodies.

In the near-term, emphasis of the program is being placed on establishing, evaluating, and providing information pertinent to interim design methods and criteria for FFTF and early LMFBR demonstration plants. Ultimately, however, criteria must be based on accurate knowledge of time- and history-dependent stress and deformation behaviors throughout a component. Analytical techniques and associated materials behavior descriptions will be identified or developed to permit detailed predictions of the long-term history-dependent structural behavior of high-temperature components. The validity of these materials behavior characterizations and analytical methods will be demonstrated by comparing theoretical predictions with results from a series of relatively simple structural tests. The central thrust of the long-range program consists, therefore, of (1) studies leading to analytical descriptions of elastic-plastic and time-dependent material behavior, (2) development of structural analysis techniques incorporating these descriptions, and (3) basic structure tests under elastic, elastic-plastic, and creep conditions for assessing the basic features of the analytical methods.

In addition to the main thrust of the program, there are several related areas of study that are being pursued. These include component-type structural testing, creep-fatigue cumulative damage criteria, the behavior of weldments in critical structural areas, ratchetting criteria, and inelastic buckling of common configurations such as piping components. Specific tasks in the near-term effort were discussed briefly in the first monthly progress report.[1]

2. ELASTIC-PLASTIC BEHAVIOR STUDIES

K. C. Liu

2.1. Experimental Tests

2.1.1. Strain-gage evaluation studies

The study of the characteristic behaviors of commercially available high-temperature strain gages, which was initiated during the last reporting period, was continued through mid-February. One type of Microdot weldable strain gage (SG-420 series for application at temperatures up to 900°F) was previously tested and the results presented in the last progress report.[2] During this reporting period another type of Microdot weldable strain gage (SG-425 series for high-temperature applications up to 950°F) was tested and the results are discussed here.

According to the literature provided by the gage manufacturer, these two types of weldable strain gages are basically identical in design and materials except for a difference in lead wire construction. The lead wires on the SG-425 strain gage are insulated by magnesium oxide and are completely sealed in a steel sheath for protection. The lead wires connected to the SG-420 strain gage are insulated only by fiberglass sleeves without any other mechanical protection, and, consequently, the fragile lead wires become the most vulnerable parts of the strain gage during installation and in high-temperature environments. However, the SG-425 strain gages are not totally trouble-free. Although magnesium oxide is an excellent insulating material at high temperatures, it easily absorbs moisture in the air, and this moisture degrades its electrical insulation

resistance. Almost all the SG-425 strain gages received by ORNL were dehydrated and resealed in the laboratory in order to maintain the minimum effective insulation resistance of 100 MΩ, as suggested by the gage manufacturer.

Two SG-425 strain gages were welded diametrically opposite to each other at the midlength of a type 304 stainless steel specimen and oriented in the longitudinal direction. The specimen and strain gages were gradually cycled between room temperature to 1200°F for three thermal cycles. The characteristic behaviors of these strain gages under the thermal cycling are shown in Figs. 2.1 and 2.2. The results indicate that the characteristic temperature curves stabilized after the initial heating cycle. Similar behavior was also observed for the SG-420 strain gages in the previous test, but the characteristic temperature curves for subsequent thermal cycles were not as stable as those reported here. On the other hand, the rate change of apparent strain versus temperature for SG-420 gages was apparently lower than that for SG-425 gages. The drift rate for SG-425 gages at 1200°F was initially about 36 μin./in./min and continued 2 to 3 μin./in./min after 1 1/2 hr at 1200°F. This drift rate was higher than that reported previously for SG-420 gages. However, when the specimen temperature was reduced to 1100°F, the drift rate became markedly lower, having a value of less than 0.2 μin./in./min.

A uniaxial tension-compression test was then performed at a temperature of 1100°F using an SG-425 gage, and the test results are shown in Fig. 2.3. The specimen was given an initial strain-controlled cycle of approximately ±0.8% strain, which is 0.2% strain in excess of the limit recommended for SG-425 strain gages by the gage manufacturer. Overstraining was carried out to examine a possible extension of the strain limit and to study the gage performance at a high strain range. The cyclic strain range was then reduced to ±0.6% strain for the second cycle as a precaution against unexpected gage failure. The specimen exhibited relatively pronounced material hardening resulting from the cyclic loadings. The hardening obtained was large in comparison with that observed at room temperature for the same strain range. For the third cyclic loading the specimen was again strained to the previous high strain level of ±0.8%.

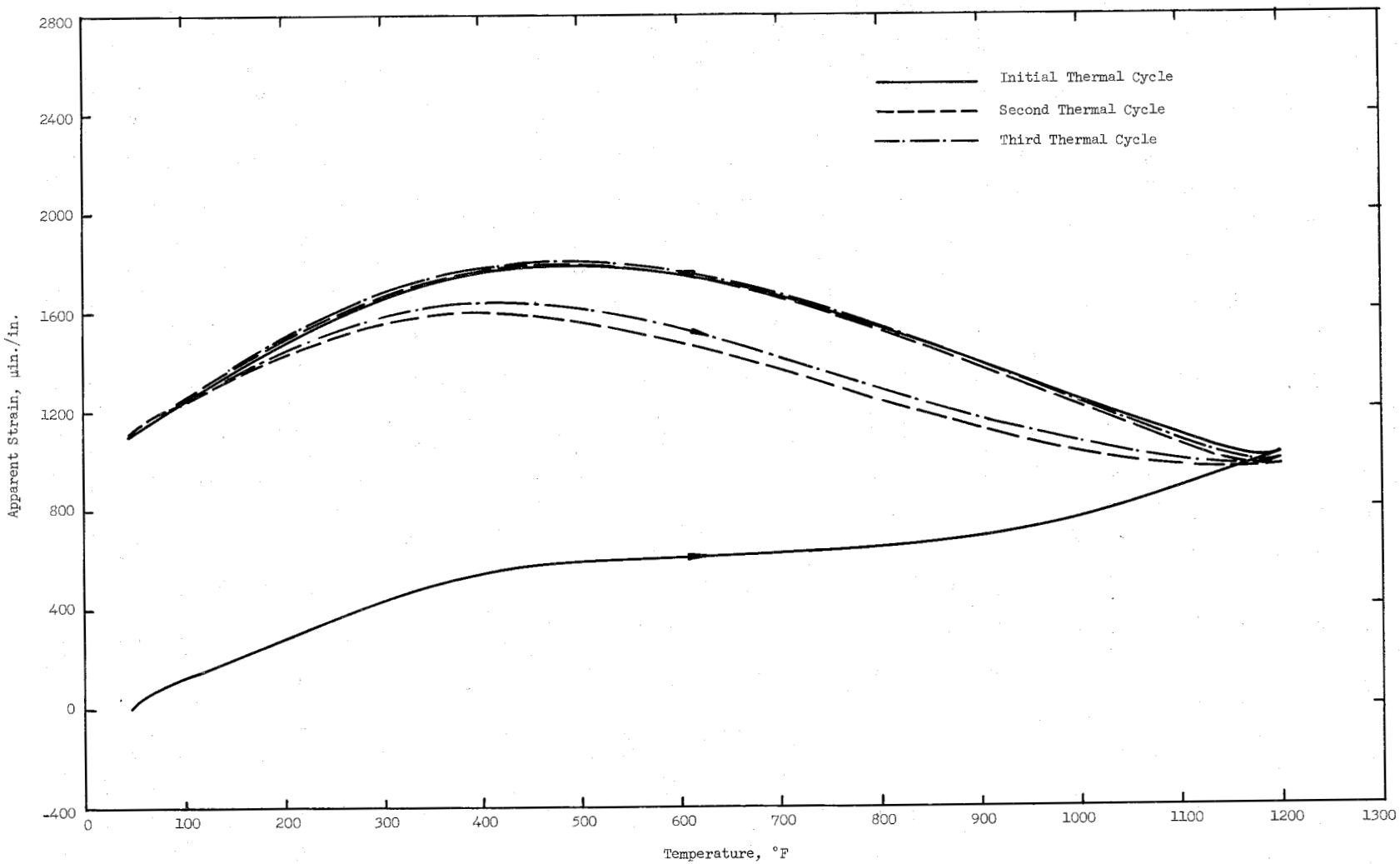

Fig. 2.1. Characteristic temperature curves for Microdot strain gage SG-425 (No. S/N 4980-1).

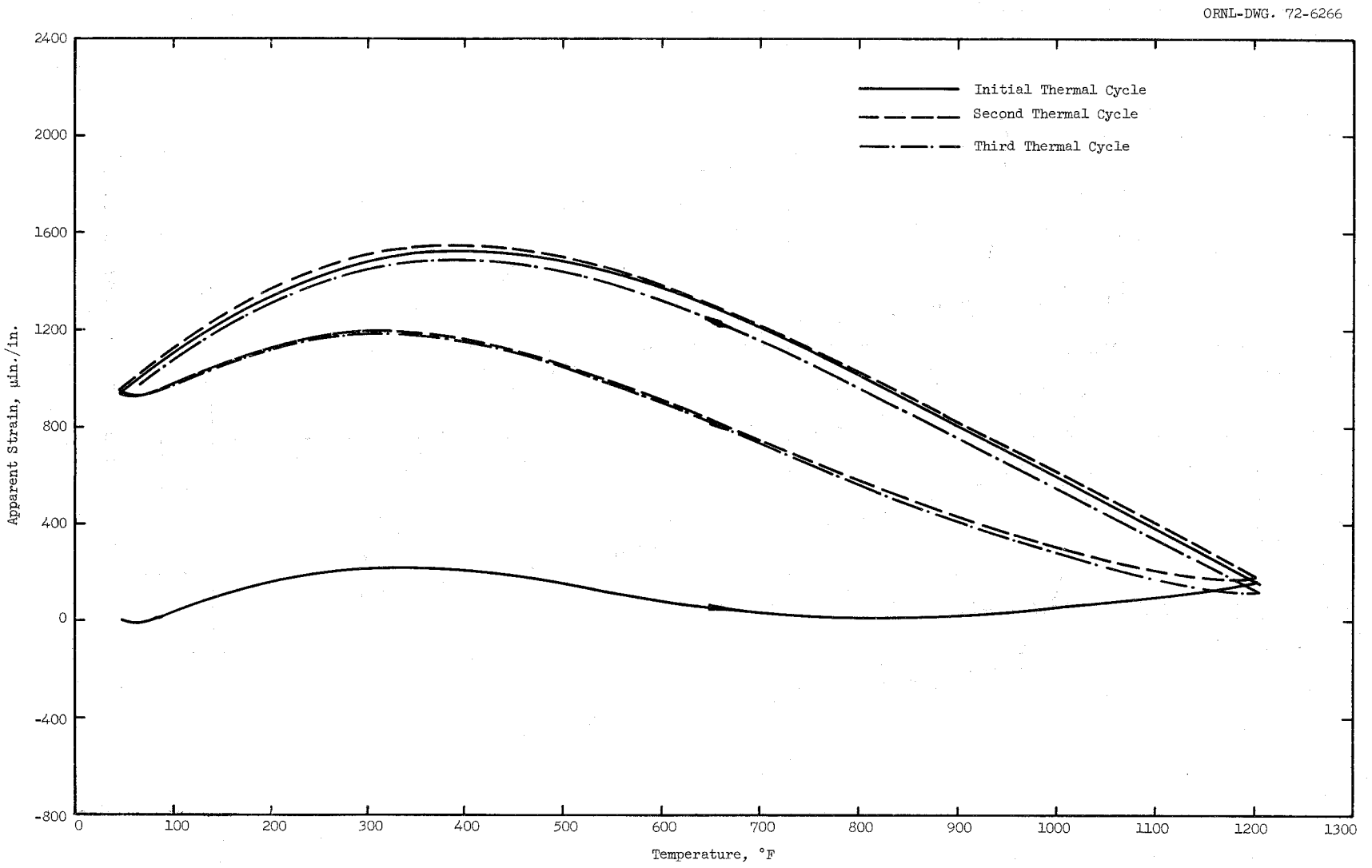

Fig. 2.2. Characteristic temperature curves for Microdot SG-425 strain gages (No. S/N 4980-2).

ORNL-DWG. 72-6267

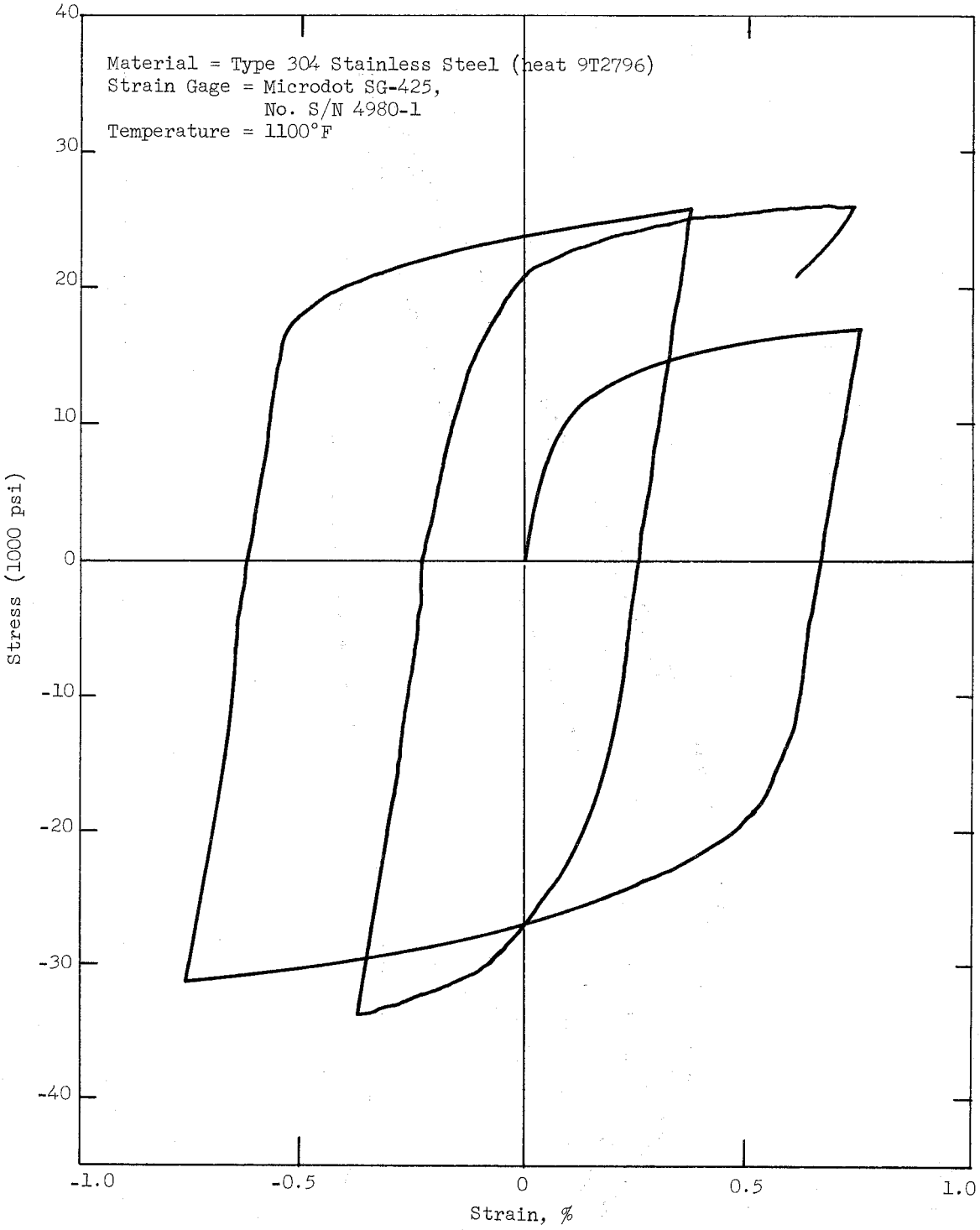

Fig. 2.3. Uniaxial tension-compression test at 1100°F.

However, the gage failed to respond on reversed loading cycle and the test was terminated.

As a closure to the investigation of high-temperature strain gages, we conclude that both the BLH and Microdot high-temperature strain gages can be used for experimental elastic-plastic behavior studies at elevated temperatures up to 1200°F provided that tests do not exceed the maximum range of strain recommended by the gage manufacturers. However, the absolute accuracy of strain readout from these gages is not known because the gage factors are given only approximately. Approximately correct strains were calculated from the gage factors provided by the gage manufacturer since we do not currently have an independent method available in the laboratory for calibrating high-temperature strain gages.

2.1.2. Room temperature biaxial tests

A series of stress-controlled biaxial tests were performed at room temperature using thin-walled tubular specimens made from the ORNL reference heat (9T2796) of type 304 stainless steel. Two 45° rosette strain gages, Micro-Measurement EA-06-125RA-120 (see Table 2.1), were bonded diametrically opposite to each other with the three strain elements oriented in the longitudinal and two 45° diagonal directions as shown in Fig. 2.4. The location of the strain gages was at the midlength of the specimen so that the end effect from the specimen grips was minimized. Five radial loading paths in a tension-torsion coordinate system (Fig. 2.5)

Table 2.1. Strain-gage data

Description	Micro-Measurement, EA-06-125RA-120
Gage material	Constantan alloy foil grid, Polyimide backing
Gage resistance	Nominal and spread: 120.0 ohms ±0.4%
Gage factor (75°F)	2.095 ± 0.5 (longitudinal gage) 2.075 ± 0.5 (45° diagonal gages)
Grid dimensions	0.125 in. long, 0.0625 in. wide
Temperature range	Cryogenic to approximately +400°F
Strain limits	3% to 5%, tension or compression

PHOTO 1734-72

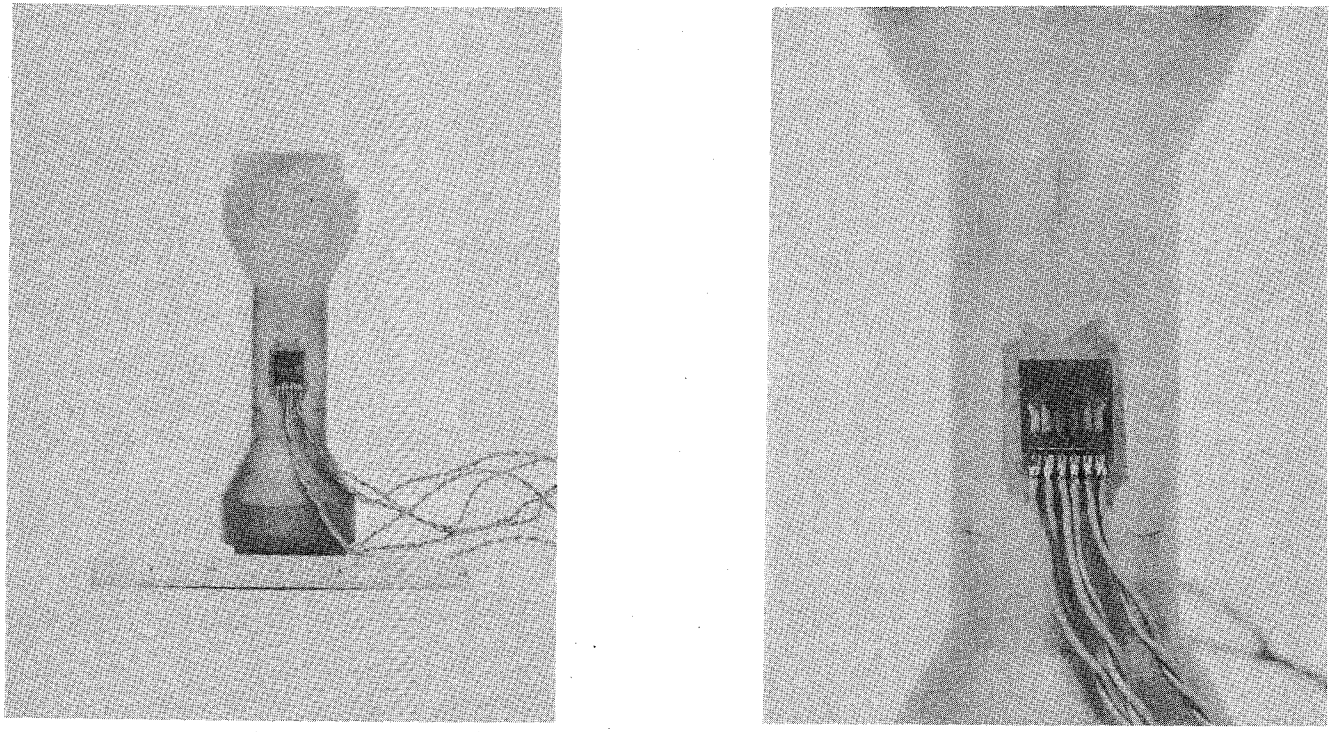

Fig. 2.4. Test specimen and strain gages.

ORNL-DWG. 72-6268

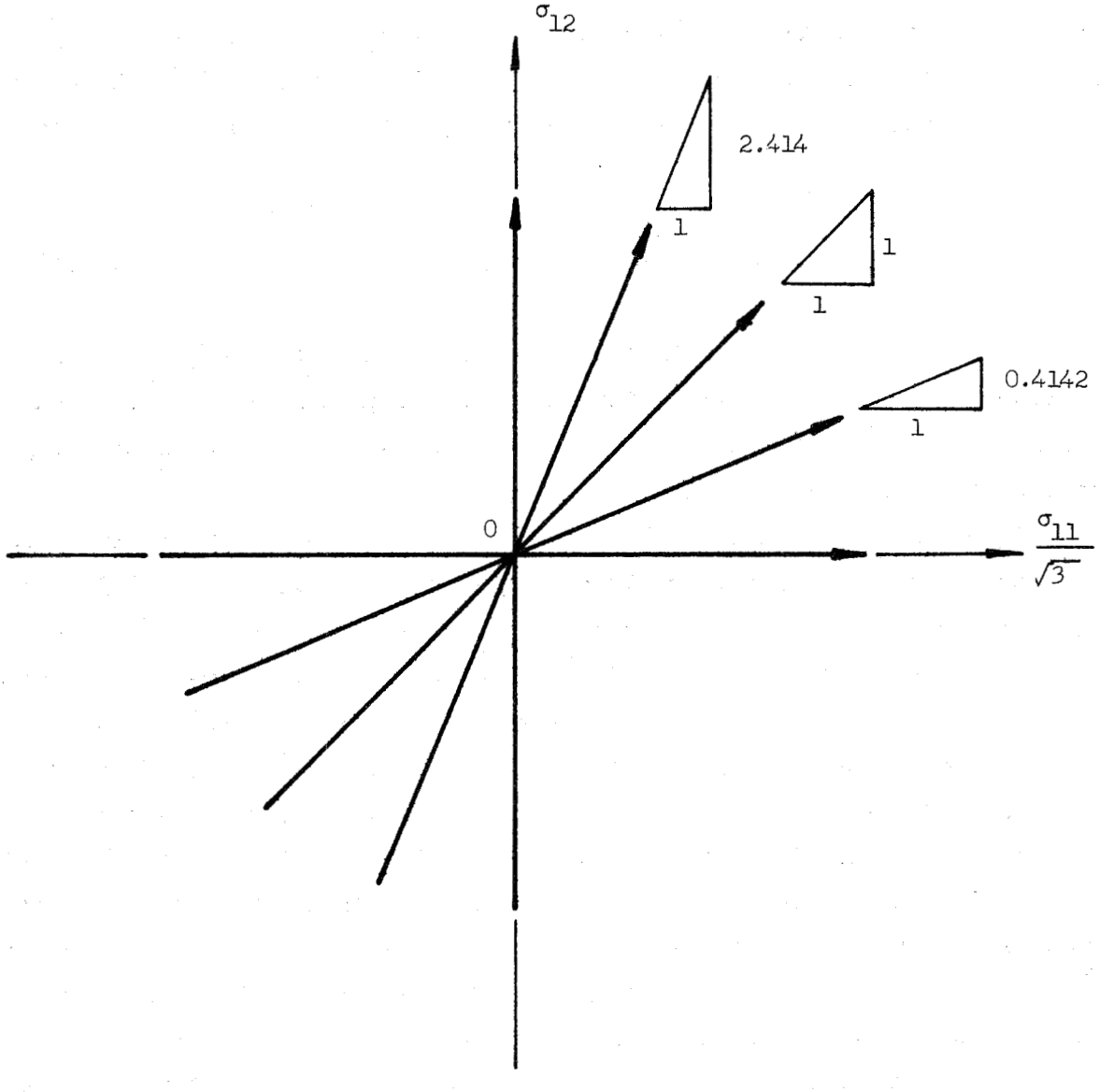

Fig. 2.5. Loading paths for combined tension-torsion tests.

were selected for these tests; the paths were evenly spaced in two quadrants of the stress space. The loading path along the horizontal axis corresponds to a uniaxial tension-compression loading and one along the vertical axis gives pure torsional cycling. The three remaining radial loading paths are combined tension-compression and torsion-reversed-torsion tests of three different stress ratios. The normal stress axis of the coordinate system shown in Fig. 2.5 is reduced by a factor of $1/\sqrt{3}$. This axis modification allows the initial yield condition of von Mises to be represented by a circle in this tension $(\sigma_{11})/\sqrt{3}$-torsion (σ_{12}) space. That is,

$$\frac{\sigma_{11}^2}{3} + \sigma_{12}^2 = k^2 , \tag{2.1}$$

where k is a constant. If the von Mises' flow rule is to apply in this subspace, it is also necessary to transform the plastic strain components simultaneously. Figure 2.6(B) is the plastic strain space corresponding to the modified stress space in Fig. 2.5.

In order to cancel possible bending effects on the test specimen, the two strain gages at diametrically opposite positions were connected to opposite arms of each bridge circuit. This allows one to read the strains in the longitudinal and two 45° diagonal directions simultaneously. Three stress-strain curves for the radial loading path [Fig. 2.6(A)] in the direction of a stress ratio, $\sigma_{11}/\sqrt{3}$: σ_{12} = 1:1, are plotted in Figs. 2.7, 2.8, and 2.9. The circumferential shearing strain component is equal to half the sum of the two strain readouts from the 45° diagonal strain gages. Axial and shearing components of plastic strain were then calculated and the plastic strain trajectory in response to the radial loading was plotted in the special strain coordinate system [Fig. 2.6(B)]. The slope of the plastic strain trajectory is close to a ratio of $\sqrt{3}/2\ \epsilon_{11}^P$: ϵ_{12}^P = 1:1. This result strongly supports (1) the normality postulate, if the initial yield surface is truly of von Mises' form, and (2) the classical kinematic hardening rule, although to prove the latter a more thorough examination of the yield surface is needed. The test results for the other radial loadings have not been completely analyzed and are not shown in this report. The analyses of the test results are continuing.

ORNL-DWG. 72-6269

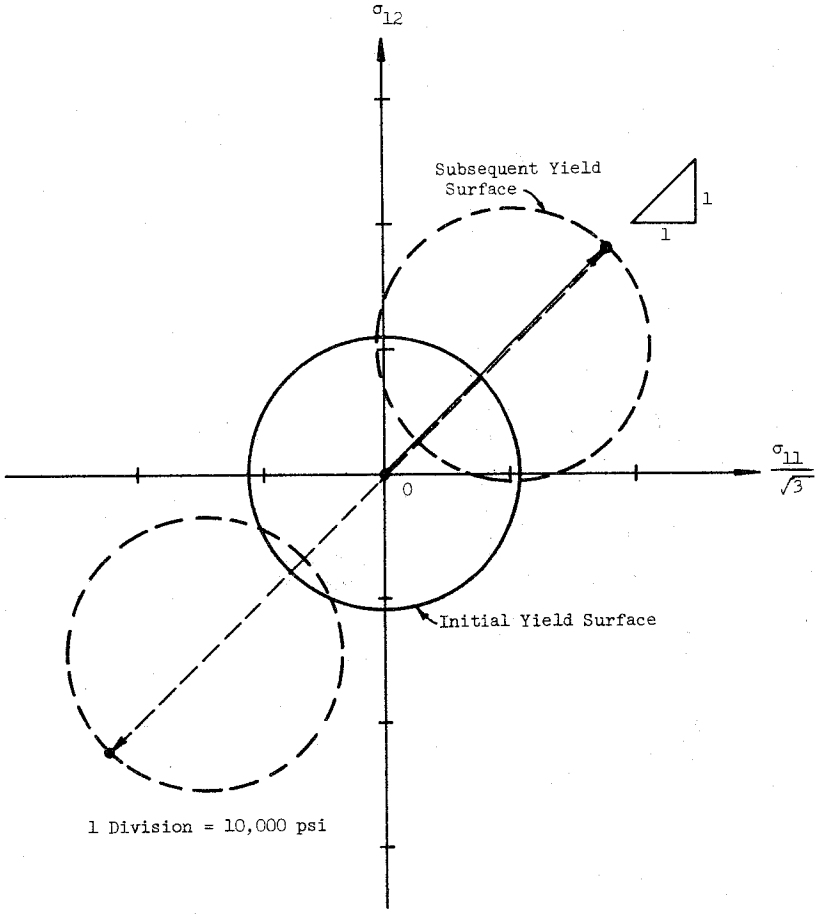

Fig. 2.6(A). Cyclic radial loading path.

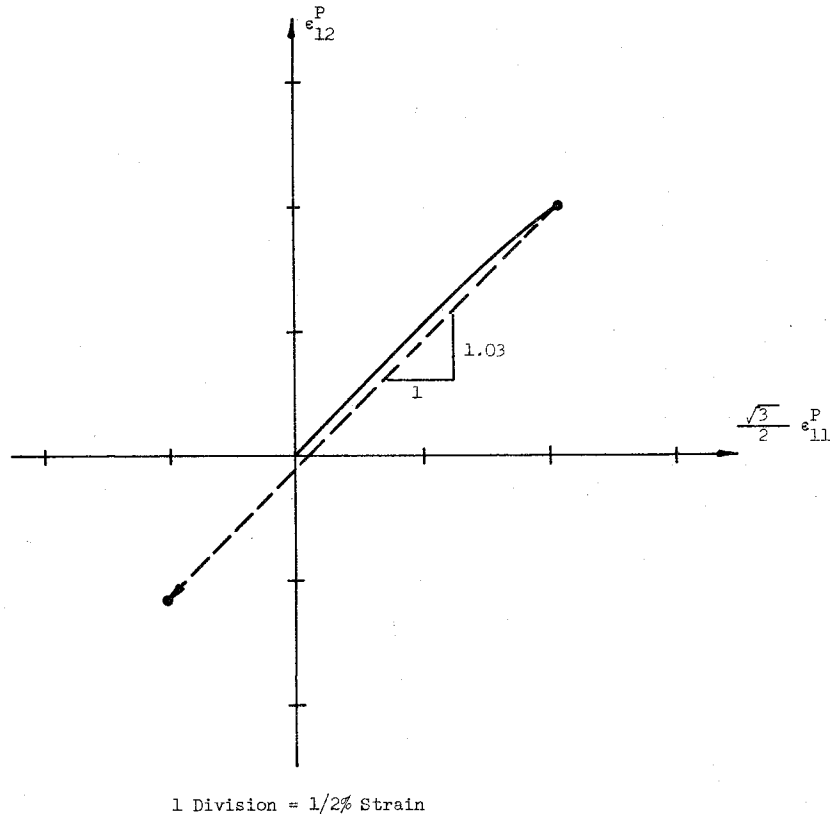

Fig. 2.6(B). Plastic strain trajectory.

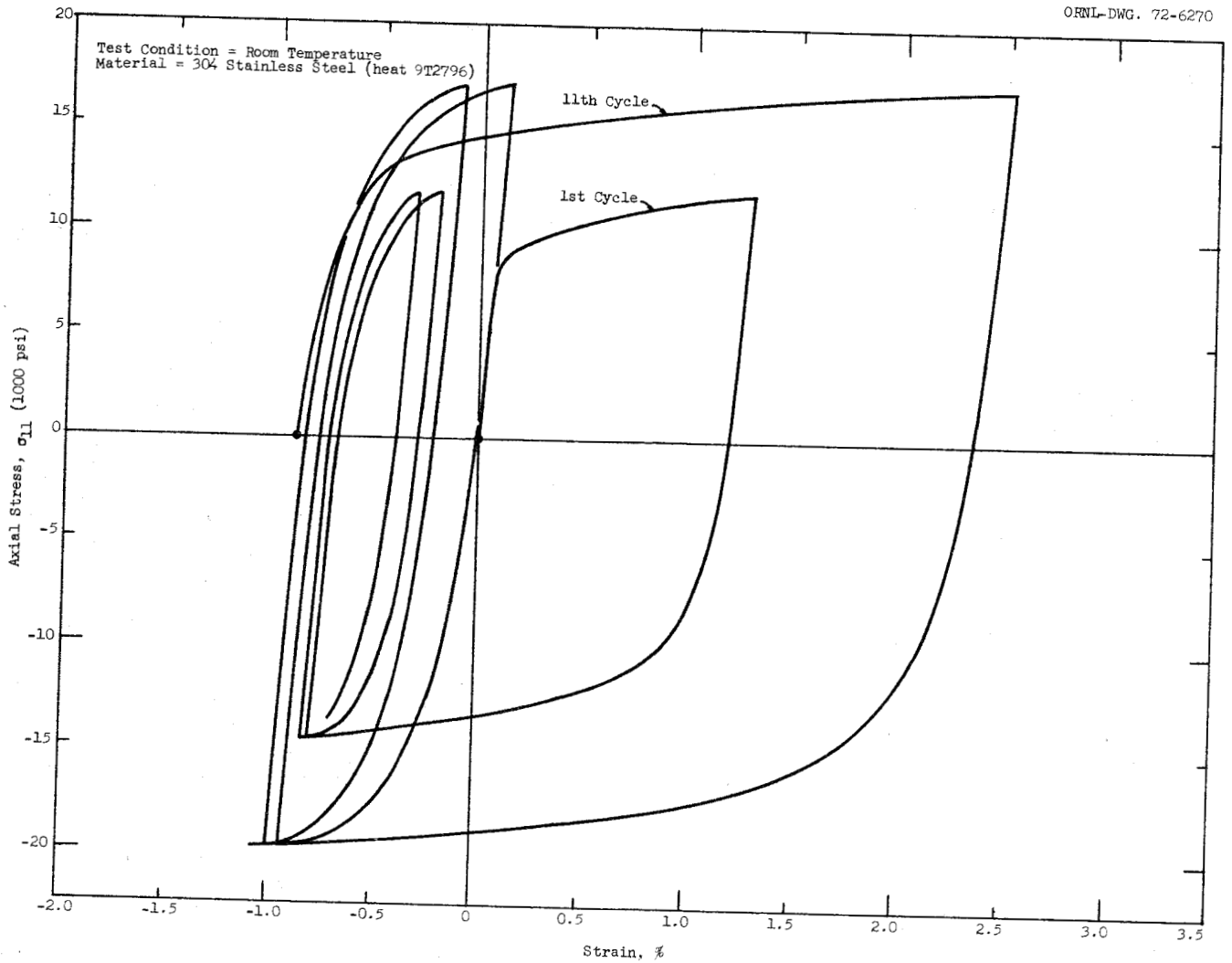

Fig. 2.7. Cyclic stress-strain curves, axial stress vs axial strain.

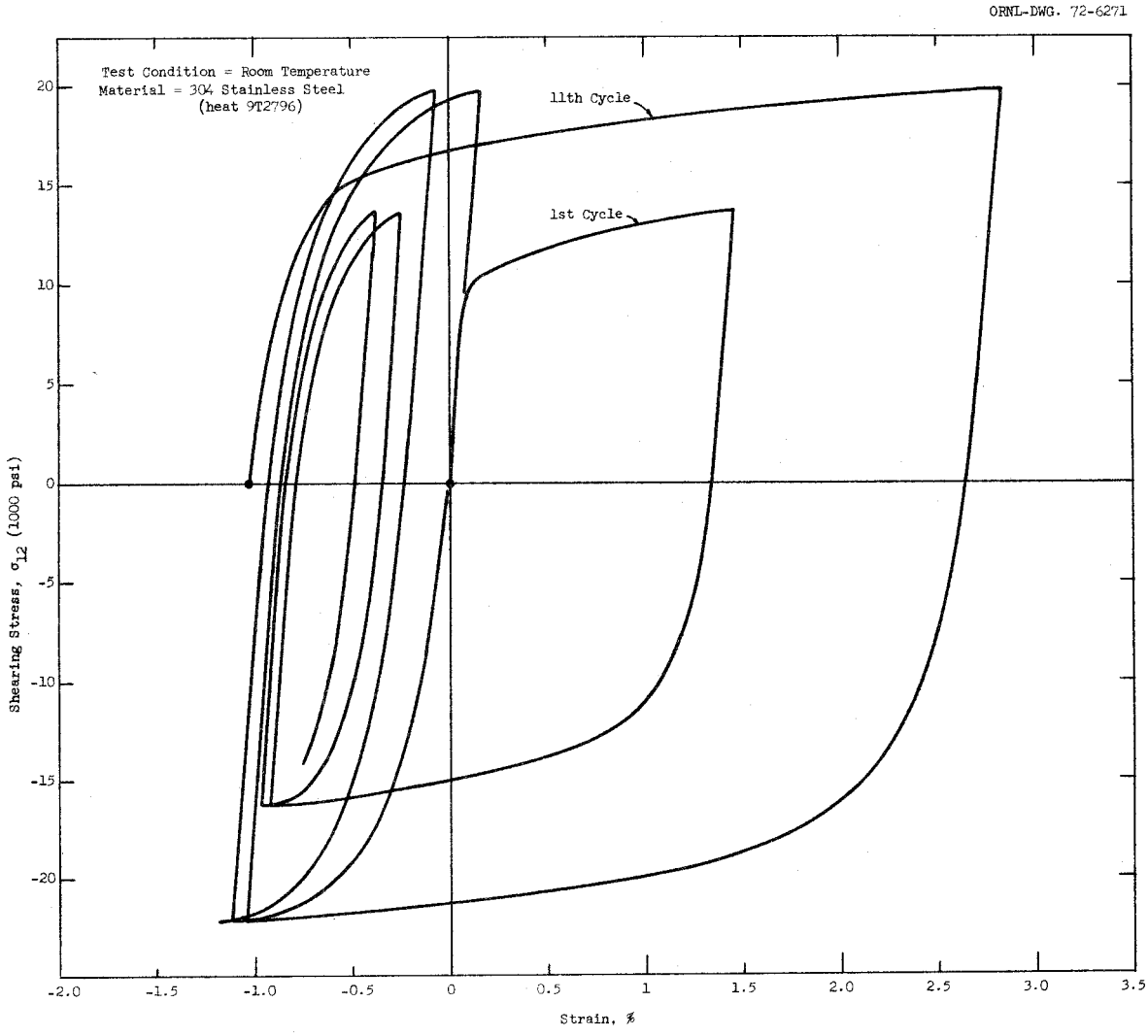

Fig. 2.8. Cyclic stress-strain curves, shearing stress vs 45° right diagonal strain.

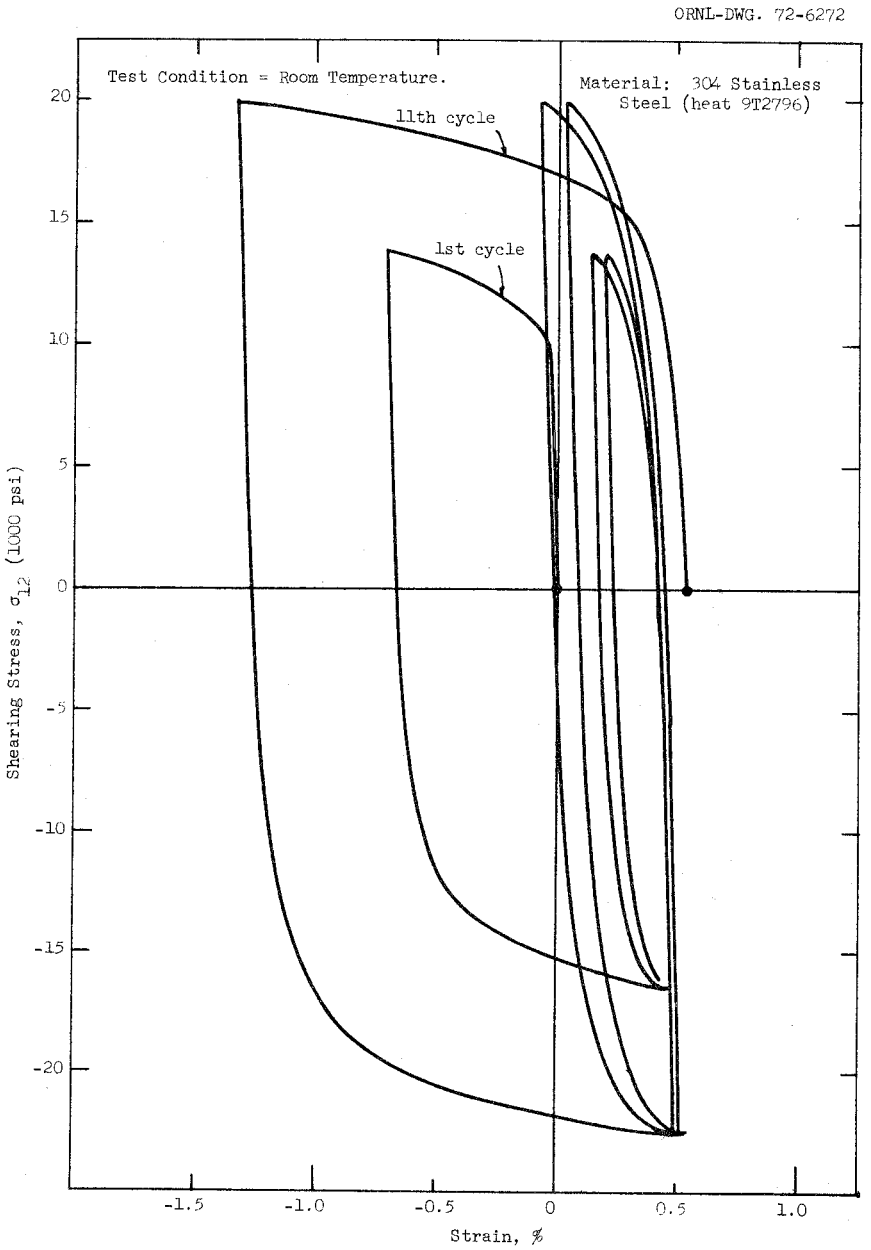

Fig. 2.9. Cyclic stress-strain curves, shearing stress vs 45° left diagonal strain.

Figure 2.10 shows the results of a tension-compression stress-controlled cyclic loading test. Upon completion of 20 loading cycles, the specimen was again loaded in tension to a stress of 42,000 psi, the highest stress previously attained. Cyclic torsion was then applied to the specimen while it was under the constant axial load. The test results revealed that the specimen underwent longitudinal elongation of approximately 2.1% when ten cycles of torsional loadings between ±7500 psi and ten between ±10,000 psi were subsequently applied. The histogram for these cyclic tests is shown in Fig. 2.11. The first torsion cycle yielded approximately 1/3% strain, but incremental elongation decreased to less than 0.06% strain per cycle at the end of the twentieth cycle. Again, this observation supports the classical kinematic hardening concept.

2.2. Theoretical Studies

In the course of examining proposed changes to ASME Code Case 1331-5, attention was given to the criteria which govern shakedown and ratchetting on the basis of Eq. (13) in Paragraph 5.2(b). The rationale of the presently proposed rules on shakedown and ratchetting was developed largely from Bree's investigative work on elastic-plastic behavior of thin tubes,[3] in which the Bree diagram was constructed on the assumption that the material is nonwork-hardening. Our effort here is to present some theoretical predictions of possible changes in the Bree diagram if the fundamental assumption of material behavior is changed to a work-hardening type. The effect of work-hardening was briefly discussed by Bree,[3] but in his analysis the Bauschinger effect, which is typical of type 304 stainless steel, was not included. In the following discussion the material behavior was assumed to be represented by a bilinear elastic-plastic stress-strain relation with the classical kinematic hardening properties [Fig. 2.12(A)]. Furthermore, in order to simplify the algebraic complexity, most of the convenient assumptions used by Bree, other than those stated above, were retained in this analysis. The analysis is lengthy and tedious. Therefore, only a few typical conditions are discussed here, but the final results are summarized and compared with the Bree diagram.

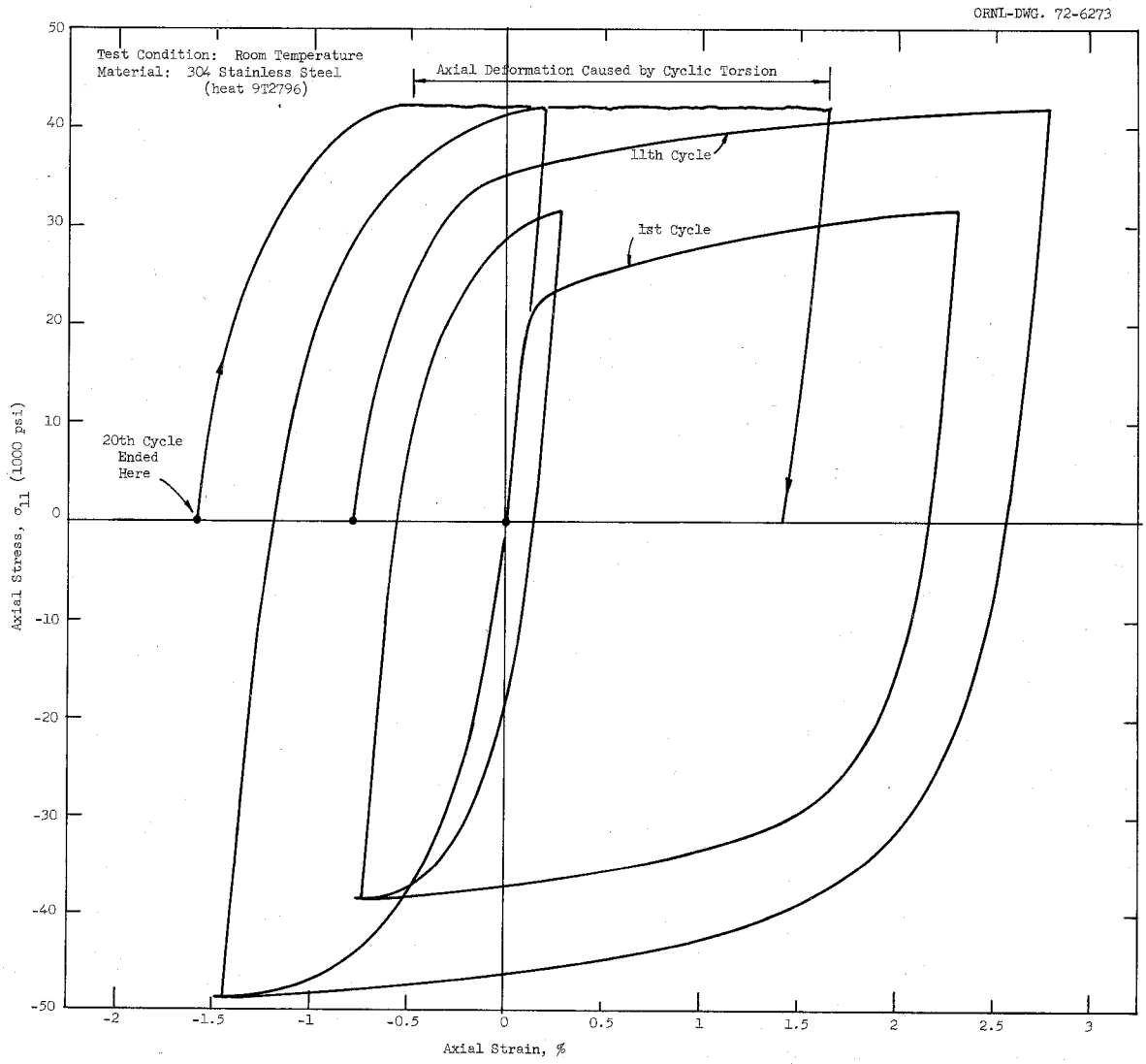

Fig. 2.10. Axial cyclic stress-strain curves and axial deformation associated with cyclic torsional loading.

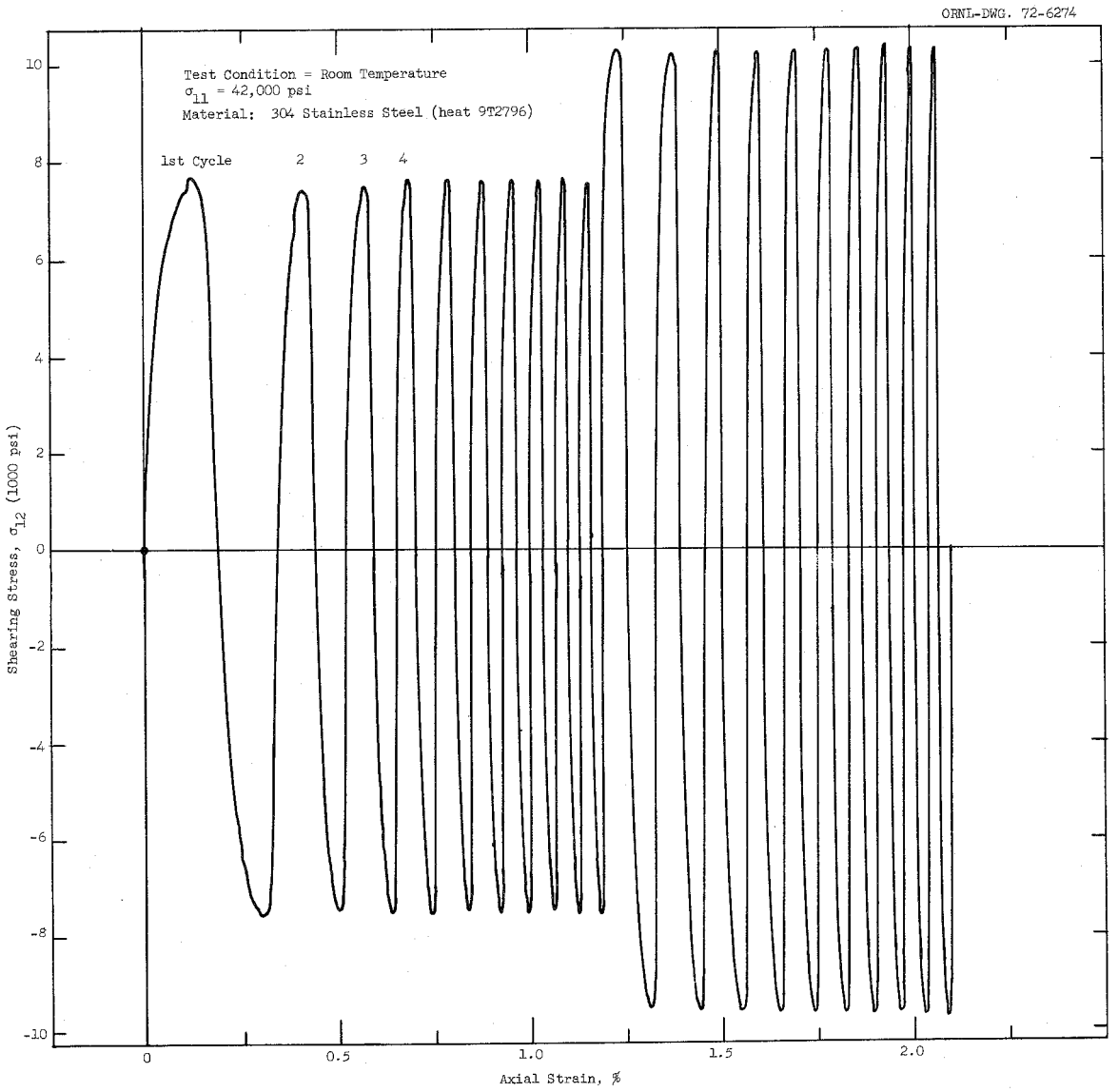

Fig. 2.11. Histogram for torsional cyclic loading.

ORNL-DWG. 72-6275

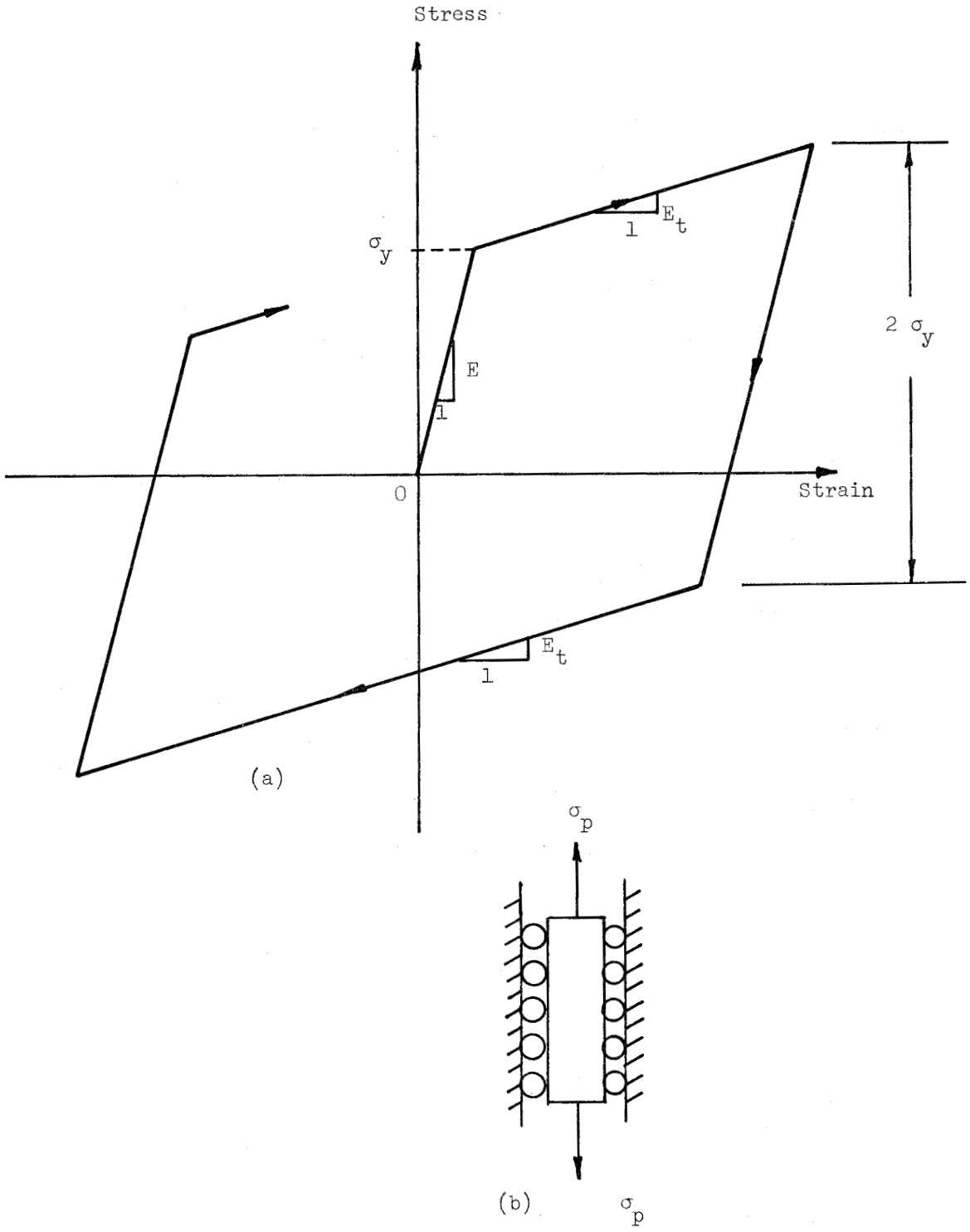

Fig. 2.12. Bilinear elastic-plastic stress-strain curve and uniaxial stress model for ratchetting study.

Consider a cyclic linear thermal gradient applied to a uniaxial stress model of the Bree type [Fig. 2.12(B)] which is subjected to a constant tensile stress of σ_p.

<u>Case I</u>: When $\sigma_p < \sigma_Y$, where σ_Y is the initial yield stress, and the secondary stress σ_t due to the cyclic thermal gradient satisfies the condition $\sigma_t > 2\sigma_Y$, the first incremental plastic strain due to the initial thermal gradient is given by

$$\Delta\epsilon_1 = \frac{(\epsilon_Y - \epsilon_t)\,\frac{E_t}{E}\,\frac{\epsilon_t \epsilon_p}{\epsilon_Y} - \epsilon_Y}{(\epsilon_t - \epsilon_Y)\,\frac{E_t}{E} + \epsilon_Y}\,\epsilon_Y\,, \tag{2.2}$$

where E and E_t are, respectively, the moduli of elastic and plastic responses in the bilinear stress-strain curve shown in Fig. 2.12(A), and

$$\epsilon_Y = \frac{\sigma_Y}{E}\,,$$

$$\epsilon_t = \frac{\sigma_t}{E}\,,$$

$$\epsilon_p = \frac{\sigma_p}{E}\,.$$

Subsequent ratchetting is given by

$$\Delta\epsilon_n = \frac{K_1\epsilon_Y}{K_1\epsilon_Y + K_o\epsilon_t}\,\Delta\epsilon_{n-1}\,, \qquad (n = 2,3,\ldots) \tag{2.3}$$

where

$$K_o = \frac{E_t}{E}$$

and

$$K_1 = 1 - \frac{E_t}{E}\,.$$

Since the term $\epsilon_t E_t/E$ is positive definite, subsequent ratchetting will decrease as the number of cycles increases. The limit of plastic cycling is determined by setting $\Delta\epsilon_1 = 0$ for Eq. (2.2). This gives

$$\epsilon_t \epsilon_p = \epsilon_Y^2 - \epsilon_Y (\epsilon_Y - \epsilon_t) \frac{E_t}{E} . \tag{2.4}$$

Since $\epsilon_Y < \epsilon_t$ in this case, the last term of Eq. (2.4) is also a positive definite quantity. As a result, the line expressed by Eq. (2.4) falls above the plastic cycling boundary of the Bree diagram. In the case of nonwork-hardening, $E_t = 0$ and Eq. (2.4) reduces to

$$\epsilon_t \epsilon_p = \epsilon_Y^2 , \tag{2.5}$$

which is equivalent to Bree's form.

Case II: When $1/2\ \sigma_Y < \sigma_p < \sigma_Y$ and the secondary stress σ_t due to thermal cycling is $4(\sigma_Y - \sigma_p) < \sigma_t < 2\sigma_Y$, the first incremental ratchetting due to an initial thermal transient is given by

$$\Delta\epsilon_1 = \frac{1}{K_1} \left\{ K_2 + \left[K_2^2 - K_1 \frac{\epsilon_p - \epsilon_Y}{\epsilon_t} \right]^{1/2} \right\} , \tag{2.6}$$

where

$$K_2 = 1 + \frac{E_t}{E} .$$

Subsequent incremental ratchetting strains are calculated from a quadratic expression and are functions of prior incremental plastic strains. Although the subsequent plastic increments do not form regular geometrical series, plastic strain increments do decrease as the number of cycles increases.

Case III: When $\sigma_p = \sigma_Y$ and the secondary stress σ_t due to thermal cycling is $\sigma_t < 2\sigma_Y$, the first incremental ratchetting strain is given by

$$\Delta\epsilon_1 = \frac{1 - \sqrt{K_o}}{\sqrt{K_o}} \epsilon_Y \tag{2.7}$$

and the second incremental ratchetting strain is

$$\Delta\epsilon_2 = \frac{K_1\Delta\epsilon_1}{K_o\Delta\epsilon_1 + K_1\epsilon_Y}\,\epsilon_Y \ . \tag{2.8}$$

Again, the subsequent incremental ratchetting strains are functions of prior incremental plastic strains as in Case II. Incremental ratchetting decreases as the number of cycles increase in this case.

Case IV: When $\sigma_p > \sigma_Y$ and $\sigma_t > 0$, incremental ratchetting behavior is analogous to the case for $\sigma_p = \sigma_Y$ since the material is assumed to behave according to the classical kinematic hardening rule. Consequently, the total accumulated plastic strain for this case will be

$$\sum_{n=1}^{\infty} \Delta\epsilon_n\Big|_{\sigma_p > \sigma_Y} = \sum_{n=1}^{\infty} \Delta\epsilon_n\Big|_{\sigma_p = \sigma_Y} + (\epsilon_p - \epsilon_Y) \ . \tag{2.9}$$

From the cases studied in the foregoing discussion, it is apparent that if the material is work-hardening and behaves with a Bauschinger effect, the incremental ratchetting due to constant thermal gradient cycling decreases as the number of cycles increases. This allows the accumulation of plastic strain increments due to thermal ratchetting to be estimated mathematically.

In order to summarize the above discussion in a more practical manner, we assumed that the hardening coefficient of the material in the plastic range was a constant value independent of temperature, and a value of $E_t/E = 0.021$ was used in a numerical example. The total accumulations of plastic strain increments due to thermal ratchetting were calculated and plotted in Fig. 2.13, which can be used to estimate total accumulated strain. As an example, material properties for type 304 stainless steel at 1200°F are: $E = 20.9 \times 10^6$ psi, and $\sigma_Y = 14{,}200$ psi. Using these values the stress limits for 1% total strain accumulation can be estimated from Fig. 2.13, as shown by the dashed line. As stated earlier, the above results are estimated on the basis of an idealized kinematical hardening model. Therefore, the effects of material hardening due to cyclic loadings are not included.

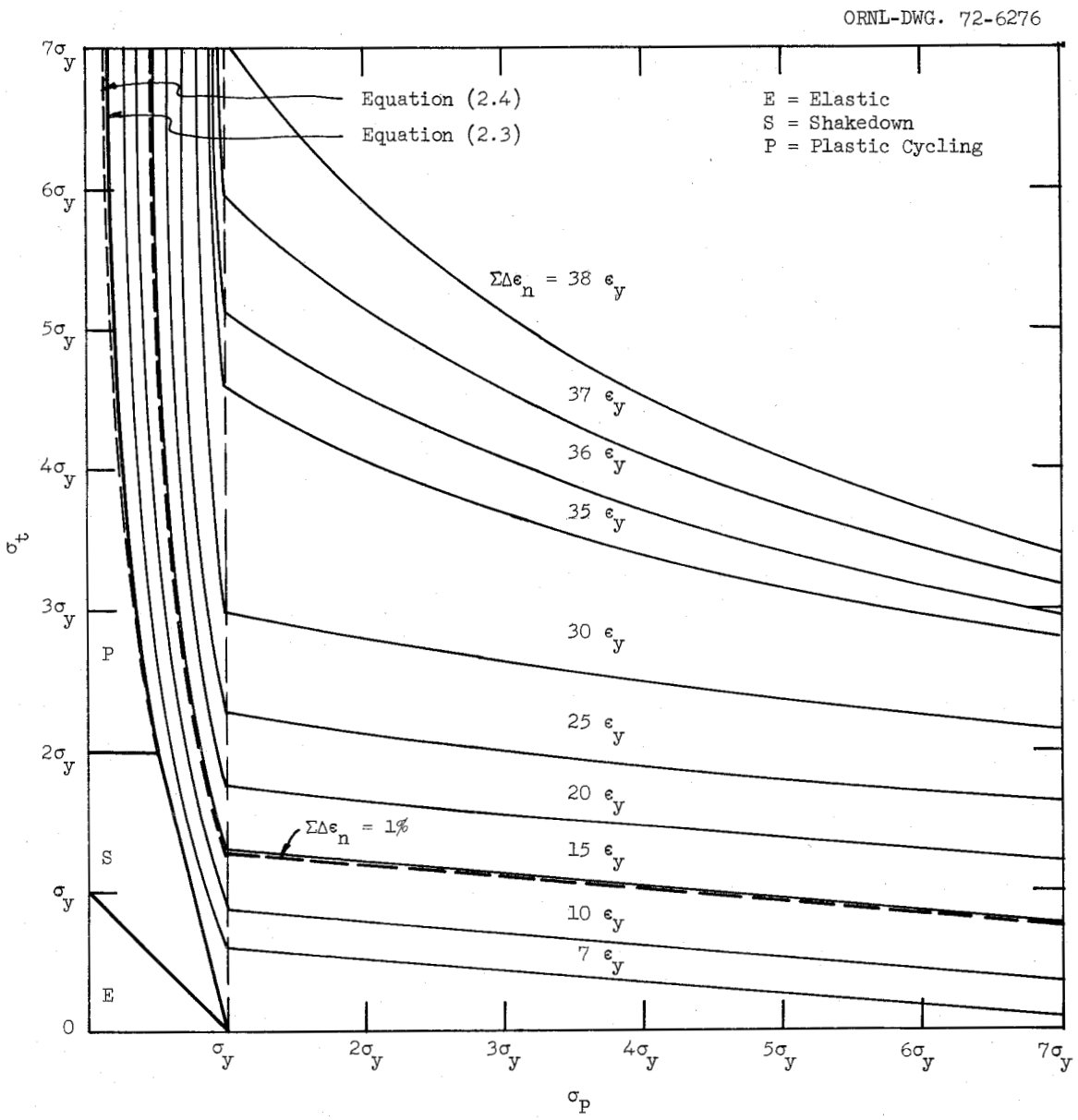

Fig. 2.13. Total plastic strain accumulation under thermal cycling.

From the above study it seems that the rules for shakedown and ratchetting based on Eq. (13) in Paragraph 5.2(b) of Code Case 1331-5 are too conservative, and the supplement to Code Case 1331-5 proposed by LMEC for SPTF is more favorable. However, this study cannot be considered conclusive since the effects of creep on thermal ratchetting at high temperatures are not included.

3. TIME-DEPENDENT BEHAVIOR STUDIES

C. E. Pugh

3.1. Representation of Time-Dependent Behavior of Structural Materials – An Interpretive Report

Professor E. T. Onat
Yale University

A copy of the final draft of the interpretive report has been received by ORNL. This draft is now being prepared for more general distribution as an ORNL report. Specifically, the report title and number are:

> E. Turan Onat and F. Fardshisheh, "Representation of Creep of Metals," USAEC Report ORNL-4783, Oak Ridge National Laboratory.

This report will be published and distributed during the next quarter. The recipients of this progress report will be included in the distribution of the interpretive report.

3.2. Multiaxial Creep Studies

Professor W. N. Findley
Brown University

3.2.1. Work completed during the month of January

1. Due to the fact that the infrared quartz heating lamp failed before 1000 hours during a trial period, investigations are being made to determine what changes are required to prolong lamp life. Subjected to extreme temperature conditions, the end seals of the lamp

deteriorated. Hopefully, special high-temperature lamps and suitable protective shielding of the end seals will eliminate any sources of electrical failure. However, if no feasible improvements are possible, the use of carbon silicon rods will be explored. The heating rods have longer life, but slower response to intentional changes in temperature.

2. A preliminary design for radial strain measurements will employ diametrically positioned DCDT's, invar extension probes and transite shielding. Fabrication of the components for the design has been initiated. Provisions have been made so that the distance between the specimen and the temperature-sensitive DCDT's can be varied. In comparison with the lever system, the proposed design will require smaller apertures in the shielding (hence, better temperature distributions), minimize errors due to vibrations, and be easier to fabricate. The performance of this experimental system of measurement will determine the final design.
3. In order to alleviate rapid wear, a different type of carbide material is being used to machine the specimen.
4. One of the yokes for compression testing has been fabricated.
5. Power controllers allowing better control over the end heaters are being purchased.
6. In order to facilitate accurate recording of the temperature distribution, various types of temperature measurement equipment are being examined.
7. Since several testing frames will be utilized concurrently, high-temperature parts for additional extensometers are being made.
8. Manufacture of additional specimens has continued.

3.2.2. Work completed during the month of February

1. High-temperature parts for additional extensometers have been completed.
2. A power controller has been received and is presently being evaluated for its performance in providing adequate control over the end heaters.
3. In an attempt to increase lamp life to 1000 hours, special high-temperature infrared heating lamps have been ordered.

4. The fabrication of the preliminary design components for radial strain measurements has been completed. During a trial run with a "dummy" specimen, the temperature-sensitive DCDT's were subjected to a temperature environment well within their operating range (less than 140°F). Instrumentation stability and the effect of temperature variations on the DCDT's (i.e., apparent strains due to thermal expansion of the extension probes) are still being investigated. Because of problems associated with the increased length of the probes, additional provisions for proper alignment of the extension probes with the DCDT's may be necessary.

3.2.3. Work completed during the month of March

1. Specimen no. 1 of 304 stainless steel is being mounted in a machine for a tension-torsion creep test at 1100°F, using a special high-temperature lamp recently received.
2. The life of the new lamp will be determined to see whether this type will provide the desired 1000 hour life.
3. The use of carbon rods in place of the lamp for heating the specimen has been under test, and evaluation will continue. It is clear that the lamp works better, but its life is in doubt.
4. The power controller seemed to be defective, was returned for checking, and has been received again.
5. Operation of a new type digital temperature indicator has been evaluated and found satisfactory.
6. A dummy specimen is set up in a tension testing frame with a lamp heater. This setup is being used to devise suitable means of achieving the desired temperature control and distribution. At present the variation of temperature with time at 1100°F is ±2.5°F, and over the 4-in. gage length the variation is ±2.3°F at 1100°F.
7. Manufacture of additional specimens has been continued.

3.3. Activities Associated with Investigations of Creep Failure Under Uniaxial and Multiaxial Conditions

C. E. Pugh

A subcontract was awarded during this quarter to the Babcock & Wilcox Co. for studies of failure under uniaxial and multiaxial creep conditions. The negotiation of this subcontract on the basis of a final proposal was noted in the Summary and Status section of Ref. 4. The principal investigator of this activity will be C. C. Schultz of B&W's Alliance Research Center. The general purpose of this study is to study failure under creep conditions in a comprehensive and consistent fashion and lead to the evaluation of methods for defining and predicting failure. The program is basically considered to be a three-year effort, with a selected number of back-up tests conducted with expected failure times of up to five years.

The overall study is to be both analytical and experimental. Tests are to be conducted over a range of temperatures, with initial emphasis on 1100°F, using specimens of type 304 stainless steel from the ORNL reference heat (9T2796). Both microscopic and macroscopic observations of deformations and rupture are to be included.

Uniaxial tests are to include tests to failure under constant load, tests to failure under stepwise-varying loads, and tests interrupted prior to failure. A number of constant load uniaxial tests will be creep tests for which deformation measurements will be made to failure and conducted under conditions which represent points dispersed throughout the overall matrix of failure tests. Similarly, deformation measurements will be obtained for some of the failure tests with stepwise-varying loads. Finally, the uniaxial rupture tests will include the simultaneous initiation of several specimens under identical conditions. At selected percentages of expected lifetimes, up to two of these tests would be interrupted; one for microscopic examinations and one for tensile testing to failure.

Tests will be conducted under multiaxial states of stress through the use of tubular specimens subjected to combinations of internal pressure and axial loadings. Some of the multiaxial tests will involve specified ratios of axial to pressure loadings that are maintained to failure.

Tubular specimens with various diameter-to-thickness ratios will be used. The ratio of axial-to-circumferential stresses will be changed in a stepwise manner during some of the tests to investigate material degradation in a direction other than the direction of maximum stress.

The analytical aspects of this activity are to lead to an evaluation of methods of predicting multiaxial failure under creep conditions. The initial activities include a literature review and will be followed by uniaxial modeling and correlation.

3.4. ORNL Studies of Time-Dependent Behavior

3.4.1. Creep law development for the ORNL reference heat of type 304 stainless steel (C. E. Pugh)

A part of the analytical ratchetting study being conducted at Teledyne Materials Research Co. (TMR)(discussed in Section 7) is to analyze the ORNL pipe ratchetting experiment[5] (discussed in Section 5). For this particular analysis, material behavior information pertinent to the material to be used in the experiment was needed. The material is the ORNL reference heat (9T2796) of type 304 stainless steel. To partially fulfill this need, a creep law of specialized form was developed on the basis of the constant uniaxial load creep data presently available from 1100°F tests.

The TMR study makes use of a creep law which is of the form

$$\frac{d\epsilon_c}{dt} = C_1 \sigma^{C_3} \epsilon_c^{C_4} + C_5 \sigma^{C_7} , \qquad (3.1)$$

where C_1, C_3, C_4, C_5, and C_7 are constants. [The indicated notation for the C coefficients is adopted to be consistent with that given in Eq. (9.1) of Ref. 6.] The variables in this equation are to be interpreted as:

ϵ_c = total axial creep strain measured in (in./in.),

σ = uniaxial stress measured in (ksi),

t = time measured in hours.

Using creep data from ORNL tests conducted at 1100°F (Ref. 6) and for uniaxial stress levels of 20 ksi and below, values were determined for the C coefficients and are shown below.

$$C_1 = 9.2878 \times 10^{-15}$$
$$C_3 = 5.6415$$
$$C_4 = -0.80082 \qquad (3.2)$$
$$C_5 = 1.9090 \times 10^{-14}$$
$$C_7 = 6.5244$$

To arrive at these values, a least-squares fit was obtained to each of the available creep curves with an equation of the form

$$\epsilon(t) = A_1 \left(1 - e^{-r_1 t}\right) + A_2 \left(1 - e^{-r_2 t}\right) + kt \ . \qquad (3.3)$$

A fit was then, in turn, obtained for Eq. (3.1) through the use of Eq. (3.3) and its time derivative for each test.

3.4.2. Creep law development for the ORNL preliminary heat of type 304 stainless steel (C. E. Pugh)

In the last quarterly progress report,[7] a creep law was given for the representation of data from constant-axial load creep tests of ORNL's preliminary heat (8043813) of type 304 stainless steel at 1200°F. It was reported that the data considered were from tests with initial stress values ranging from 8 to 25 ksi. Inadvertently, however, the expression given for $r(\sigma)$, see Eq. (4.14) in Ref. 7, was not the one intended. The creep law given in Ref. 7 is not recommended for use in analyses associated with this material, except at high stress levels.

The expression given in Ref. 7 had been developed on the basis of information from tests with initial stress values ranging from 12.5 to 25 ksi. An expression for $r(\sigma)$ that had been developed while including some information from tests with stress values as low as 8 ksi is

$$r(\sigma) = 1.275 \times 10^{-3} \, e^{0.1375\sigma} \ , \qquad (3.4)$$

where r is in $(\text{hours})^{-1}$ and σ in ksi. That is, the intended statement was

$$\epsilon(\sigma,t) = A(\sigma) \left[1 - e^{-r(\sigma)t}\right] + K(\sigma)t \ , \qquad (3.5)$$

with

$$A(\sigma) = 8.26 \times 10^{-4} \sinh (0.20\sigma) , \tag{3.6}$$

$$r(\sigma) = 1.275 \times 10^{-3} e^{(0.1375\sigma)} , \tag{3.7}$$

$$K(\sigma) = 1.632 \times 10^{-10} [\sinh (0.1858\sigma)]^4 , \tag{3.8}$$

with σ in ksi, creep strain in (in./in.), and time in hours. Although this particular representation was being stated, other expressions for the stress-dependence of these parameters were considered by the earlier investigations. In particular, power law relations were obtained for $A(\sigma)$ and $r(\sigma)$:

$$A(\sigma) = 2.079 \times 10^{-6} \sigma^{3.11} , \tag{3.9}$$

$$r(\sigma) = 3.991 \times 10^{-5} \sigma^{2.094} , \tag{3.10}$$

where $A(\sigma)$ is in (in./in.), $r(\sigma)$ in $(\text{hours})^{-1}$, and σ in ksi.

When compared with the data available when these relations were developed, there is little difference between the agreement given by the two sets of expressions for $A(\sigma)$ and $r(\sigma)$. However, when extrapolated to stress levels below that for which data were available, the predictions of the two sets of representations may differ substantially. In particular, Eqs. (3.9) and (3.10) predict smaller primary creep values and longer durations of primary creep.

The observations made above demonstrate some of the uncertainties associated with the extrapolation of a creep law into ranges for which data do not exist. Since creep analyses of structures critically depend on the creep law as input, the necessity of having creep data over the ranges of variables which apply to the problems to be analyzed is again pointed out. For the design of reactor components, this means that data must exist for ranges of variables, such as stress, temperature, and time, that are representative of design conditions. Recommendations for testing of materials under representative LMFBR design ranges have been made and were discussed in Ref. 8.

Some additional creep information, a part of which is shown in Fig. 6.4 of Ref. 6, is now available for the preliminary heat at stress levels of 10 ksi and below. This information is currently under investigation

and will give further definition to the creep law at the lower stress values. Preliminary observations suggest that the creep law given by Ref. 7 and the law given by Eqs. (3.6) through (3.8) in this report tend to over-predict the primary creep at low stress values (below 10 ksi). The correlations given by Eqs. (3.9) and (3.10) with Eq. (3.8) give better predictions at these low stress values. The law defined by Eqs. (3.8) through (3.10) is essentially that which was used to make the predictions shown in Ref. 9 (Figs. 4.4 through 4.6). Efforts to establish a more definitive creep law on the basis of all available information is in progress and will be discussed in the next quarterly progress report.

The attempts have been, in developing primary and secondary creep correlations, to provide a representation for the entire span of data, in both stress and time. When such a representation is applied to a specific limited range of stress or time, variations in the detailed accuracy of the representation can result. For example, an expression of the form given by Eq. (3.5) cannot exactly represent all points of long-duration creep-time curves. In this connection, other forms for representing the time dependence of the creep law have been[10] and are being studied. However, if only short-time creep behavior (times $\ll$ 2000 hours in this case) is of interest, a correlation can be developed from data over the limited range and most probably provide improved accuracy of representation in this restricted region. The same is true for specific limited stress ranges.

The beam analysis, discussed in Subsection 4.2 of this report, for example, applied the creep law given in Ref. 7 and that given by Eqs. (3.8), (3.9), and (3.10) of this report to low stress and relatively short-time situations. Observations are made there of features which substantiate some of the before-mentioned features of these particular creep laws in this low stress regime. Since the structural test and analysis study reported in Subsection 4.2 is one of examining the overall basic features and principles fundamental to existing analytical methods, it is important that use be made of the creep law which most accurately represents material behavior over the appropriate ranges of stress and time. Therefore, as noted earlier, efforts are continuing to establish

a creep law which includes the most representative description of the information available from low stress tests.

4. STRUCTURAL ANALYSIS

J. M. Corum

4.1. Development of Elastic-Plastic-Creep Finite Element Computer Programs

4.1.1. Development of general three-dimensional thick-shell elastic-plastic-creep finite element program (Z. Zudans, The Franklin Institute Research Laboratories; W. K. Sartory, ORNL)

The complete EPACA program has been assembled and is being debugged. This debugging procedure is taking considerably more time than expected. Also, minor changes and modifications are continuing to be made in the program. Thus, the program is not yet available; the best current estimate is that it will be ready to deliver to ORNL in May.

The major portion of the User's Manual for EPACA has been finished. The expected Table of Contents is reproduced below.

THEORY AND USER'S GUIDE FOR EPACA

TABLE OF CONTENTS

Section	Description
I	GENERAL INTRODUCTION
II	THEORY AND METHODS
	1. Introduction
	2. Technical Discussion of Analysis Methods
	2.1. Brief Summary
	2.2. Solution Method and Incremental Variational Principle
	2.3. Constitutive Relations
	2.3.1. Isotropic Strain Hardening
	2.3.2. Kinematic Strain Hardening
	2.3.3. Yielding from Elastic State

Section	Description
	2.3.4. Reduction of Constitutive Relations to Generalized Plane Stress Case
	2.3.5. State of Loading
	2.4. Time-Dependent Creep
	2.5. Eigenvalue Computation
	2.6. Forward Integration
	2.7. Solution and Decomposition
	2.8. References
	3. Element Types
	3.1. Brief Summary
	3.2. Element NKØD = 3
	3.3. Element NKØD = 4
	3.4. Element NKØD = 5
	3.5. Element NKØD = 6
	3.6. Isoparametric Elements NKØD = 7 to NKØD = 8
	4. Reference Frames, Reference Surface, and Shifts
	5. Materials Properties
III	PROGRAM DESCRIPTION
	1. Introduction
	2. Load History Concept
	3. Types of Analyses
	4. Overall Program Layout
	5. I/O Units and Their Storage Requirements
	6. Function of Major Subroutines
IV	INPUT GUIDE
	1. Introduction
	2. Concise Input
	2.1. Input Flow Chart
	2.2. Card-by-Card Concise Input
	3. Detailed Card-by-Card Input Instructions
V	SAMPLE PROBLEMS

Section II, Theory and Methods, and Section IV, Input Guide, have been submitted to ORNL, as has a preliminary complete program listing.

Specifically, during January the main emphasis was placed on debugging the creep analysis, load-history scheme, and nonisothermal plasticity portions of the program. Also, work was continued to modify the program so that the equation formation, solution, and decomposition is optionally done by using external storage devices. Relative to the creep analysis, the auxiliary creep hardening rules recommended by ORNL[11] in connection with strain hardening were incorporated via the subroutine AUXRU. This subroutine was reviewed and approved by ORNL.

During February the assembly of the overall program with the inclusion of creep, nonisothermal plasticity, load-history concept, single and double precision, and in-core and out-of-core strategy was completed, and the debugging stage was begun. A large number of new and modified subroutines were written and the input layout was extensively changed. The overall user's manual outline was prepared and the manuscript for Section II was completed.

The debugging and testing of computational modules proceeded in parallel with the overall program debugging by the use of the in-core, single precision program version first assembled. This version of the program had previously satisfactorily solved a small problem for loading into the plastic zone followed by creep relaxation and then by a complete unloading. Bugs found in this version were immediately corrected in the final complete version of EPACA.

During March major emphasis continued to be placed on debugging of the overall program. The final input layout was generated and a card-by-card input map was prepared and placed as an element on the program tape as well as used as the manuscript of Subsection 2.2 of Section IV of the "Theory and User's Guide for EPACA."

Problems were encountered with the Univac 1108, Exec 8, Level 26 operating system in the transfer of labeled commons. System experts of the Univac computer services supplier are studying the question and promise to resolve the problem as soon as possible.

The complete program listing, including a number of superseded subroutines, was sent to ORNL. From the overall program point of view, this listing represents the program in its final form, except for the restart feature with respect to some of the computational modules; however, further

changes are presently being worked on. Also, some of the double precision subroutines have not been punched as yet from the corresponding single precision subroutines.

As mentioned in the previous program report, ORNL has obtained a preliminary version of the EPACA program. The preliminary version that we have does not have complete facilities for inelastic calculations or automatic mesh generation capabilities. Documentation, particularly with regard to input data preparation for the preliminary version, is also incomplete. Nonetheless, several elastic and inelastic analyses involving thermal and pressure loading of flat plates have been attempted on this program, but with only minimal success. When a complete version of the program and documentation are available, a more intensive effort to test and evaluate the program and its many options will be made by ORNL.

4.1.2. Development of two-dimensional elastic-plastic-creep finite element program (Y. R. Rashid, General Electric Co.; J. M. Corum and J. S. Crowell, ORNL)

The CREEP-PLAST program is currently undergoing final checkout and evaluation at ORNL. Two reports have been prepared by General Electric to aid the program user. One of these, Part II: User's Manual for CREEP-PLAST Computer Program, has been received at ORNL in final form. The second, Part I: Theory for CREEP-PLAST Computer Program, is presently at the printers and will be ready in mid-May.

Two versions of the program were developed — a research version and a production version. The research version, which is primarily for ORNL in-house use, is the more versatile of the two with respect to the constitutive equations that can be handled and the manner in which they are treated. This versatility is achieved at the cost of efficiency and capacity in terms of the number of time steps (80) that can be handled. Thus the research version is for examining the use of various constitutive theories (particularly those of the memory type), not for analyzing structures with realistic load-temperature histories.* The production version

*Both load steps and time increments, in the 'time increment-initial strain' approach, are treated as time steps by CREEP-PLAST. The limitation of 80 time steps in the research version is overly restrictive for realistic histories.

is geared to the more efficient handling and solution of realistic problems. Because it does not have provisions for integrating over the entire previous history at each time step (as required in a general memory theory approach), there is no real limit to the number of time steps that can be used in a given analysis. Currently each run is limited to 200, but restart capabilities can be used to extend this to any number. It is the production version, not the research version, that will be made generally available to the public.

Although the CREEP-PLAST program was made operational on an IBM 360 computer system, the programming was done to take advantage of Univac 1108 Input/Output software. Consequently, both research and production versions of the program are 'I/O bound.' The result is that the total machine time for a run is excessively large relative to the actual CPU time used on the IBM 360 system.* At ORNL we can get around this very real problem by using more of the available fast memory of the 360/91 system.** However, we are looking at other ways of improving the situation in order to keep the program relatively small and machine independent for public use.

We have spent, at ORNL, considerable time checking and correcting various aspects of the research version, and more recently of the production version. Several problems have been successfully run, one of which is described in the next section. A small number of additional sample problems must be run and a number of fairly small modifications that were made by General Electric must be incorporated before the production version will be generally distributed to the public. The program will be available from, and kept updated by, ORNL. The program will be released with the agreement that any changes and modifications that are made will be coordinated with ORNL for at least a period of one year. In this way everyone will benefit from any corrections, modifications, or extensions made to the program, and a current updated version will always be available.

The General Electric subcontract has been extended for eight months to extend the capability of CREEP-PLAST to include the solution of the

---

*This is probably true also for a CDC 6600 system.

**The CREEP-PLAST program currently requires 400K bytes of fast memory (for 900 nodes, 1800 elements). User programs can currently use up to 1500K of the 2000K 360/91 fast memory.

transient heat conduction problem for plane and axisymmetric structures. Also, arrangements have been made with Y. R. Rashid to include in the program all of the ORNL constitutive equation recommendations as previously described.[11] These latter changes will be available about June 1.

4.2. Elastic-Plastic-Creep Analyses of Beam B3

J. A. Clinard
J. M. Corum
W. K. Sartory

The initial elastic-plastic loading of beam B3 (Ref. 12) to 1900 lb and the 312-hr creep period at that load level have been analyzed using both the CREEP-PLAST program, which was developed at General Electric, and the PLACRE program, which was developed at ORNL. Initially, both analyses used the creep equation given in the previous quarterly progress report[13] for the preliminary heat of 304 stainless steel at 1200°F. For the initial loading stress-strain curve, both analyses used a representation of the actual curve which is recommended later in Section 5.1.2 of this report (see Fig. 5.9).

To obtain a valid comparison of the two analyses, identical finite element layouts were used. One-half of the 2 in. high by 26 in. long, simply supported, center-loaded beam was represented for the plane stress analysis. A uniform square mesh consisting of 832 constant strain triangular elements and 477 nodes was used. Both programs use the tangent stiffness method, with kinematic hardening, for elastic-plastic analyses, and in both cases 11 load steps were used to reach 1900 lb (one step to 900 and ten steps between 900 and 1900 lb). For creep, both programs used the equation-of-state approach with strain hardening. Primary strain hardening was used by CREEP-PLAST, whereas total strain hardening was used by PLACRE. For CREEP-PLAST, 18 time steps were used in the creep analysis and these were chosen and input by hand. PLACRE has an automatic time step selection procedure, and this resulted in 48 time steps over the 312-hr creep period.

The results of the two analyses are typified by Figs. 4.1 and 4.2 where the predicted center deflection behavior of the beam is compared with the measured behavior. The elastic-plastic loading predictions

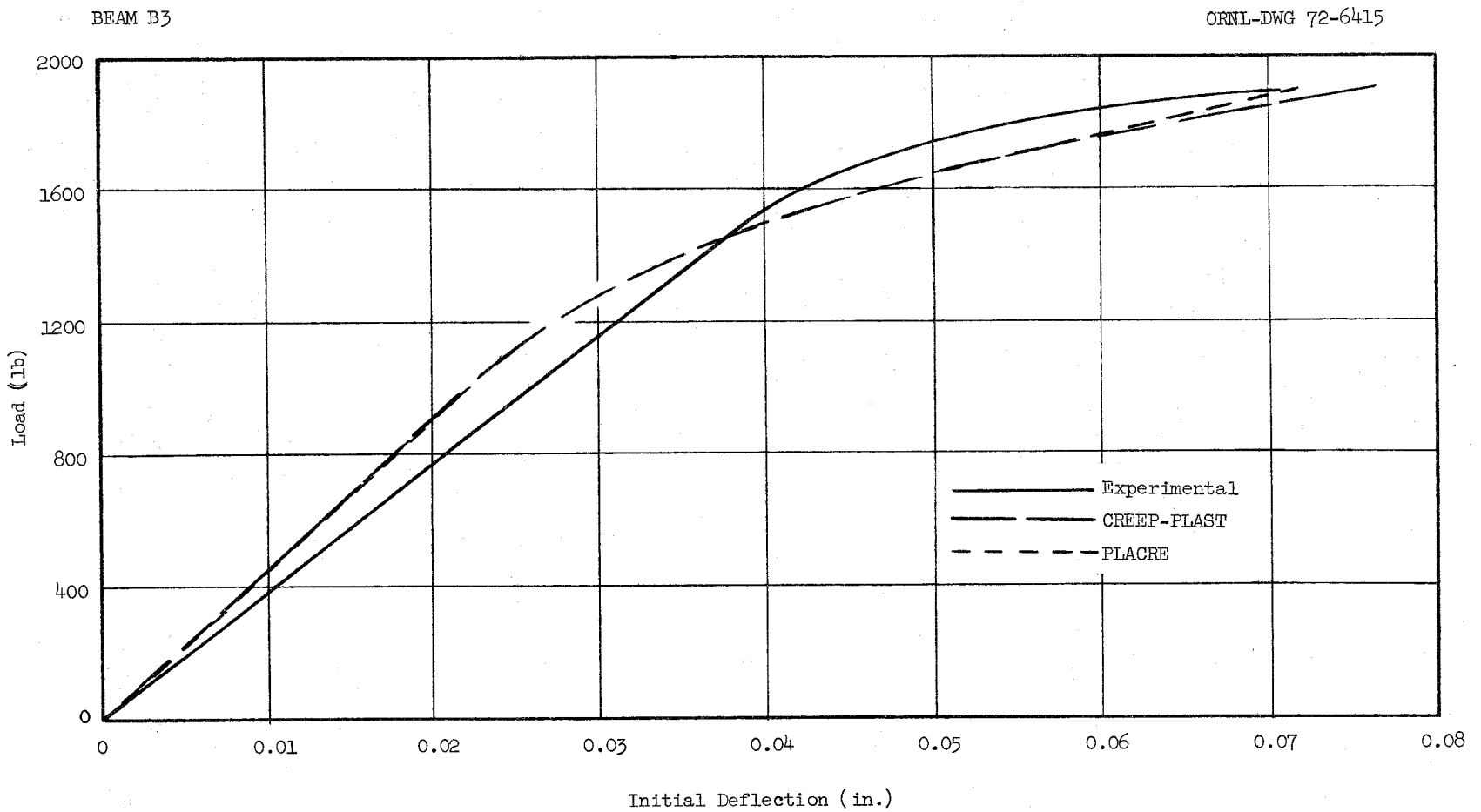

Fig. 4.1. Predicted and measured load versus center deflection behavior of beam B3 for initial loading to 1900 lb.

ORNL-DWG 72-6416

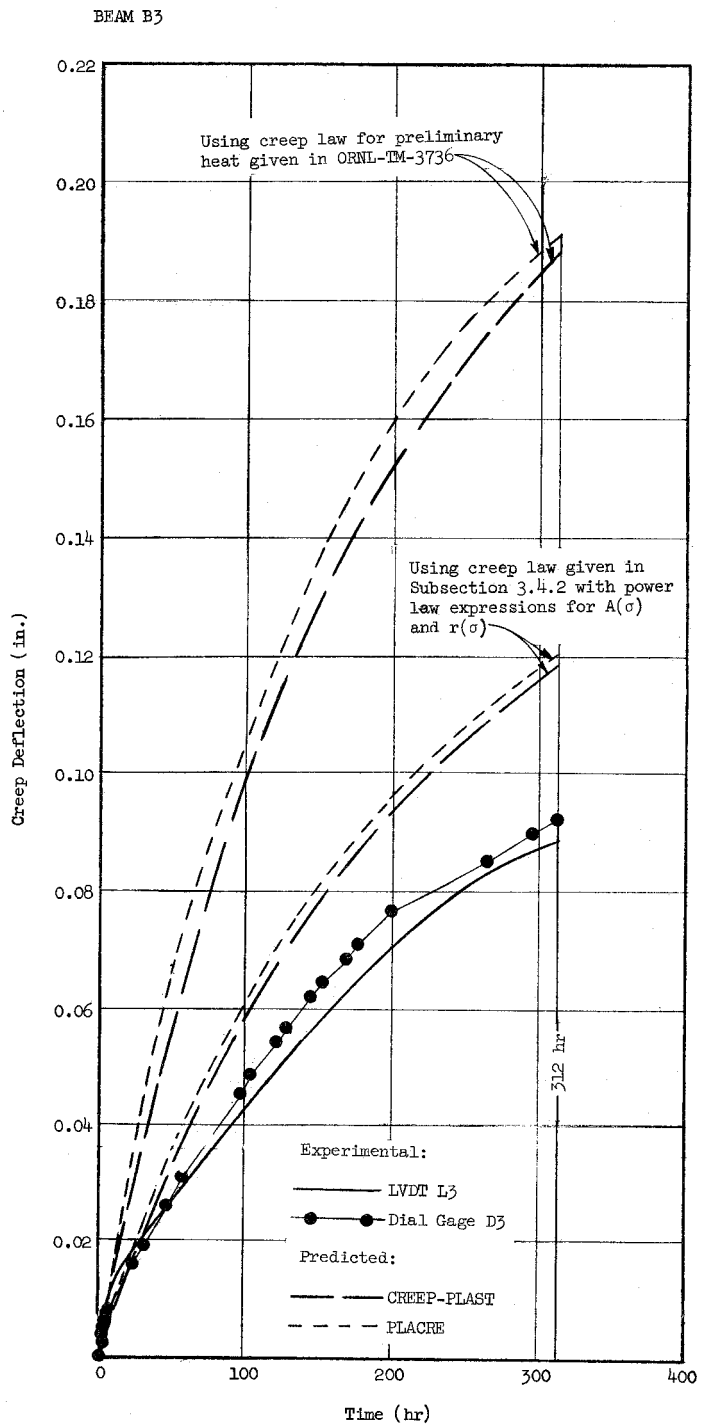

Fig. 4.2. Predicted and measured creep deflection versus time for center of beam B3 during initial 312-hr creep period at 1900 lb. Note that although the deflection is labeled 'creep deflection,' plastic behavior also occurred simultaneously, and both analyses accounted for this behavior.

shown in Fig. 4.1 agree reasonably well with the measured behavior. The initial creep predictions, which are represented by the two upper curves in Fig. 4.2, do not do as well. Here the main problem probably arises from the fact that the creep equation used to describe the uniaxial creep data overestimates the measured primary creep data at the low stress levels and relatively short times existing in the beam test. For example, at 8000 psi the predicted creep at the end of 300 hours is about 1.8 times the creep strains measured in two uniaxial creep tests performed at ORNL. Two uniaxial creep tests at 6000 psi seem to indicate that very little measurable creep occurs at that low stress level.

To further illustrate the influence of the creep equation on the analysis predictions at these low stress levels, a second beam analysis was carried out using one of the alternate creep equations given in Subsection 3.4.2 of this report, and the results are also shown in Fig. 4.2. The creep equation used is given by Eqs. (3.5), (3.8), (3.9), and (3.10), and uses power law expressions for $A(\sigma)$ and $r(\sigma)$. The extrapolation to low stress levels using this equation provides better agreement with the uniaxial creep data than does the equation given in Ref. 13, and, not surprisingly, the predicted beam behavior agrees better with experiment.

As mentioned in Subsection 3.4.2, efforts are underway to obtain a creep equation that better predicts the low stress creep behavior. This equation will take into account additional low-stress creep data that were not available when the previous equations were developed.

4.3. Elastic-Plastic-Creep Analyses of First Proposed ORNL Pipe Thermal Ratchetting Test

4.3.1. ORNL pipe ratchetting sensitivity studies (W. K. Sartory)

To assist in the design of the ORNL pipe thermal ratchetting tests (see Section 5.2 of this report), a series of analyses was carried out to determine the sensitivity of the ratchetting to variations in a number of test conditions. The reference conditions during the thermal shock portion of the first test are:

1. A coolant temperature drop from 1100°F to 800°F at a constant rate of 30°F/sec, followed by a hold period at 800°F until the wall temperature is uniform.

2. A constant pressure of 700 psi during the shock itself. (The pressure is removed and reapplied later at 800°F.)

3. No axial temperature gradient.

Since these conditions cannot be met precisely in the test, a study was made to determine the effect of altering the rate of temperature drop during the shock, of a temperature undershoot below 800°F at the end of the shock, of a pressure drop during the shock, and of an axial temperature gradient during the shock.

The axial temperature gradient was simulated by introducing a pure time delay into the coolant temperature at locations downstream from the entrance to the test section. The coolant temperature T (°F) at time t (sec) at a location z (in.) downstream from the entrance was taken to be:

$$T = \begin{cases} 1100 & \text{for } t < z/15 \ , \\ 1100 - 30\ (t - z/15) & \text{for } z/15 < t < 10 + z/15 \ , \\ 800 & \text{for } 10 + z/15 < t \ . \end{cases}$$

This results in an axial coolant temperature gradient of 2°F/in. during the shock. Axial heat conduction in the pipe wall was ignored. The results of the sensitivity study are shown in Table 4.1.

The effect of a temperature undershoot in particular appeared to be excessive, so a further investigation was made. For the calculation reported above, the coolant temperature was dropped from 1100°F to 750°F at a constant rate of 30°F/sec, held at 750°F until the wall temperature equalized, and then very slowly reheated to 800°F. The coolant temperature undershoot which could actually occur in the test is somewhat less severe and is given in Table 4.2.

Pipe ratchetting calculations were repeated for the coolant temperature transient prescribed in Table 4.2. The results are summarized in Table 4.3. These deviations from the reference conditions are considered acceptable.

These sensitivity calculations indicate that the possible deviations from the reference conditions do not result in excessive variations in the axial and circumferential strains to be measured. After the ratchetting test is performed, the actual conditions will, of course, be known, and they can be factored into the final structural analysis of the specimen.

Table 4.1. Study of percentage effects due to deviations from reference thermal transient cycle

Condition	Variation in outside circumferential strain (%)	Variation in axial strain (%)
1. Raising the shock rate to 32°F/sec		
1st cycle	3	3
2nd cycle	3	4
2. A 50°F undershoot (to 750°F) in downshock at 30°F/sec		
1st cycle	10	13
2nd cycle	8	12
3. A 50-psi pressure drop throughout transient		
1st cycle	−5	0
2nd cycle	−10	−5
4. A 2°F/in. axial temperature gradient during the shock		
1st cycle	−1	−3
2nd cycle	−2	−4

Table 4.2. Possible coolant temperature transient undershoot in test

Time (sec)	Temperature (°F)
0	1100
10	800
11	772
12	756
13	750
14	751
15	757
16	764
30	800

Table 4.3. Study of the percentage effects of replacing the reference shock by the coolant temperature anticipated in the test

	Variation in outside circumferential strain (%)	Variation in axial strain (%)
1st cycle	+6	+8
2nd cycle	+5	+7

4.3.2. Teledyne analysis of ORNL ratchetting test specimen using ANSYS computer program (T. R. Branca, J. L. McLean, Teledyne Materials Research Co.)

As a part of the TMR ratchetting study (see Chapter 7 of this report) the ANSYS computer program was used to perform a preliminary analysis of the first ORNL pipe thermal ratchetting test specimen. The analysis was preliminary in that the creep equation and the stress-strain curves used to describe the material behavior were very preliminary. They do, however, describe reasonably well the expected behavior of the pipe ratchetting specimen material. Tests of specimens taken from the actual pipe will be used to better establish the behavior.

The ratchetting specimen is 8.44 in. outside diameter with a 0.375 in. wall. The reference test conditions are:

1. a normal temperature and pressure of 1100°F and 700 psi, respectively,
2. a downshock in the sodium of 30°F/sec for 10 sec,
3. a hold period at 800°F during which the pressure is removed and then reapplied,
4. a gradual heating (50°F/hr) to 1100°F, and finally,
5. a 500-hr hold period at 1100°F and 700 psi.

The cycle is then repeated.

The finite element model is the same one as depicted in Fig. 7.1 (Chapter 7 of this report). It consisted of 16 quadrilateral axisymmetric elements through the pipe thickness. Generalized plane strain was assumed.

The heat transfer coefficient furnished by ORNL for the inner surface was 34 Btu/hr-in.^{2}-°F. The outer surface was assumed to be insulated.

Other properties used in the analysis are given in Table 4.4. The stress-strain data used were based on ORNL tests on rod material from the reference heat of 304 stainless steel and are tabulated in Table 4.5.

Finally, the creep law used was provided by ORNL in a strain-hardening form available on ANSYS at the time. The equation is

$$\frac{d\epsilon_c}{dt} = C_1 \sigma^{C_3} \epsilon_c^{C_4} + C_5 \sigma^{C_7} ,$$

where

$C_1 = 9.2878 \times 10^{-15}$,

$C_3 = 5.6415$,

$C_4 = -0.80082$,

$C_5 = 1.9090 \times 10^{-14}$,

$C_7 = 6.5244$,

with

ϵ_c = total creep strain (in./in.),

σ = stress measured in ksi,

t = time in hours.

The results are typified by the computer plots shown in Figs. 4.3 and 4.4. Figure 4.3 shows the circumferential stress-strain history for the outside element for five test cycles. The initial downshock begins at point 0 where the 700 psi pressure is acting at 1100°F. The 500-hr hold period after the thermal shock is shown for 1′ to 1 for cycle 1, and from 2′ to 2 for cycle 2, etc. The elastic downspike immediately proceeding the hold period represents the pressure removal at 800°F.

The circumferential stress-strain history for the inside element is shown in Fig. 4.4. Again, the initial thermal downshock begins at point 0, and the behavior during the hold periods is represented by 1′–1, 2′–2, etc. The upper tips of the loops represent the stress-strain state after approximately 10 seconds (at about the time the sodium temperature reaches 800°F). As the wall temperature evens out to 800°F, the inside undergoes elastic unloading and then yielding in compression. The pressure unloading, which produces further yielding in compression, begins just before the lower tips are reached, and reloading occurs beginning at the lower tips.

Table 4.4. Properties assumed for 304 stainless steel

Temperature (°F)	Modulus of elasticity (psi)	Instantaneous coefficient of thermal expansion (in./in.-°F)	Poisson's ratio	Thermal conductivity (Btu/hr-in.-°F)	Specific heat (Btu/lb-°F)	Density (lb/in.^{3})
600	25.4×10^6	10.43×10^{-6}	0.30	0.8558	0.128	0.285
700	24.8×10^6	10.66×10^{-6}	0.30	0.9250	0.130	0.285
800	24.1×10^6	10.90×10^{-6}	0.30	0.9625	0.132	0.284
900	23.3×10^6	11.09×10^{-6}	0.30	0.9917	0.134	0.283
1000	22.5×10^6	11.28×10^{-6}	0.30	1.0350	0.137	0.282
1100	21.7×10^6	11.47×10^{-6}	0.30	1.0750	0.139	0.281
1200	20.9×10^6	11.65×10^{-6}	0.30	1.1083	0.141	0.280

ORNL-DWG 72-6417

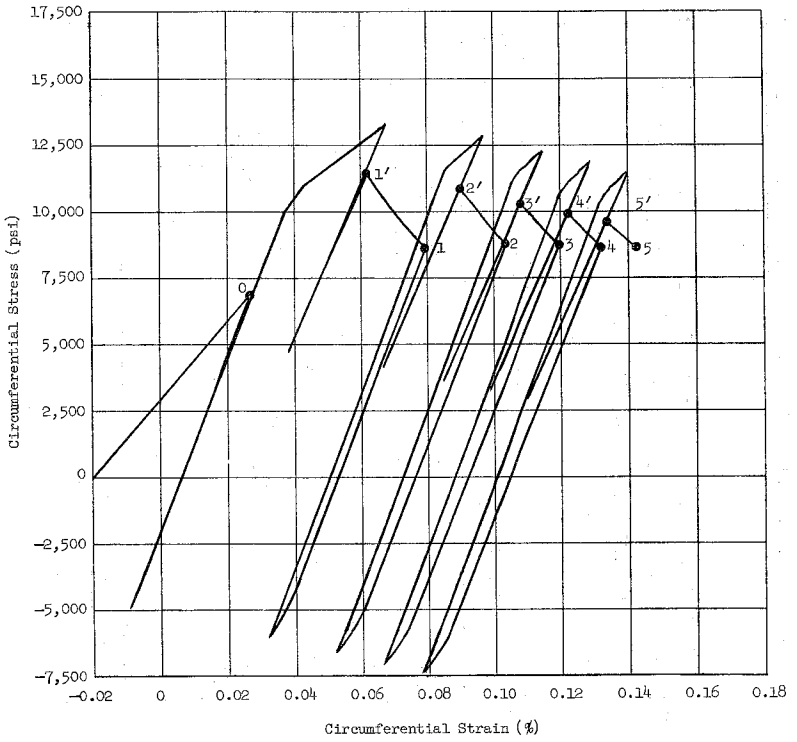

Fig. 4.3. Stress versus strain history for outside element. History shown is for five test cycles.

ORNL-DWG 72-6418

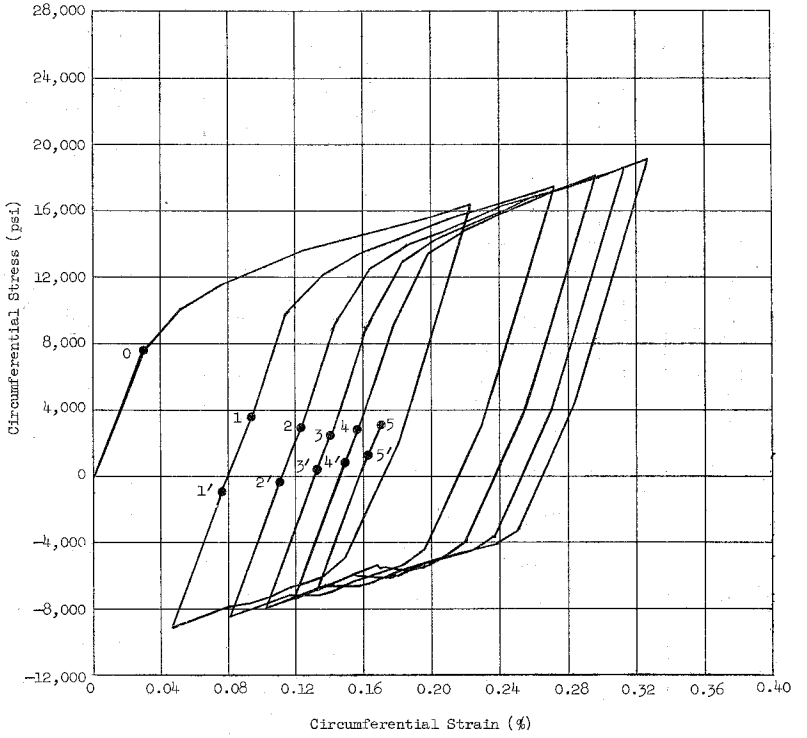

Fig. 4.4. Stress versus strain history for inside element. History shown is for five test cycles.

Table 4.5. Stress-strain input for ANSYS solution of ORNL ratchet case

Temperature (°F)	Strain (in./in.)				
	0.000392	0.001	0.002	0.006	0.03
	Stress (psi)				
600	9956	14,200	16,600	20,300	27,700
800	9447	13,100	15,300	18,900	26,400
1000	8820	11,700	13,900	17,500	25,200
1100	8506	11,000	13,300	16,900	24,500
1200	8193	10,300	12,700	16,300	23,200

The predicted circumferential and axial strains in the outside element are summarized in Table 4.6. These quantities are near those that we would expect to measure on the outside surface.

The predicted incremental circumferential strains accumulated during the 500-hr hold periods are, from Table 4.6, 151, 108, 85, 72, and 63 μin./in. for the first through fifth cycles, respectively. Preliminary

Table 4.6. Predicted circumferential and axial strains in outer element at beginning and end of 500-hr hold period at 700 psi and 1100°F

Cycle No.	Strain at start of 500 hr (μin./in.)		Strain at end of 500 hr (μin./in.)	
	Circumferential	Axial	Circumferential	Axial
1	645		796	244
2	929		1037	266
3	1110		1195	267
4	1249		1321	264
5	1364		1427	258

values, considerably larger than these, were previously reported.[14] These early values were based on preliminary design analyses using materials data from a different heat of 304 stainless steel. Additional analyses will be performed as more data and better representations of the data become available.

4.4. A Preliminary Analysis of Three Uniaxial Ratchetting Tests – PVRC Sponsored Testing at Mar-Test, Inc.

W. K. Sartory
C. E. Pugh

4.4.1. Test definition

The Pressure Vessel Research Committee, through the Plastic Fatigue Strength Subcommittee to the Fabrication Division, is sponsoring a testing effort at Mar-Test, Inc. The tests simultaneously employ two uniaxial specimens in two testing machines whose controls are coupled so that the system represents the behavior of a classical three-bar ratchetting model.[15] Figure 4.5 shows the two-specimen arrangement. The system is controlled in a manner such that a constant total load P is carried by the two specimens and such that the total axial strain is the same in each specimen. In addition to carrying the load, each specimen is subjected to a thermal history and the resulting deformations are followed. The basic type of thermal history of interest is shown in Fig. 4.6.

Reference 16 tentatively recommended three tests for the PVRC sponsored testing at Mar-Test, Inc. These tests are outlined in Table 4.7 and are to utilize specimens from the ORNL reference heat (9T2796) of type 304 stainless steel. In order to give better insight into the expected behavior of these specimens, preliminary elastic-plastic-creep analyses were performed for a total of six different cases of each test. The results of these analyses will be retained for comparison with the experimental results when they become available.

ORNL-DWG 72-6419

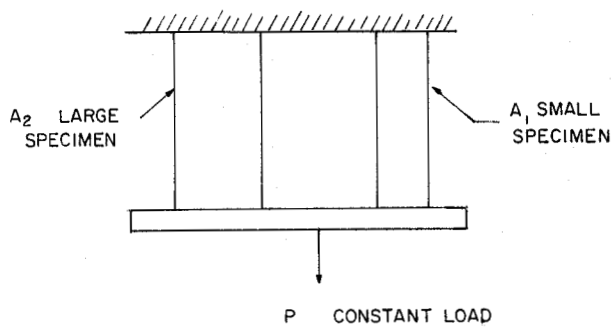

Fig. 4.5. Basic arrangement of specimens in Mar-Test, Inc. studies.

ORNL-DWG 72-6420

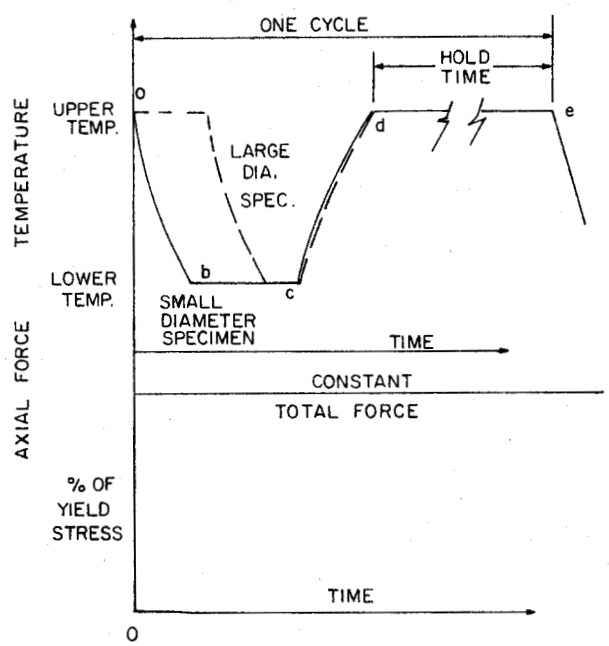

Fig. 4.6. Thermal and mechanical loading histories for Mar-Test, Inc. studies.

Table 4.7. Tentative specification test requirements

Parameter	Test No. 1	Test No. 2	Test No. 3
(1) Specimen gage diameter (in.)			
Large	0.375	0.375	0.375
Small	0.200	0.200	0.278
(2) Total applied axial force, % yield stress	60%	60%	30%
(3) Test parameters per cycle	(a) (b) (c)	(a) (b) (c)	(a) (b) (c)
(a) Upper temperature, °F (b) Lower temperature, °F (c) Hold time			
Cycle 1	1100°F, 900°F, 5 min	1100°F, 900°F, 1 day	1200°F, 800°F, 8 hr
Cycle 2	1100°F, 900°F, 5 min	1100°F, 900°F, 1 day	1200°F, 800°F, 8 hr
Cycle 3	1100°F, 900°F, 5 min	1100°F, 900°F, 1 day	1200°F, 800°F, 8 hr
Cycle 4	1100°F, 900°F, 5 min	1100°F, 900°F, 1 day	1200°F, 800°F, 8 hr
Cycle 5	1100°F, 900°F, 1 hr	1100°F, 900°F, 1 day	1200°F, 800°F, 8 hr
Cycle 6	1100°F, 900°F, 1 hr	1100°F, 900°F, 1 week	1200°F, 800°F, 4 days
Cycle 7	1100°F, 900°F, 16 hr	1100°F, 900°F, 1 week	1200°F, 800°F, 4 days
Cycle 8	1200°F, 1000°F, 5 min	1100°F, 900°F, 4 hr	1200°F, 800°F, 4 hr
Cycle 9	1200°F, 1000°F, 5 min		
Cycle 10	1200°F, 1000°F, 5 min		
Cycle 11	1200°F, 1000°F, 1 hr		
Cycle 12	1200°F, 1000°F, 1 hr		
Cycle 13	1200°F, 1000°F, 8 hr		

4.4.2. Analyses of tests

The analyses were based on the limited material properties information currently available on the ORNL reference material. The guidelines given in Ref. 17 and discussed in Ref. 18 were generally followed. Five of the six cases analyzed were based on initial yield stress information pertinent to specimens taken from plates of the ORNL material and the other one case on information from rod material. Since the information currently available on this material is very limited, the properties used in this study must be considered to be unrefined and uncertain representations. For example, the creep law, which relates axial creep strain to uniaxial stress and temperature for constant uniaxial stress conditions, used throughout this study is an adjusted version of that given in the LMFBR Materials Handbook[19] for type 304 stainless steel. The creep law coefficients are adjusted to provide general agreement with the creep data now available for the ORNL reference material at 1100°F.

The six cases considered are listed below.

Case I. This case utilizes properties associated with plate material and makes use of the cyclic hardening rule. Except for the load P applied to the system which is 10% more than indicated, the tests are identical to those in Table 4.7.

Case II. The difference between Case II and Case I is that the load P applied to Case II is that given in Table 4.7.

Case III. Cyclic hardening is omitted from Case III; otherwise it is the same as Case II.

Case IV. This case is the same as Case II, except that the yield properties used are those associated with rod material.

Case V. This case is the same as Case I except that the load P applied to the system is 20% more than indicated in Table 4.7.

Case VI. This is identical to Case V except that the temperature changes here are also 20% greater than given in Table 4.7. (The hold-time temperatures remain unchanged.)

As noted earlier, the purpose of these analyses was to provide added assistance in developing a feeling for the amount of deformation that can be expected for various cycles and tests. Such information gives an added basis for assessing required measurement and control accuracies that need to be employed in the conduct of the tests.

The PVRC test recommendations have been revised from that shown in Table 4.7, in part, on the basis of the results of these analyses. The revision made is to increase the total load carried by the system to 1.20 times that shown in Table 4.7.

5. STRUCTURAL TESTS

J. M. Corum

5.1. Elastic-Plastic-Creep Beam Tests

J. M. Corum
M. Richardson

The second elevated temperature beam test (beam B4) was completed. The test temperature was 1200°F, and the loading history consisted of a short-time cyclic loading, a step-loading creep test period, and finally a second, post-creep, short-time cyclic loading. Like the previous eleevated temperature test (beam B3), beam B4 was machined from the preliminary heat of type 304 stainless steel (heat 8043813). Creep data, developed for this material at 1200°F, are available, as are cyclic stress-strain curves obtained at 1200°F. Thus the experimental data from beams B3 and B4 together with the material properties data developed for this heat of material provide the analyst with a means for performing a check on his inelastic analysis procedures.*

---

*As mentioned in the two previous chapters, the creep equation that was given in the previous progress report[20] provides a good description of the creep data for stress levels of 12,500 psi and above. It does not adequately describe the lower stress short-time creep data that are of most interest for analyzing beam tests B3 and B4 and should not be used for analyzing these beams. Additional low stress creep data are now available, and a modified equation, more suitable for beam analyses, is being developed.

The test of beam B4 completed the initial series of beam tests, which was designed to check out the test facility and to provide some structural test data for the preliminary heat of material. Following the test of beam B4, the beam test facility was modified to improve both the temperature control and the cyclic load control. We are now ready to begin a new series of elevated temperature tests using beams from the reference heat of 304 stainless steel (heat 9T2796). The initial two tests in this new series will be conducted at a temperature of 1100°F, and the loading histories will essentially duplicate those used for beams B3 and B4.

5.1.1. Elastic-plastic-creep test of beam B4 at 1200°F

Beam B4 was simply supported and center loaded. It had a height of 2 in., a nominal width of 1 in. (the actual measured width was 0.967 in.), and a length, between supports, of 24 in. The total length was 26 in. The loading sequence used for the test was:

1. ten short-time load cycles between nominal limits of ±1900 lb,
2. constant load creep test, 1900 lb for 312 hr,
3. step increase in load to 2250 lb, and then held constant for 312 hr,
4. step decrease in load to −1900 lb, held constant for 332 hr,
5. removal of load followed by 12 short-time load cycles between nominal limits of ±1900 lb.

The loading rate for all step-load changes and for the short-time cyclic loading was controlled to maintain a near-constant beam center deflection rate of 0.2 in./min. This latter value corresponds approximately to a maximum strain rate (calculated on an elastic basis) of 0.005/min. Except for the initial short-time load cycles, which beam B3 did not have, the load history for beam B4 essentially duplicated that for beam B3. The test results for beam B3 were described in the previous quarterly report.[20]

In addition to quartz rods, which were attached to the beam midsurface, for measuring lateral deflection, and Microdot weldable strain gages, which were used primarily for gage evaluation purposes, beam B4 was instrumented with ten thermocouples, located on the top and bottom surfaces, within the middle 16 in. of the span. These thermocouples were located near the center of the beam, 4 in. from the center, and 8 in. from the center. These locations are the same as those at which deflection measurements were made.

The thermocouples used were sheathed Chromel-alumel, 1/16-in.-diam × 24-in. long, and were individually calibrated before and after the beam test. The measured temperature range, over the middle 16 in. of the beam, is shown plotted in Fig. 5.1 for various times during the test. Generally, the measured temperatures over the beam surface differed by 10°F or less at any given time throughout the 956-hr test. However, the mean temperature varied somewhat from 1200°F over the duration of the test. The trend in the variation that is depicted in Fig. 5.1 was also exhibited by beam B3, and is related to the relative position of the beam to the heaters during the test. Modifications, which will be described later, have been made to the heating system to correct this mean-temperature variation.

The measured maximum and minimum loads for each of the ten short-time load cycles to which beam B4 was subjected prior to the creep test are tabulated in Table 5.1. The numbers in parentheses in the table are the percentages that the actual loads were over, or under, the specified load levels of ±1900 lb. The beam behavior during the precreep cyclic test is typified by the cyclic deflections at the center of the beam, as shown in Fig. 5.2. The amount of plastic work hardening that rapidly occurs is apparent from the decreased loop width in going from the first to

Table 5.1. Maximum and minimum measured loads in precreep cyclic test on beam B4

Cycle	P_{max} (lb)	P_{min} (lb)
1	1970 (3.7)[a]	−1900 (0)
2	1925 (1.3)	−1960 (3.2)
3	1935 (1.8)	−1930 (1.6)
4	1935 (1.8)	−1925 (1.3)
5	1935 (1.8)	−1925 (1.3)
6	1920 (1.1)	−1965 (3.4)
7	1930 (1.6)	−1915 (0.8)
8	1940 (2.1)	−1950 (2.6)
9	1925 (1.3)	−1890 (−0.5)
10	1940 (2.1)	−1925 (1.3)

[a]Numbers in parentheses denote the percentage that the measured load was over, or under, the specified levels of ±1900 lb.

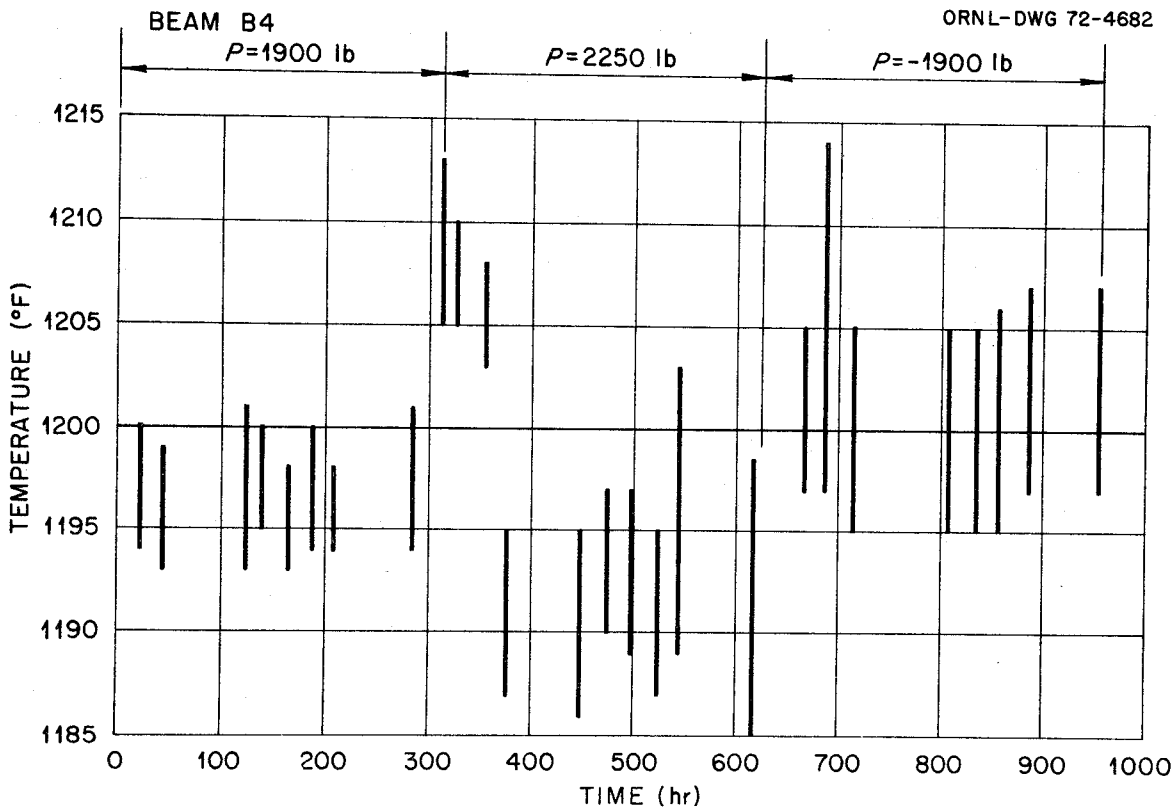

Fig. 5.1. Measured temperature range over middle 16 in. of beam B4 during 1200°F test.

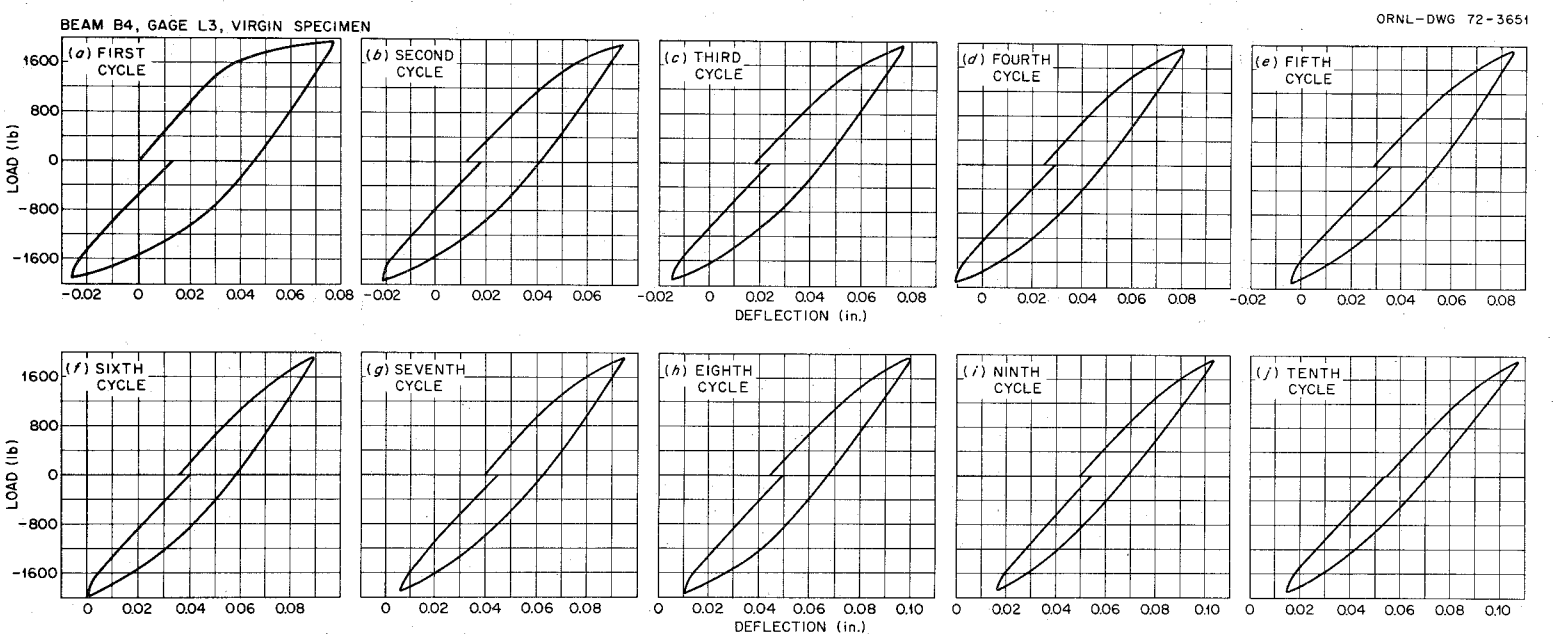

Fig. 5.2. Center deflection of beam B4 for the ten precreep short-time load cycles at 1200°F.

the second cycle. Further hardening occurs in subsequent cycles, but by the eighth or ninth cycle the loops become fairly stable. Note that the hardening has produced a plastic ratchetting in the positive deflection direction. The initial loading deflection of 0.065 in. at 1900 lb agrees reasonably well with the initial loading deflection of 0.071 in. measured for beam B3.

The measured creep deflections for beam B4 are shown as a function of time in Figs. 5.3, 5.4, and 5.5. The data shown are dial-gage readings. Also shown in these figures are the 'instantaneous' elastic plus plastic deflections obtained at each load change (0 to 1900 lb, 1900 to 2250 lb, 2250 to −1900 lb, and −1900 lb to zero load).* The two sets of dial-gage data shown in Figs. 5.4 and 5.5 are from symmetrically located gages on either side of the beam centerline. These gages exhibited close agreement throughout the test.

The creep response curves shown in Figs. 5.3, 5.4, and 5.5 agree relatively closely with the creep response curves presented previously for beam B3 (Ref. 20). Thus, it appears that despite the fact that considerable plastic hardening occurred during the precreep cyclic test period, this hardening had little effect on the subsequent creep behavior.

Following the creep portion of the test, beam B4 was subjected to 12 postcreep short-time load cycles between nominal load levels of ±1900 lb. The measured maximum and minimum loads for each of these postcreep cycles are tabulated in Table 5.2. The postcreep cyclic beam behavior is typified by the cyclic deflections at the center of the beam, as shown in Fig. 5.6. Two significant observations can be made from Fig. 5.6. First, the loops are relatively stable in shape, considering the varying peak load levels, and they are somewhat narrower in width than the latter-cycle loops in the precreep cyclic loading (see Fig. 5.2). This indicates that some additional hardening due to creep has occurred. The second observation is that there is a progressive plastic ratchetting in the negative deflection direction. This may or may not be a true characteristic of the structural

---

*The creep test was begun immediately at the end of the precreep cyclic test. Thus dial-gage readings were not obtained immediately before the initial 1900-lb load was applied. The initial instantaneous deflection values shown are from LVDT data.

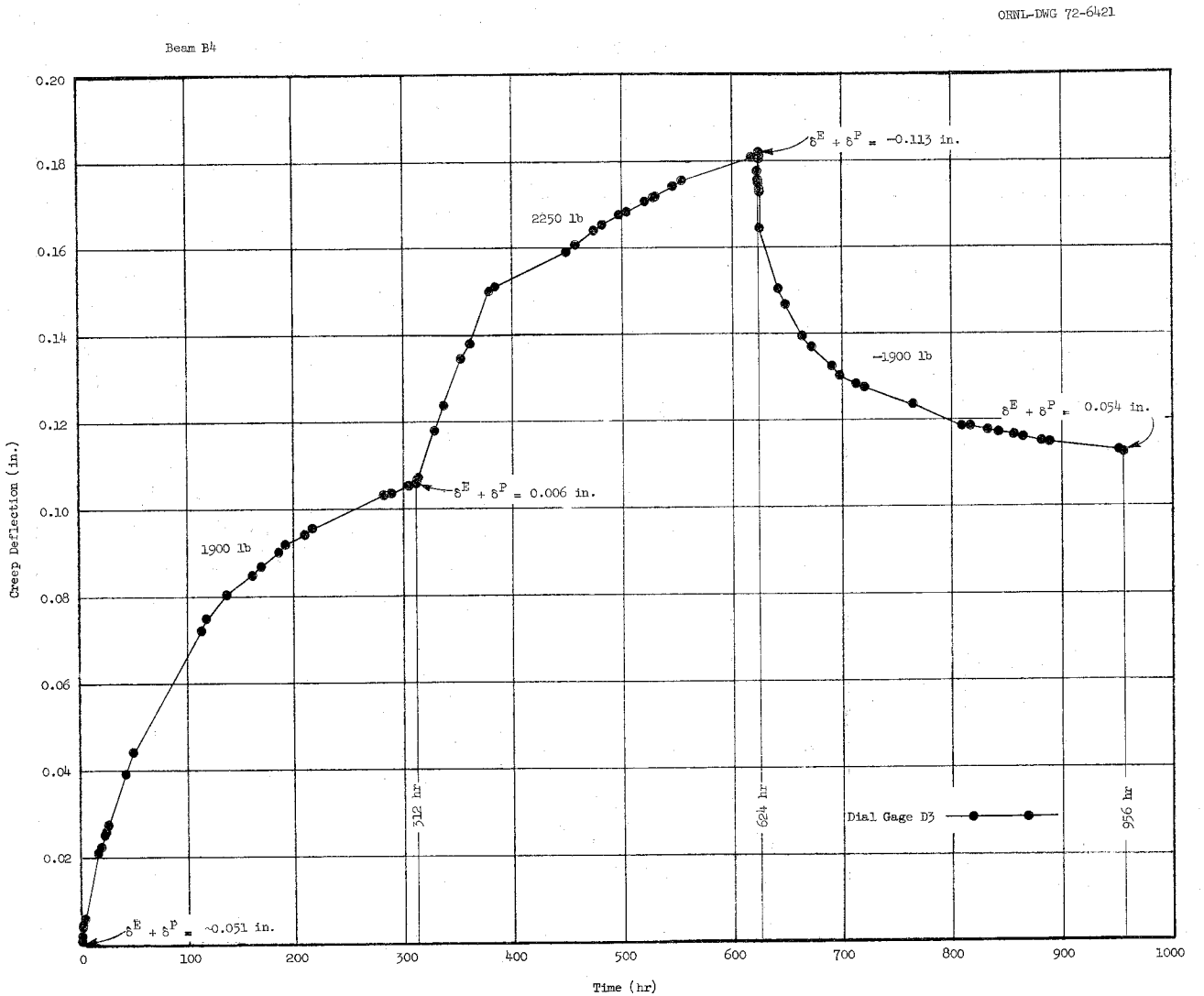

Fig. 5.3. Measured creep deflection versus time for center of beam B4.

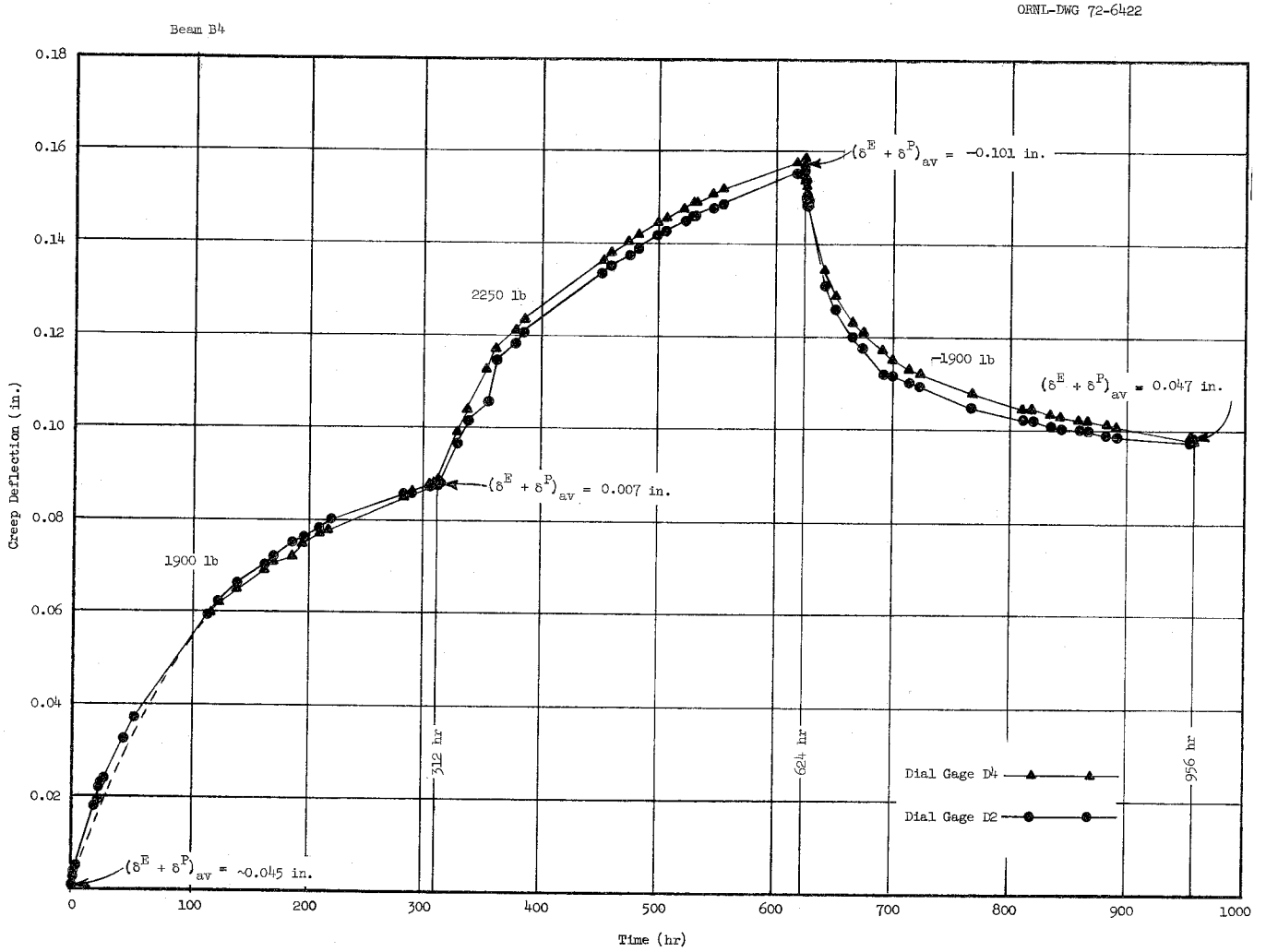

Fig. 5.4. Measured creep deflection versus time for points 4 in. from center of beam B4. Instantaneous elastic plus plastic deflection values given are average of those measured by dial gages D2 and D4.

ORNL-DWG 72-6423

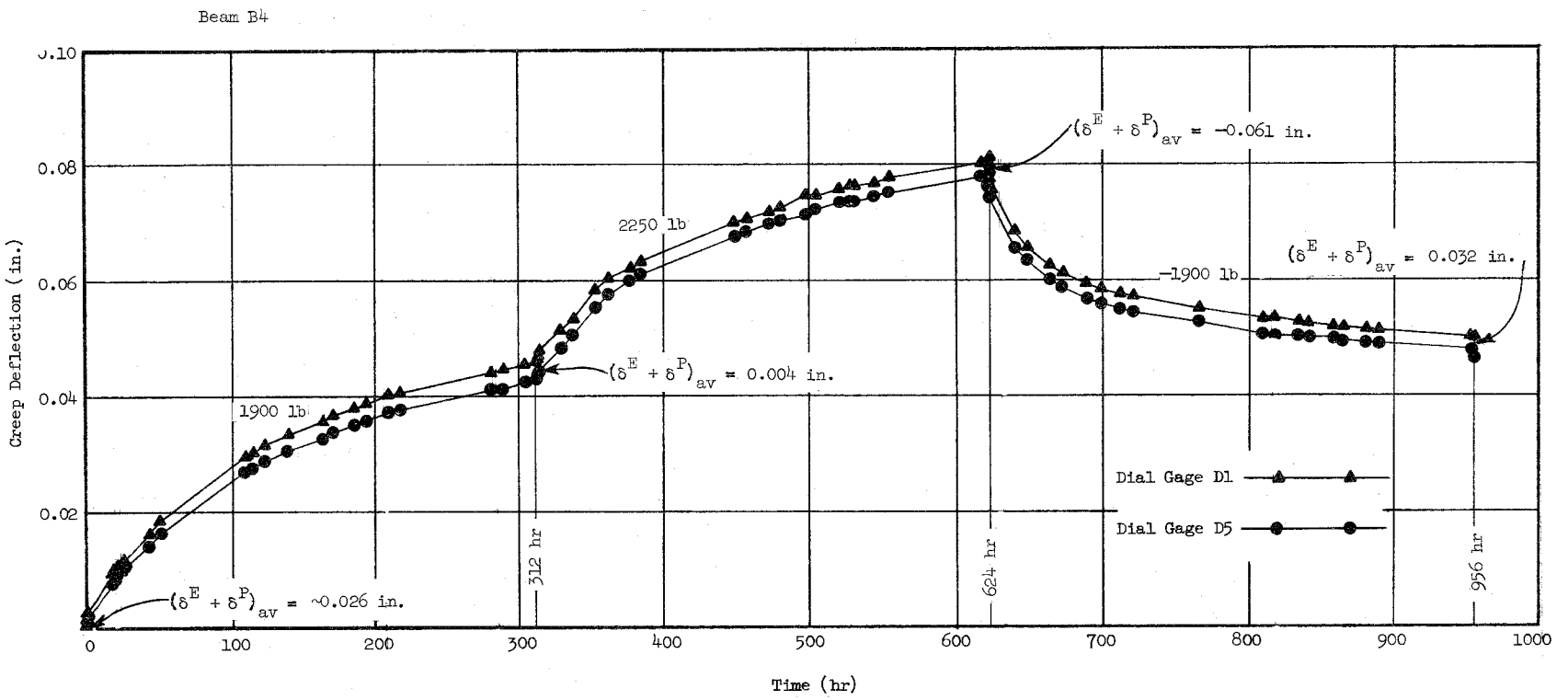

Fig. 5.5. Measured creep deflection versus time for points 8 in. from center of beam B4. Instantaneous elastic plus plastic deflection values given are average of those measured by dial gages D1 and D5.

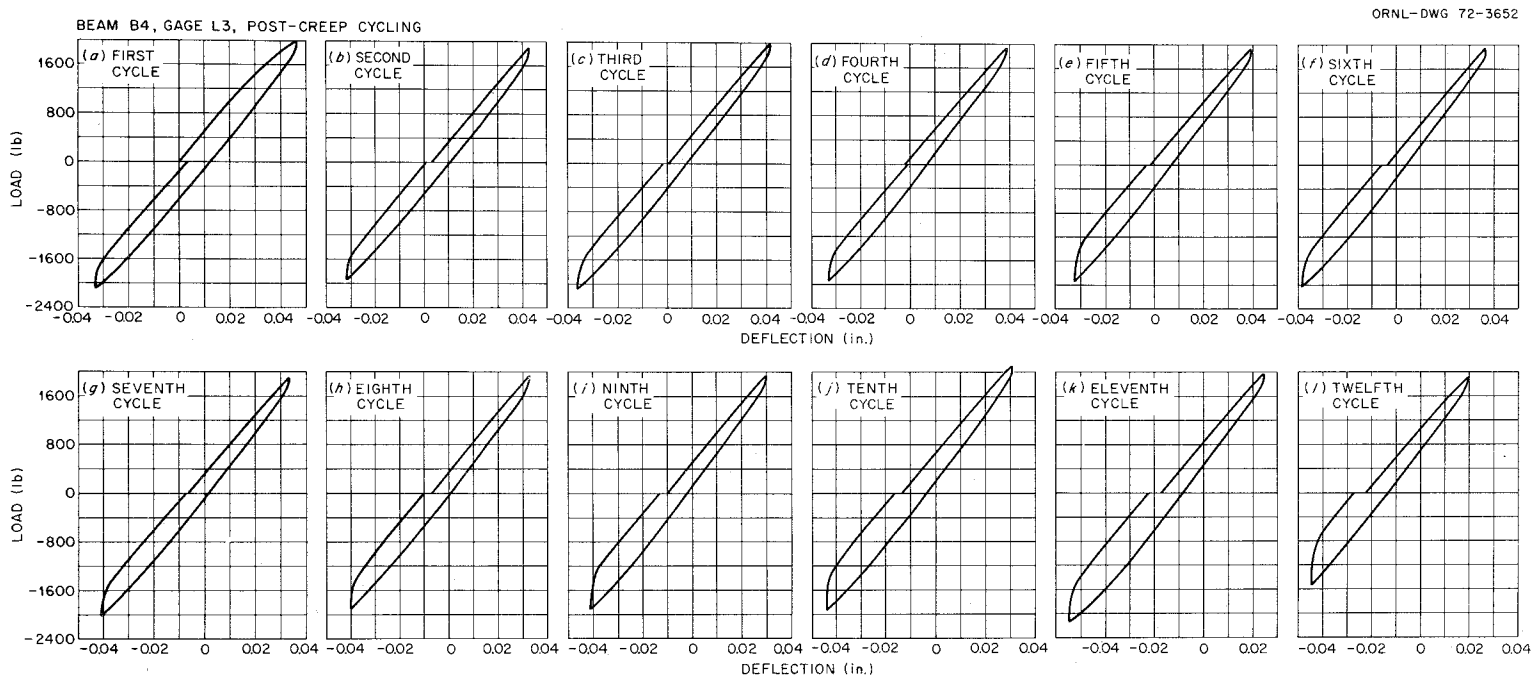

Fig. 5.6. Center deflection of beam B4 for the 12 postcreep short-time load cycles at 1200°F.

Table 5.2. Maximum and minimum measured loads in postcreep cyclic test on beam B4

Cycle	P_{max} (lb)	P_{min} (lb)
1	2020 (6.3)[a]	−2075 (9.2)
2	1910 (0.5)	−1940 (2.1)
3	1965 (3.4)	−2070 (8.9)
4	1935 (1.8)	−1915 (0.8)
5	1925 (1.3)	−1935 (1.8)
6	1935 (1.8)	−2010 (5.8)
7	1890 (−0.5)	−2005 (5.5)
8	1935 (1.8)	−1910 (0.5)
9	1935 (1.8)	−1920 (1.1)
10	2090 (10.0)	−1945 (2.4)
11	1955 (2.9)	−2135 (12.4)
12	1915 (0.8)	−1535 (−19.2)

[a]Numbers in parentheses denote the percentage that the measured load was over, or under, the specified levels of ±1900 lb.

behavior of the beam. If it is, we might reason that the behavior is the result of some sort of difference in hardening that has been accumulated in the positive and negative portions of the loading cycle. On the other hand, we have observed that our control was a little more sluggish in the negative part of the load cycle than in the positive part. In other words, slightly more time was expended in reversing the deflection rate at the lower end of the cycle than at the upper end. This could possibly result in some additional time-dependent deflection being accumulated in the negative portion of the cycle relative to that accumulated in the positive portion.* In any event, more test data will be necessary before too much significance can be placed on the observed differences. Modifications that have been made to the control system will provide identical control of positive and negative loadings in future beam tests.

*A counterpoint is that the same time delay in changing the deflection rate was observed in previous cyclic tests, but an effect on the cyclic curves was not apparent.

5.1.2. Cyclic stress-strain data at 1200°F for analyzing beams B3 and B4

As reported previously, we made arrangements with Southern Research Institute in Birmingham, Alabama, to perform a number of uniaxial cyclic stress-strain tests on both the preliminary heat and the reference heat of type 304 stainless steel. These curves will be used for analyzing the various structures, including beams, that are being tested as a part of the ORNL High-Temperature Design Methods Program. The test matrix for the preliminary heat (beams B3 and B4) was given in the previous progress report.[20] Preliminary results from three tests performed at the standard strain rate of 0.005/min and a total strain range of 2% have been obtained from SRI and are presented here. These results are the basis for the stress-strain data which should be used for analyzing the elastic-plastic behavior of beams B3 and B4. The specimens were taken from the same plate as were the beams, and the pretest heat treatment used for the specimens was essentially the same as used for the beams.

A typical cyclic stress-strain curve is shown in Fig. 5.7. An optical extensometer in the axial direction was used for both measurement and control in the SRI tests. The strain control was much closer to ±1% than is indicated in Fig. 5.7. This is because the actual loop tips were slightly rounded due to the time delay required for reversing the strain rate. In drawing the final curves, the straight-line portions of the unloading curves were extrapolated back to the loading curves to obtain the sharp tips shown.

To perform analyses in accordance with the procedures for inelastic analyses that have been recommended by ORNL,[21] the initial loading curve and the tenth cycle curve are required. These are shown in Fig. 5.8 for the three duplicate SRI tests. A single representative initial loading and tenth cycle stress-strain curve obtained from these SRI results is shown in Fig. 5.9. The bilinear equivalent curves, which were obtained in accordance with previous recommendations,[21] are also shown. The stress-strain curves in Fig. 5.9 should be used in elastic-plastic analyses of beams B3 and B4.

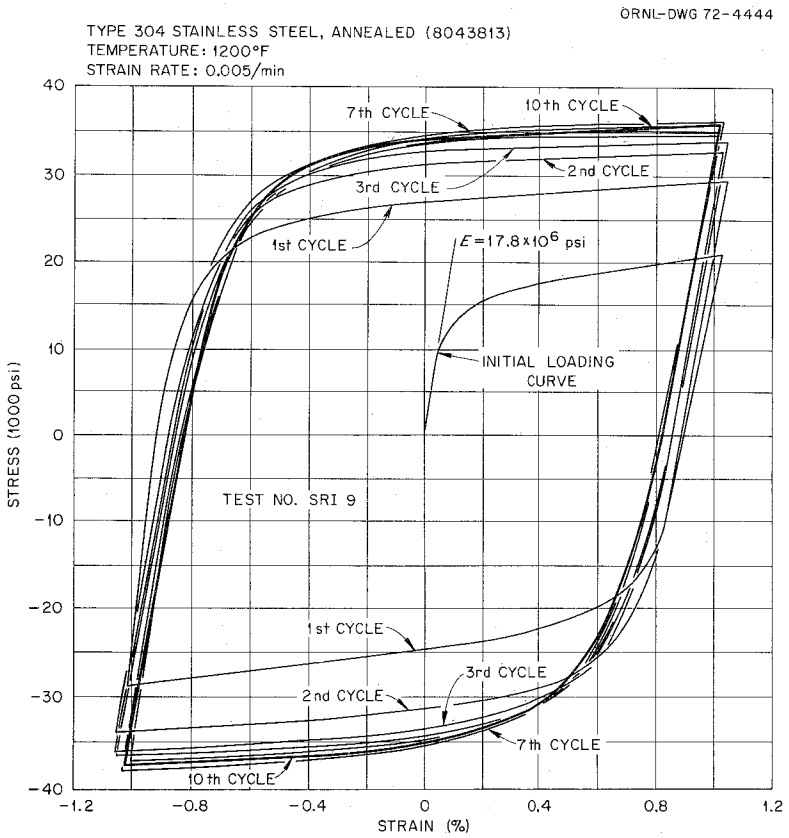

Fig. 5.7. Typical uniaxial cyclic stress-strain curve for type 304 stainless steel (heat 8043813) at 1200°F (from Southern Research Institute test no. 9).

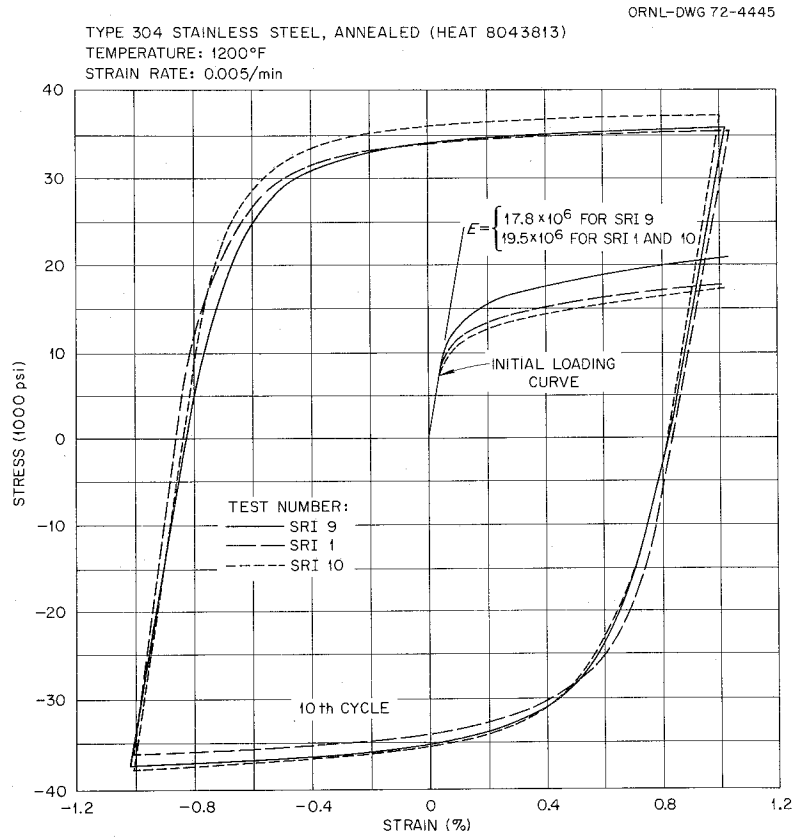

Fig. 5.8. Initial loading and tenth cycle stress-strain curves from SRI test nos. 1, 9, and 10.

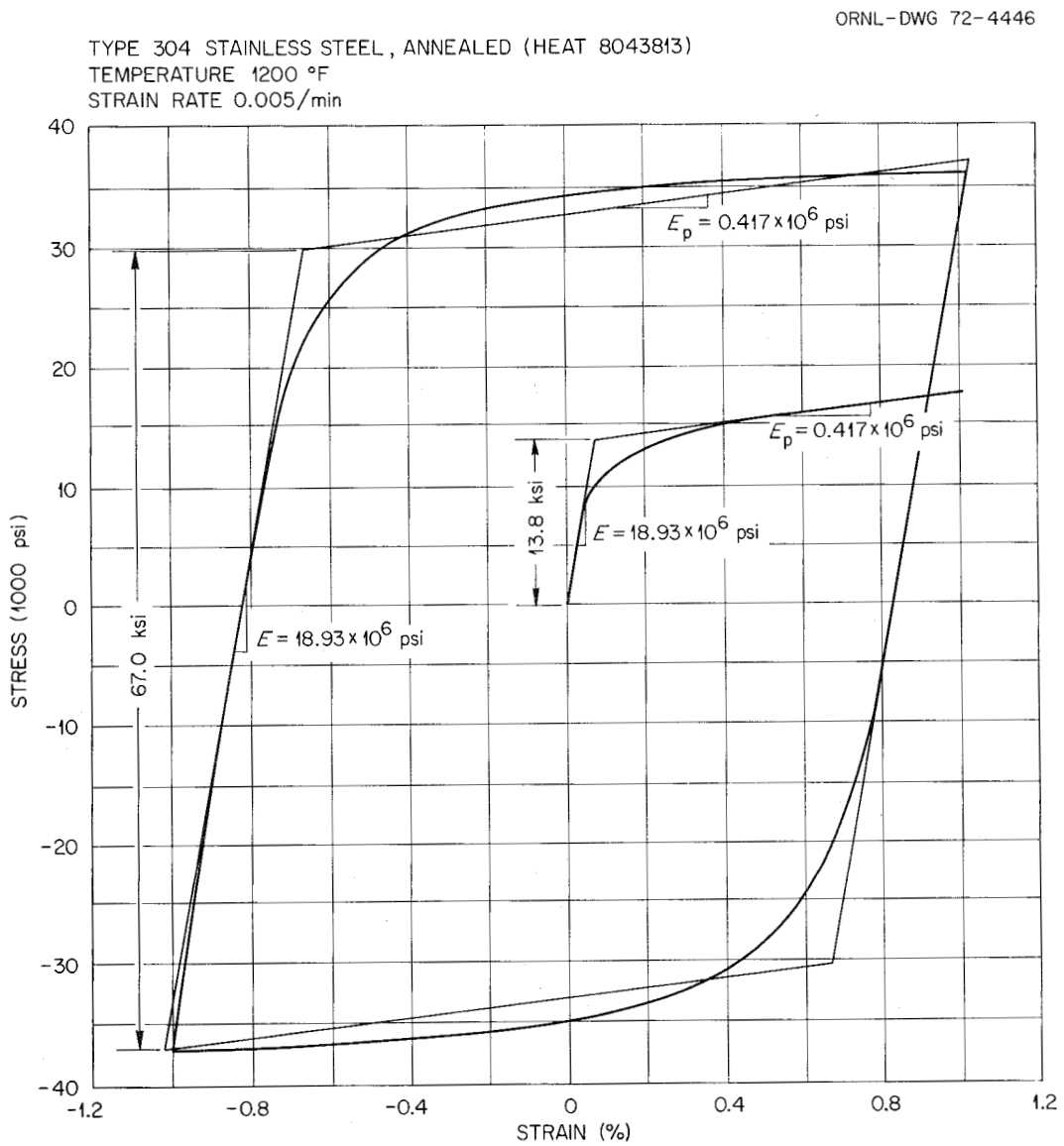

Fig. 5.9. Representative initial loading and tenth cycle stress-strain curves, and their bilinear equivalents, for type 304 stainless steel (heat 8043813) at 1200°F.

5.1.3. Beam test facility modifications

Following the test of beam B4, four significant modifications were made to the beam test facility. Two of these improvements were aimed at obtaining better temperature control, both over the beam surface and with time. The importance of very close temperature control is emphasized by the fact that a temperature variation of just 10°F at 1200°F can produce a 20 to 24% change in total creep strain (at the end of 300 hours) for stress levels ranging from 12,000 psi to 8,000 psi.* These are the stress levels at which beams B3 and B4 were tested.

The furnace heater mounts were modified to permit small manual adjustments to be remotely made to the heater positions throughout a test. This will help to eliminate the temperature variation with time as well as over the beam surface. Secondly, since future beam tests on the reference material will be conducted at 1100°F and below, the upper limit of the temperature controller range has been reduced from 2000°F to 1200°F. This will provide tighter control at 1100°F.

The third change was in the load control system, which has now been modified by the addition of a servo-valve in the hydraulic system that supplies oil to and from the double-acting hydraulic loading ram. This servo-amplifier-controlled valve is used in conjunction with a function generator to apply cyclic loadings, or deflections, with a variety of wave shapes. The modified system has been checked out and provides excellent control. For the next two high-temperature beam tests, beams B5 and B6, a sinusoidal load waveform will be used for the short-time cyclic loadings and load changes. The period of the sine wave will be 2 minutes and will produce strain rates in the beam of the order of 0.005/min.

Finally, the LVDT's used in the previous beam tests have been replaced with DCDT's. These direct current devices contain built-in amplifiers, thus eliminating the need for an external carrier amplifier system with its attendant drift problems.

Testing of beam B5 will begin early in May, and the beam B6 test is scheduled to begin in mid-June. Details of future tests will depend, in part, upon the results from these first two reference heat beams.

---

*These numbers are based on the creep equations for type 304 stainless steel currently given in the LMFBR Materials Handbook.

5.2. Pipe Thermal Ratchetting Tests

A. G. Grindell
H. C. Young

The Quality Assurance Program Plan[22] for the Thermal Transient Test Facility[23] was completed. The mechanical and structural and the thermal hydraulic studies portions of the design are approximately 80% complete.

Two modifications were made to the layout which will (1) permit possible installation of another flow path parallel to the present path to accommodate a second test piece, and (2) provide for the near-isothermal operation of the sodium flow control valve during thermal transient operation of the facility. As indicated in Fig. 5.10, the source and storage tanks and the piping (pipe nest) needed for the temperature-graded sodium would be common to both test pieces. However, each test piece would require separate sodium control valves, orifice runs, and thermal capacitance tanks. Presently two capped tees are provided to accommodate a future installation of a second flow path.

Conceptual schemes to eliminate or reduce the thermal shock to the sodium flow control valve during the thermal transient were studied. The sodium freeze valve was rejected because of the difficulties associated with timing the quick release of the sodium at the initiation of the thermal transient and with stopping the flowing sodium in positive fashion at the termination of the transient. It was decided to install a thermal capacitance tank just upstream of the sodium valve. This tank will contain a sufficiently large volume of sodium at control valve temperature to permit performing the thermal transient operation with the valve practically isothermal. The tank will be approximately 1-ft in diameter, approximately 15 ft long, and will be filled with stainless steel Raschig rings. With this arrangement, there will be very little mixing with the ingressing thermal transient sodium, and the long slender tank will discharge nearly isothermal stored sodium to the flow control valve.

Originally, we had planned to reduce the sodium pressure[24] after each thermal transient to aid making strain measurements of the test piece and to permit recharging the source tank with sodium from the storage tank. Although we still plan to reduce sodium pressure at least during initial

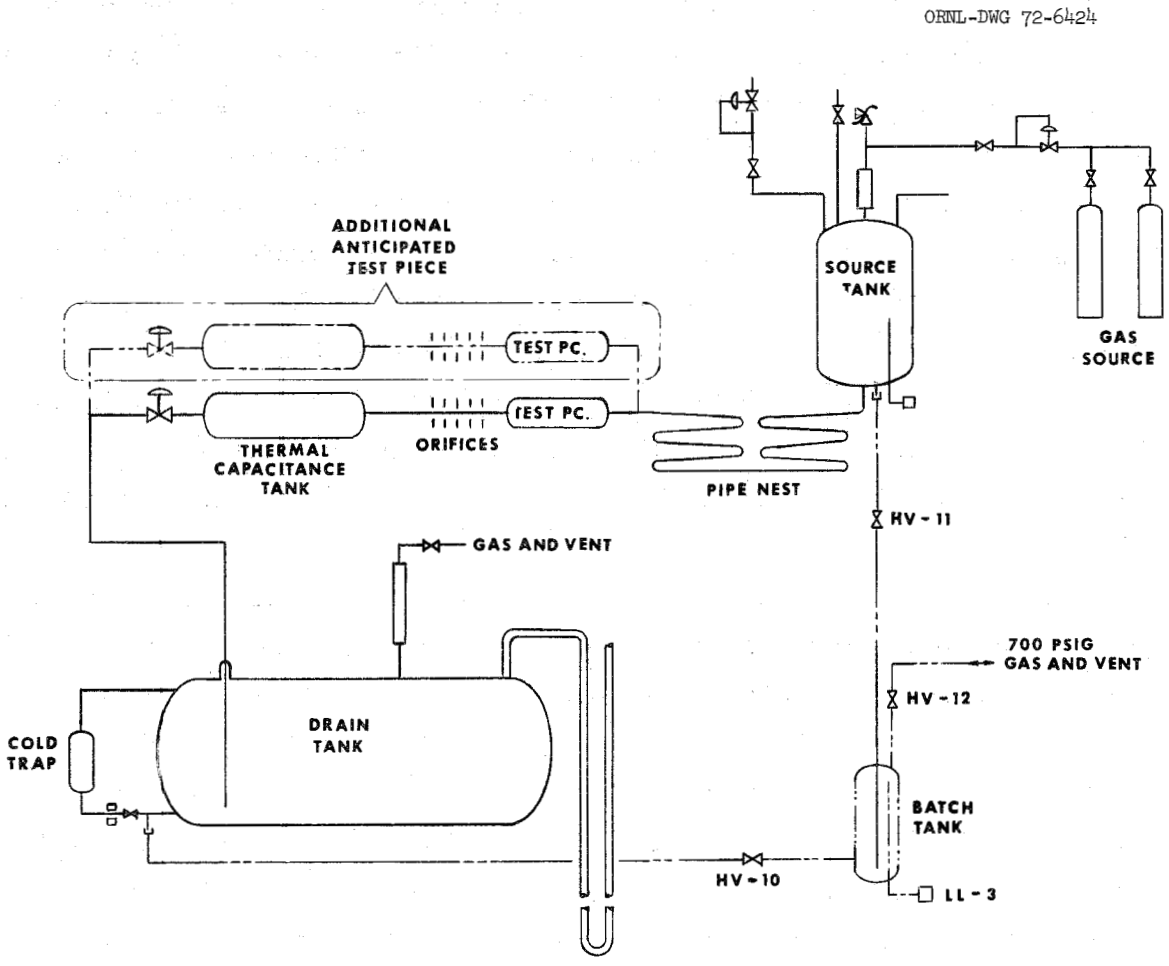

Fig. 5.10. Schematic of the thermal transient test facility. Modified to show thermal capacitance tank and parallel sodium flow path to accommodate anticipated second test piece.

ratchetting tests, we are preparing to install a batch tank which will permit recharging the source tank without reducing the sodium pressure in the test piece.

Although the mechanical design of the pipe nest is complete, the method of controlling the temperature gradient of the sodium in the pipe nest is still under study. Starting with sodium at 800°F in the source tank, the temperature will decrease to 744°F at the rate of 2°F per ft in a 28-ft pipe run. It will rise to 1024°F at the rate of 7°F per ft in a 40-ft pipe run, and finally it will reach 1100°F at the rate of 4°F per ft in a pipe run of 20 ft.* Prior to modifying the existing sodium test facility, a portion of the existing facility will be used in a test to obtain design information on the heater length, controls, and temperature instrumentation requirements to attain the specified thermal gradients.

The design of the orifice run is essentially complete. It will consist of five orifices, each about 3/4 in. in diameter, installed in 2 1/2-in.-diam pipe approximately 10 ft long and located just downstream of the test piece.*

A list of all the stainless steel requirements for the facility was compiled, and plans for obtaining the material in advance of the issuance of formal drawings are being formulated.

The test pieces will be made from piping which was fabricated from the reference heat of 304 stainless steel material. Because of surface roughness, the original hot-rolled piping could not be ultrasonically inspected and was, therefore, not truly RDT material. Consequently, a quality assurance procedure was prepared to upgrade the machined pipe specimens to RDT standard M3-3T.

---

*These data are based on the test conditions for the initial pipe ratchetting test: a downshock of 30°F/sec for 10 sec with an internal pressure of 700 psi.[25]

5.3. Weldment Creep-Rupture Studies

W. J. McAfee
M. Richardson

5.3.1. Results of creep-rupture tests

Only one specimen was tested to completion during this reporting period, specimen no. 2A. One of the main purposes of this test was to gather further information on the behavior of an unwelded flat head to cylinder junction. It was decided that failed specimen no. 2 could be used as the vehicle for this test by simply replacing the ruptured lower half of the specimen with a new component and continuing the test.

This specimen no. 2A failed after 88 hours at pressure and temperature. The failure, as shown in Fig. 5.11, was similar to that of specimen no. 2, that is, a separation of flat head and cylinder. Since there was no possibility of interaction between the core and specimen in this test, and since the total test time was comparable, considering normal data scatter, to that of specimen no. 2, it was felt that the results of specimen no. 2 could be considered valid.

A preliminary comparison of some of the results obtained to date is shown in Fig. 5.12. Specimen nos. 1 and 3, as discussed previously,[26] failed by a longitudinal rupture in the cylinder. The data points for bar and plate material are uniaxial creep rupture data as reported in Chapter 6 of Ref. 26. The data for the weldment creep-rupture specimens (WCR) are based on the effective von Mises stress in the membrane section of the cylinder. All specimens, uniaxial and biaxial, underwent similar heat treatment prior to testing.

Postmortem dimensional inspection of specimen nos. 1 and 2 has been completed. The results for specimen no. 2 are shown in Fig. 5.13 where the average circumferential strain in the cylindrical section of the specimen is indicated. The strain curve is shown up to the point of rupture. The head was badly distorted and has not yet been inspected. The weld region underwent much less circumferential strain (~1/2%) than the base metal (2-3%). Note also that the scatterband for the data in the weld is generally slightly larger than that in the base metal. This is probably caused to some degree by the anisotropy associated with welds.

PHOTO 79445

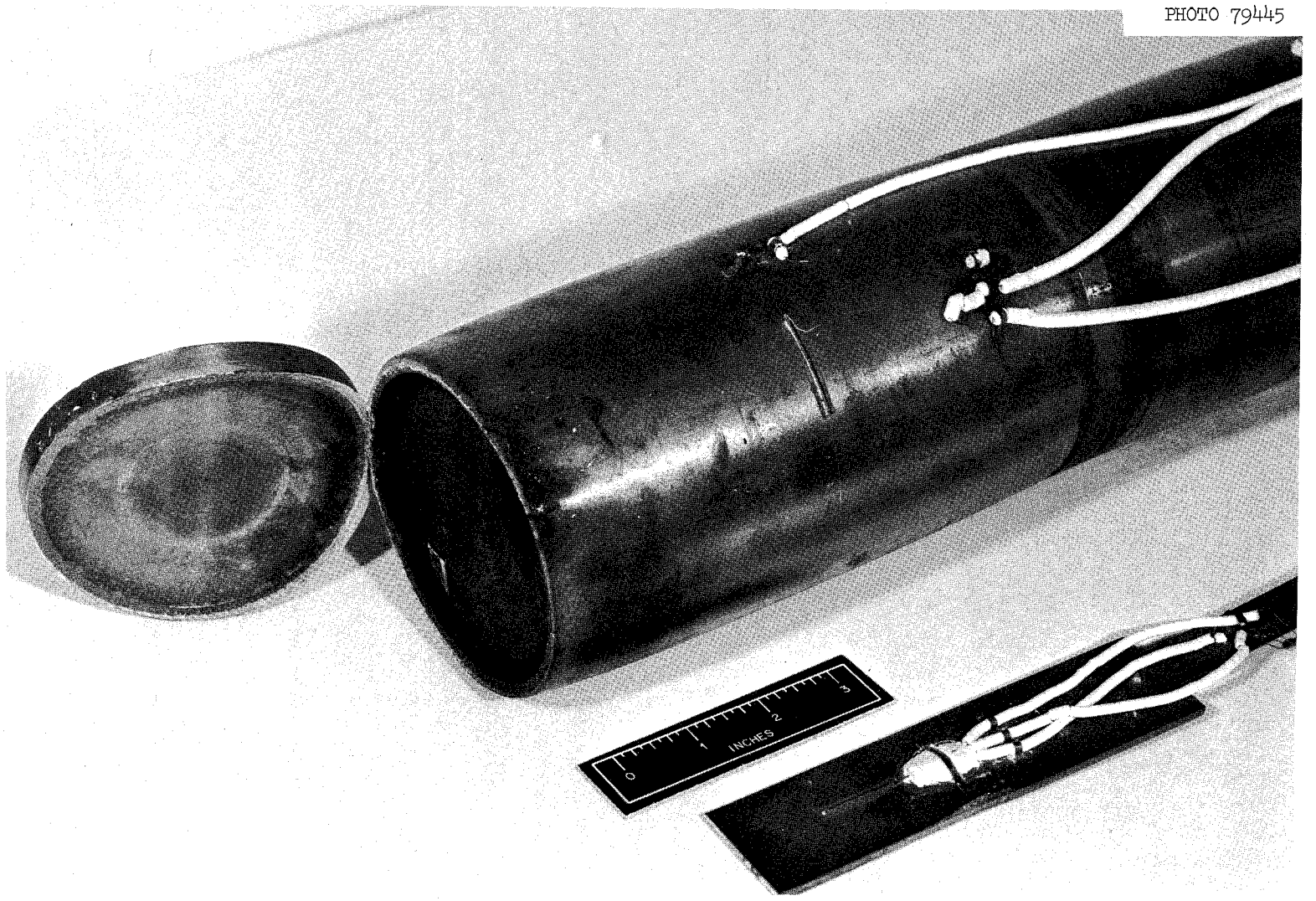

Fig. 5.11. End view of specimen no. 2A showing rupture opening and core.

ORNL-DWG 72-6425

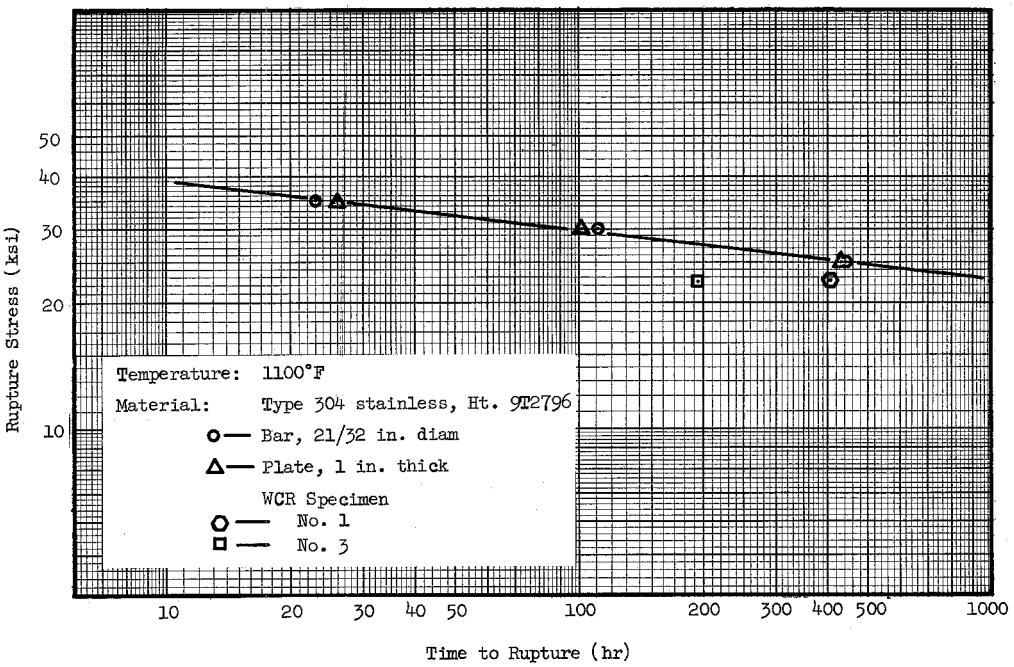

Fig. 5.12. Comparison of creep rupture data from uniaxial tests and WCR tests.

ORNL-DWG 72-6426

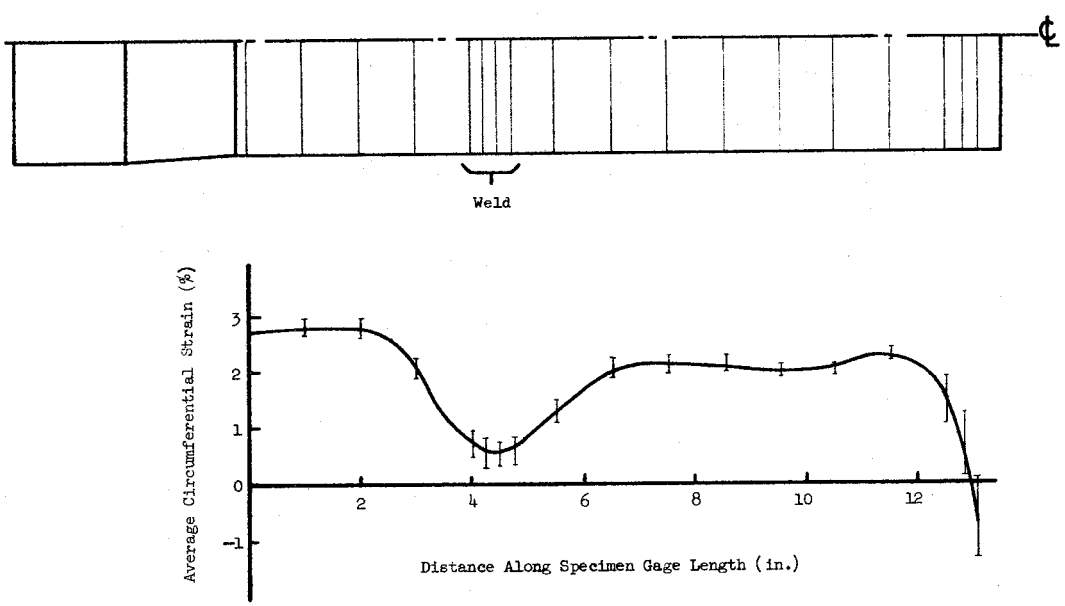

Fig. 5.13. Average circumferential strain profile for the cylindrical portion of WCR specimen no. 2.

The deformation behavior of specimen no. 1 is shown in Fig. 5.14. For the cylindrical portion of the specimen, change in radius versus gage length is shown for each of the six radii measured. These six radii and the nomenclature used are also indicated on the figure. Where the data lines are shown as interrupted, dimensional measurements could not be made due to the ruptured area of the specimen. The rupture opening was between the C and D radii being generally about 10° off the C radius. The head deformation is shown as the average change in head height versus head radius. This was done because the head deformation was symmetrical, and the average data well represented the head profile. Specimen strains have not been calculated awaiting a complete evaluation of the data obtained.

5.3.2. Description of weld used in WCR tests

The weld type used in the first generation of WCR specimens was chosen to be representative of current (current at time of program initiation) thinking for FFTF pipe welds. It was thought that for type 304 stainless steel pipe type 308 stainless steel alloy weld rod and inert gas tungsten-arc welding would be used. The exact weld rod, that is, the additive elements or coatings, had not been decided upon at the time of finalization of WCR specimen design. It was thus decided to use the best 304-308 stainless weld available for the first generation of these specimens. The weld specification chosen was ORNL Welding Procedure Specification WPS-302 which, for the weld geometries used, is qualified to RDT F6-5 and is for the TIG welding process. These specifications require dye-penetrant and 100% radiographic inspection.

The weld geometry is of two types as shown in Fig. 5.15. The single-U geometry was used for only one weld, the plug to head weld of WCR specimen no. 3. The single-V geometry was used for all other welds including the specimen to cap closure weld.

Each specimen component, except core and closure cap, was annealed, using the reference anneal, prior to welding. No postwelding heat treatment was conducted as per present plans for FFTF pipe welds. However, the specimens were held at 1100°F (nominal) for approximately 24 hours prior

ORNL-DWG 72-6427

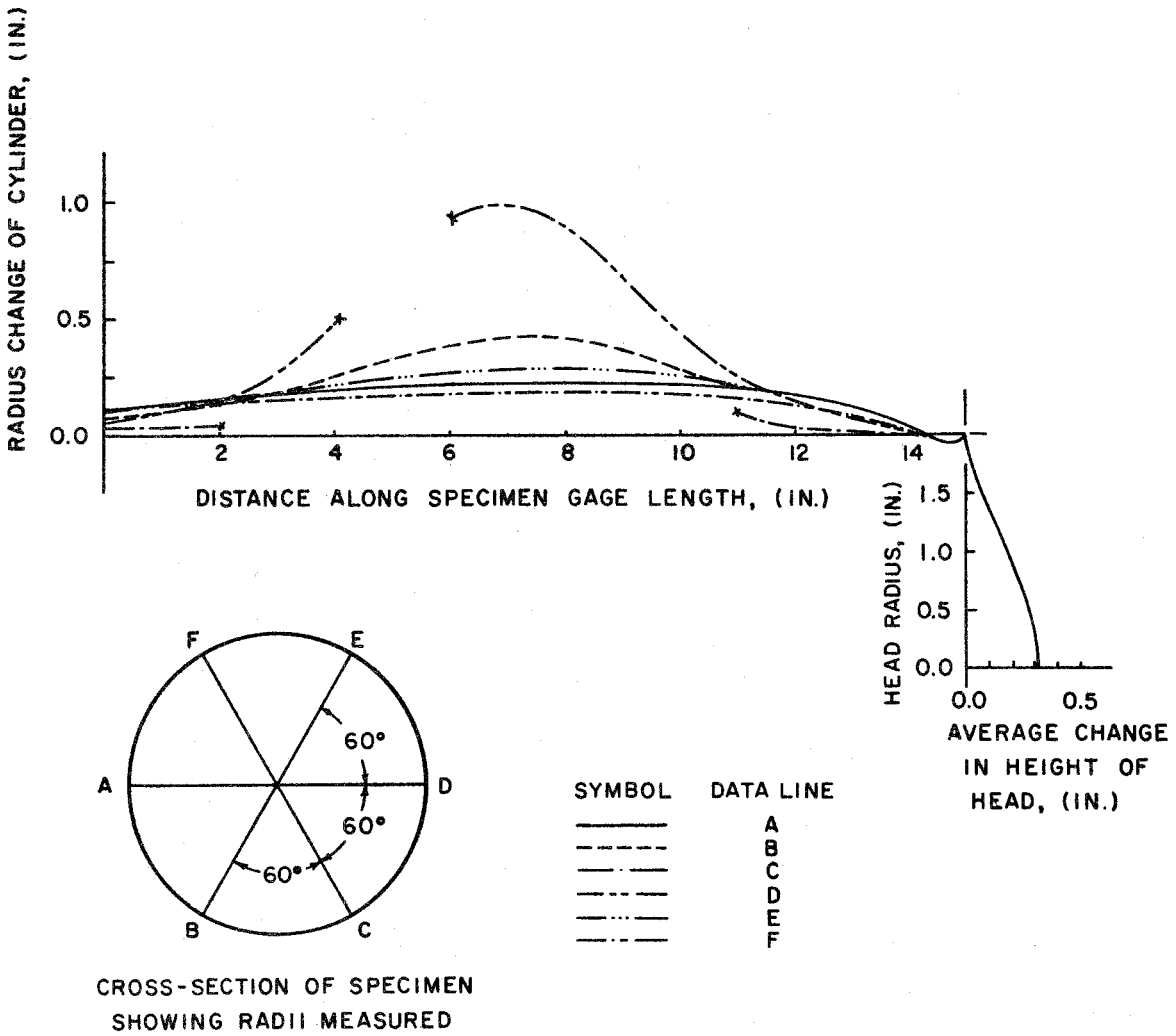

Fig. 5.14. Displacement behavior of cylinder and head portions of WCR specimen no. 1.

ORNL-DWG 72-6428

Groove Type	Groove Dimensions					Thickness
	B (deg)	G (deg)	RF (in.)	RO (in.)	R (in.)	(in.)
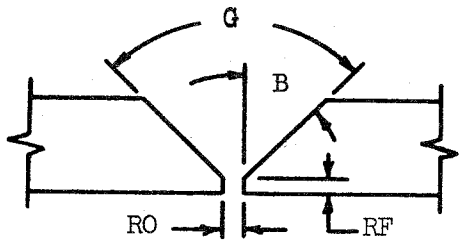 Single-V	45 ± 2.5	90 ± 5	0.010 ±0.005	$\frac{1}{16}{}^{+0}_{-\frac{1}{64}}$		0.100 to 0.500
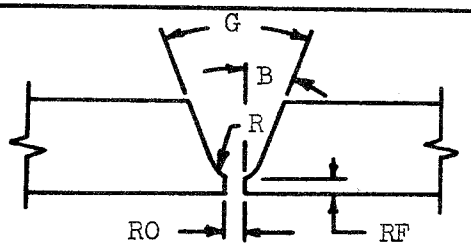 Single-U	20 ± 2.5	40 ± 5	0.062 +0.016 −0	$\frac{1}{16}{}^{+0}_{-\frac{1}{64}}$	0.094 +0.016 −0	0.375 to 1.0

Fig. 5.15. Weld geometries used for WCR specimens.

to load application. This was required to allow the specimen to fully reach thermal equilibrium and for the furnace temperature to stabilize.

For the second generation of WCR specimens, a reevaluation of weld type was made based on present knowledge of FFTF weld specifications. This review was in the form of discussions with personnel in the ORNL Metals and Ceramics Division who are currently involved in weld evaluation studies. The decision was made to use the same 304-308 stainless weld for the second generation of WCR specimens as was used for the first. This will allow more continuity between test series. In addition, M&C Division is to provide further support in the form of test welds on flat plate using the same process and heat of 308 weld rod as is being used for the WCR specimens. These test welds will be characterized (time-independent and short-term time-dependent mechanical properties, metallography, etc.) thus generating some data for elastic-plastic-creep analyses of welded specimen behavior as well as some additional baseline data for M&C Division's programs in weld evaluation. The welding of this second generation of specimens will be coordinated by M&C personnel. Presently, the specimens are in the machine shop in various stages of completion.

6. MATERIAL INVESTIGATIONS

R. W. Swindeman

6.1. Material Characterization

The short-time evaluation of the 5/8-in.-diam bar product of the reference heat of type 304 stainless steel (heat 9T2796) has been nearly completed. The comparison of ORNL chemistry for this material with the vendor ladle analysis and two other product forms is shown in Table 6.1. The carbon level determined at ORNL for the 5/8-in.-diam bar was more in line with the ladle analysis than was the 0.059% value reported by the vendor based on a check analysis.[27] The tensile properties before and after the standard 2000°F reannealing treatment were presented previously.[28] Some of these data are reported again in Table 6.2. The purpose is to

Table 6.1. Chemistry for type 304 stainless steel heat 9T2796

Element	Vendor ladle	ORNL			ASTM specification A-240, A-479
		1-in. plate	1-in. bar	5/8-in. bar	
Carbon	0.048	0.051	0.048	0.047	0.04 to 0.06
Manganese	1.22	1.37	1.34	1.22	2.00 max
Phosphorous	0.028	0.041	0.039	0.029	0.045 max
Sulfur	0.015			0.012	0.03 max
Silicon	0.48	0.40	0.50	0.47	1.00 max
Chromium	18.60	18.50	18.60	18.50	18 to 20
Nickel	9.70	9.87	10.1	9.58	8 to 12
Cobalt	0.18	0.10	0.10		
Molybdenum	0.32	0.30	0.30		
Columbium	0.003	0.002	0.002		
Titanium	0.010				
Boron					
Copper	0.24	0.20	0.20		
Nitrogen		0.31	0.030	0.031	

NOTE: All data weight %.

Table 6.2. Effect of heat treatment on the room temperature tensile properties and grain size of type 304 stainless steel heat 9T2796

Specimen no.	Product form	Condition[a]	0.2% yield[b] (ksi)	Ultimate tensile strength (ksi)	Elongation[b] 4 × diam (%)	Reduction in area (%)	ASTM grain size number
RP36	Plate	A240	29.8	82.0	84	80.9	1-3
RP51	Plate	A240	33.1	83.3	84	85.9	1-3
RP42	Plate	1800 annealed	26.6	84.6	86	81.7	1-3
RP44	Plate	1900 annealed	28.0	83.6	90	81.7	1-3
RP46	Plate	1950 annealed	26.8	83.6	92	83.4	1-3
RP49	Plate	2000 annealed	27.0	84.2	91	77.9	1-3
RP37	Plate	2000 annealed	25.6	80.2	90	78.5	1-3
RR7	1-in. bar	A479	31.3	83.6	85	82.0	1-5
RR14	1-in. bar	2000 annealed	26.2				1-5
RR20	5/8-in. bar	A479	43.6	91.4	77	83.0	3-5
RR48	5/8-in. bar	1850 annealed	32.5	88.0			2-4
RR21	5/8-in. bar	2000 annealed	28.8	86.8	85	84.0	1-3

[a]Hot rolled and pickled for A240 and A479 condition.

[b]Nominal strain rate was 0.05 min^{-1}.

show the influence of the reannealing temperature. No detectable change in the grain size of the 1-in. plate was noted for reanneals in the temperature range from 1800 to 2000°F. The grain size, already coarse, remained the same. Photomicrographs are shown in Figs. 6.1(A) and 6.1(B) for the A-240 and reannealed conditions. On the other hand, some loss in the yield strength was observed after reannealing, and we feel that this loss was due to the elimination of slight cold work.

The 1-in.-diam bar in the A-479 condition exhibited a mixed grain size. Some areas were as fine as ASTM No. 5, while other areas were as coarse as No. 1. Even after reannealing we found some relatively fine-grained areas. The tensile yield data for the 1-in.-diam bar were very similar to data obtained on plate for both the A-479 and the reannealed conditions.

The 5/8-in.-diam bar, in the A-479 condition, was fine-grained and quite strong. This was probably due to a large amount of cold work in addition to the fine-grain size. Reannealing at 1850°F eliminated all traces of cold work and increased the grain size. The standard 2000°F reanneal produced a further increase in grain size and a corresponding drop in yield strength.

For the most part, the microstructures for all three product forms were fairly clean. Although it is not evident in Figs. 6.1(A) and 6.1(B), the 1-in. plate showed minor compositional variation in the thickness direction. This conclusion was based on the response to etching. Stringers of slag and delta-ferrite were observed also in the plane perpendicular to the thickness. All of the above observations are probably typical of type 304 stainless steel plate.

Although the creep behavior of bar and plate is discussed in Section 6.2, the rupture studies to 1000 hr fall within the scope of characterization. A data summary is contained in Fig. 6.2. The rupture strength of the bar and plate was remarkably similar. Included in the figure are curves drawn through the minimum expected rupture strengths for type 304 stainless steel. These data were obtained from Table 16 of the ASME Pressure Vessel Code Case 1331-5. The reference heat (9T2796) exceeds the minimum expected strength, but not by much. In Figs. 6.3 and 6.4, comparisons of the rupture lives at 35 and 30 ksi are made for a number of

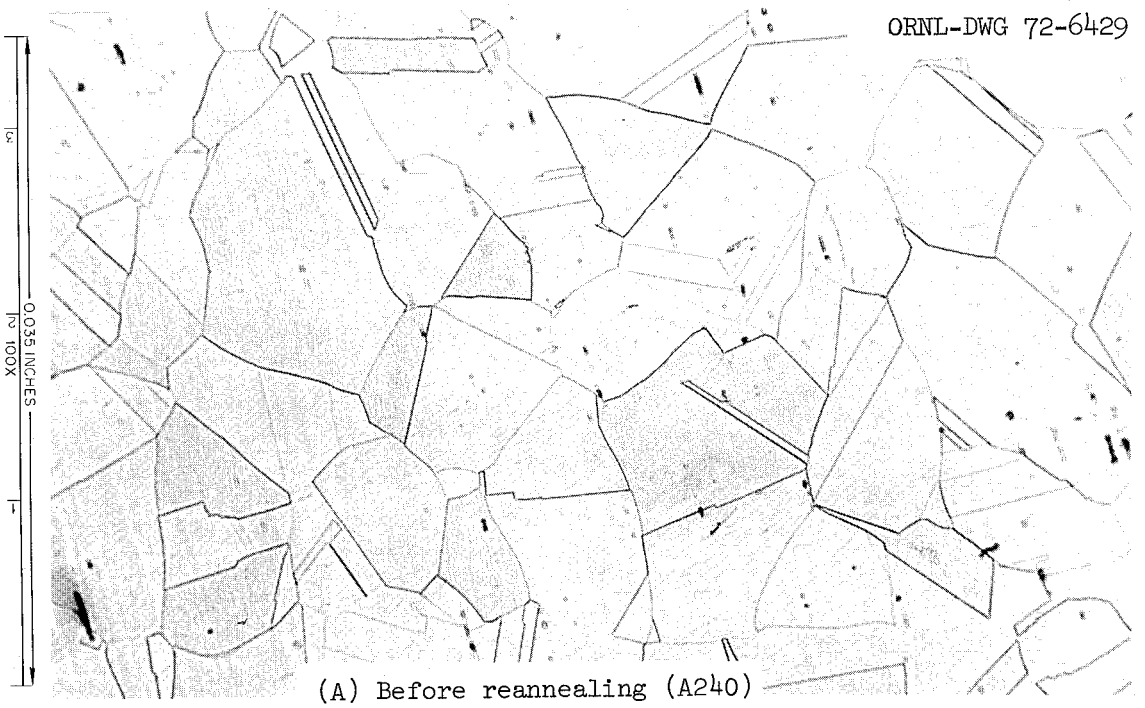

(A) Before reannealing (A240)

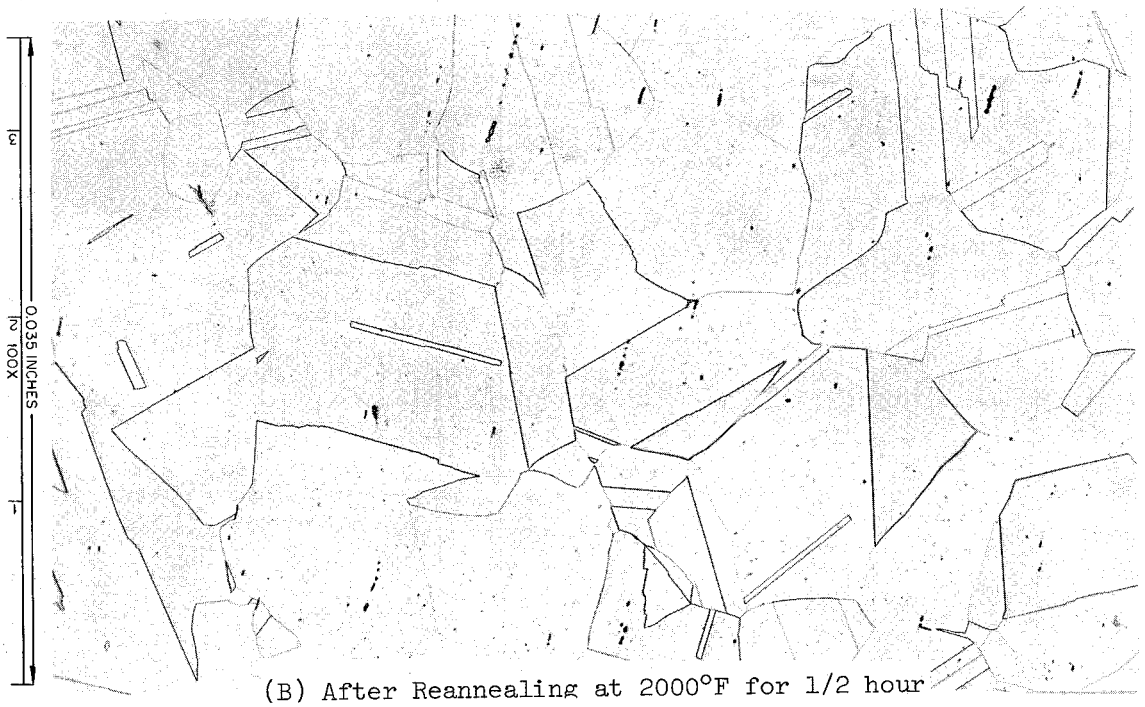

(B) After Reannealing at 2000°F for 1/2 hour

Fig. 6.1. Comparison of the microstructure of 1-in. plate of type 304 stainless steel (heat 9T2796) before and after reannealing (1/2 hour at 2000°F). Etchant: glyceria regia. Original magnification: 100X.

ORNL-DWG 72-6430

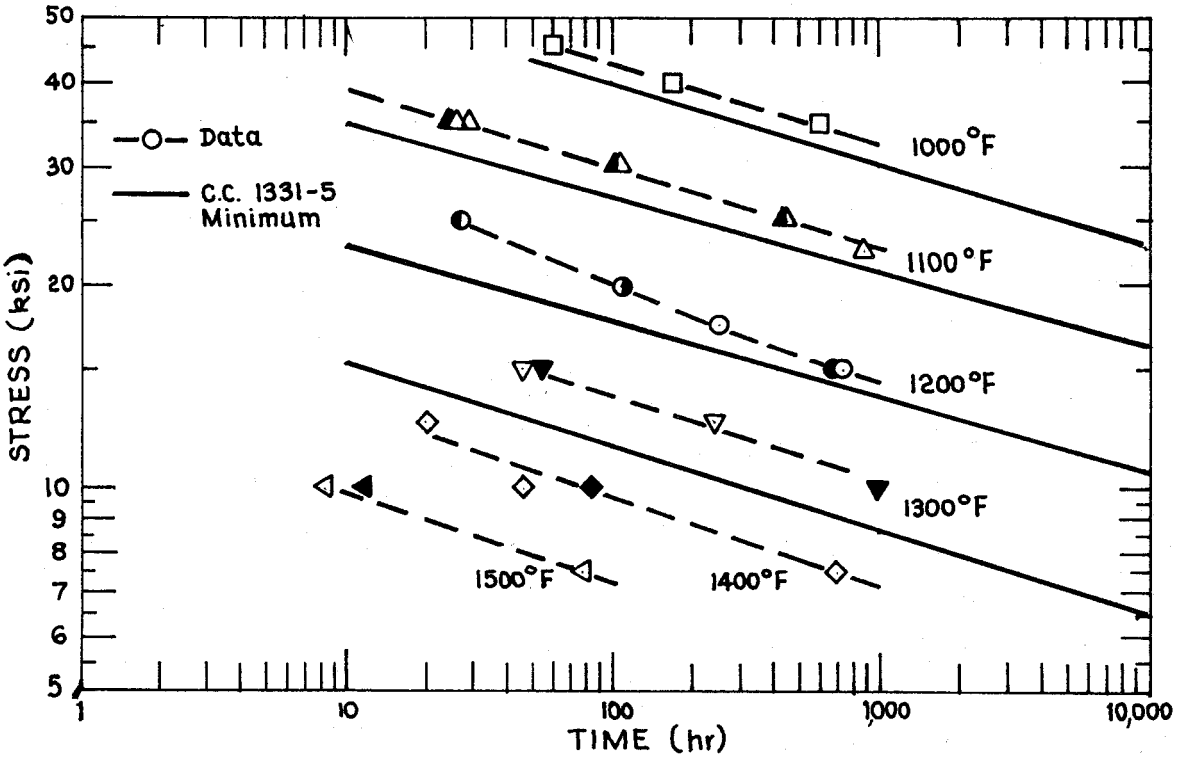

Fig. 6.2. Comparison of stress rupture data for type 304 stainless steel (heat 9T2796) with minimum values tabulated in ASME Code Case 1331-5. Open symbols are for plate, and closed symbols are for bar. All data obtained on reannealed specimens (1/2 hr at 2000°F).

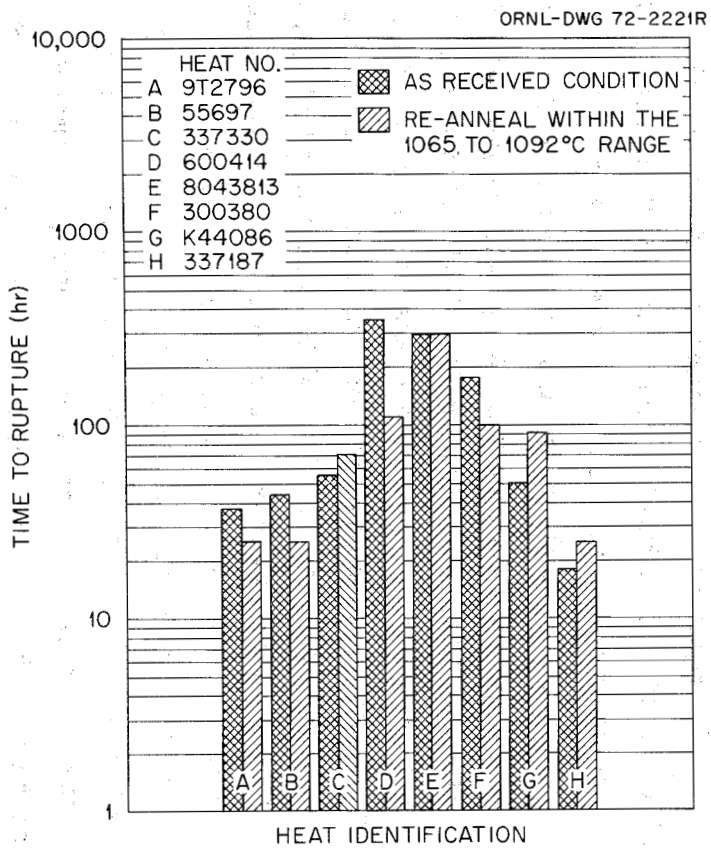

Fig. 6.3. Comparison of the times to rupture for several heats of type 304 stainless steel tested at 1100°F and 35,000 psi.

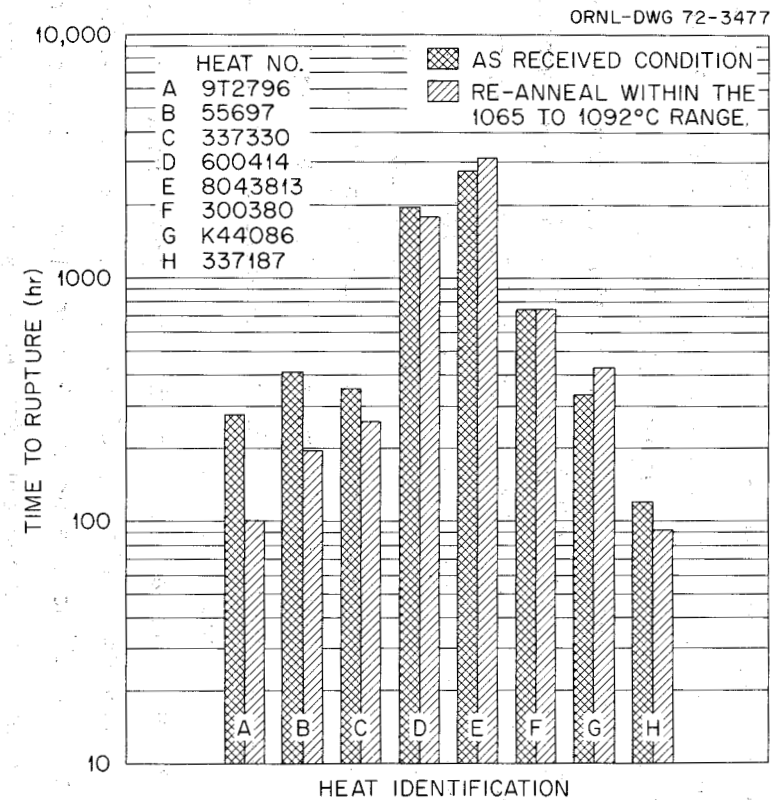

Fig. 6.4. Comparison of the times to rupture for several heats of type 304 stainless steel tested at 1100°F and 30,000 psi.

heats of type 304 stainless steel in two thermo-mechanical conditions and at 1100°F. These data have been generated at ORNL under another program.[29] The reference heat, 9T2796, was again among the weakest. Possibly, poor ductility contributes to this. The material tended to go into third stage creep quite early and fractured at a low strain relative to a strong heat such as the preliminary heat (8043813). In Fig. 6.5, we compare the ductilities of these two heats at 1000, 1100, and 1200°F. Although not relevant to LMFBR conditions, the ductility of heat 9T2796 at temperatures in excess of 1200°F was quite good. We also saw anisotropy in the plate product form. The deformation in the width direction of the plate was consistently less than that in thickness direction. Stated in another way, specimens tested in the longitudinal direction, the rolling direction, developed oval cross sections.

Another area of material characterization into which we are moving deals with the structural stability of the reference heat (9T2796). Several specimens were sent to the University of Cincinnati for inclusion in their light and electron microscopy studies on austenitic stainless steels.[30] A small in-house effort is beginning also. We obtained electron transmission photographs of the preliminary heat (8043813) earlier and these proved interesting. Examples are shown in Figs. 6.6, 6.7, and 6.8 which were taken from specimens tested in creep. Figure 6.6 represents the structure developed after testing 1642 hr at 20,000 psi and 1200°F (specimen P-3). Figure 6.7 represents 5033 hr at 17,000 psi plus an additional 2207 hr at 20,000 psi (specimen P-5). Both specimens exhibited a reasonably well-defined substructure. A coarse dispersion of $M_{23}C_6$ carbides developed throughout the matrix and on grain and twin boundaries. Figure 6.8 was obtained from specimen P-9, which was tested at 30,000 psi and 1100°F for 3184 hr. Some regions of the specimen, such as shown in the figure, developed a substructure. More significant, perhaps, were the clusters of very fine precipitates ($M_{23}C_6$) which formed. A question to be resolved is whether these precipitates contributed to creep strength by immobilizing strain-induced dislocations or signify a time-dependent decrease in strength via the loss of solid solution hardening.[31,32]

ORNL-DWG 72-6431

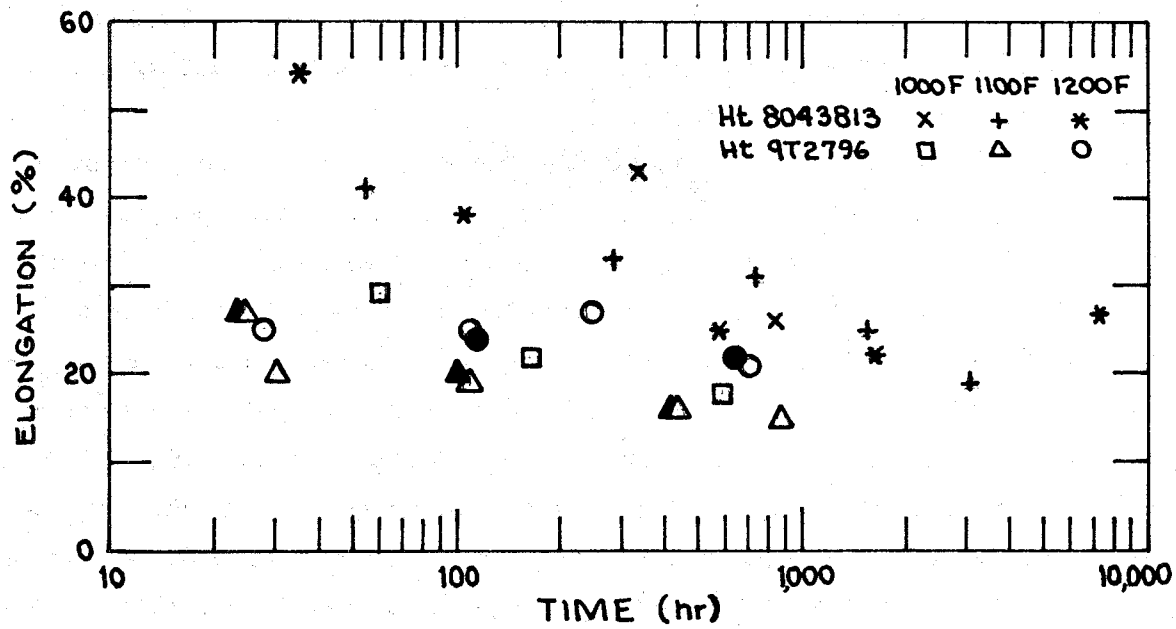

Fig. 6.5. Stress rupture ductilities for two heats of type 304 stainless steel at 1000, 1100, and 1200°F. Heat 8043813 was reannealed at 1950°F and heat 9T2796 was reannealed at 2000°F. Open symbols are for plate, and closed symbols are for bar.

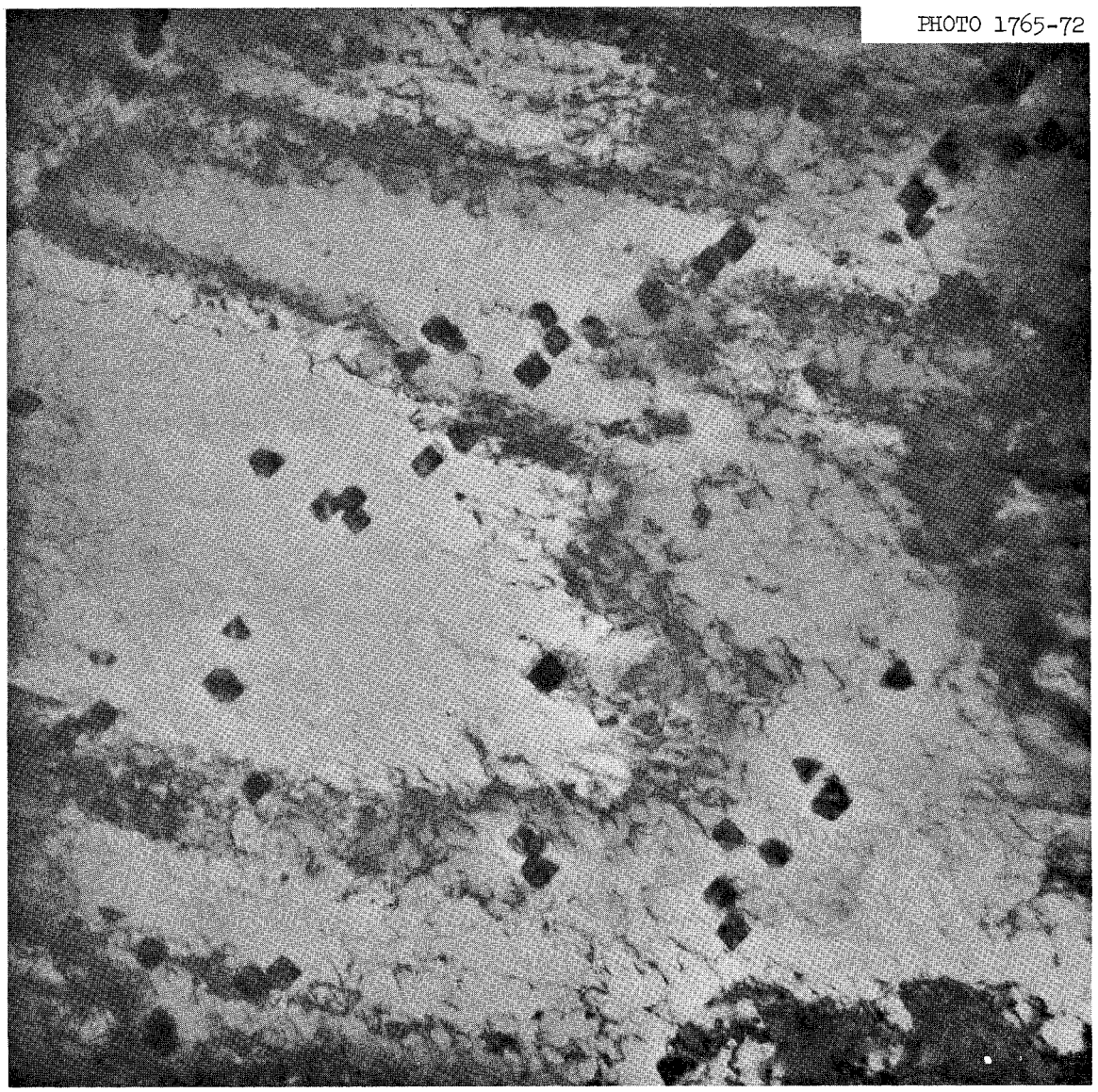

Fig. 6.6. Structure developed in type 304 stainless steel after 1642 hours at 1200°F and 20,000 psi. Heat 8043813 (specimen P3). The large particles are $M_{23}C_6$ carbides. Original magnification: 25,000X.

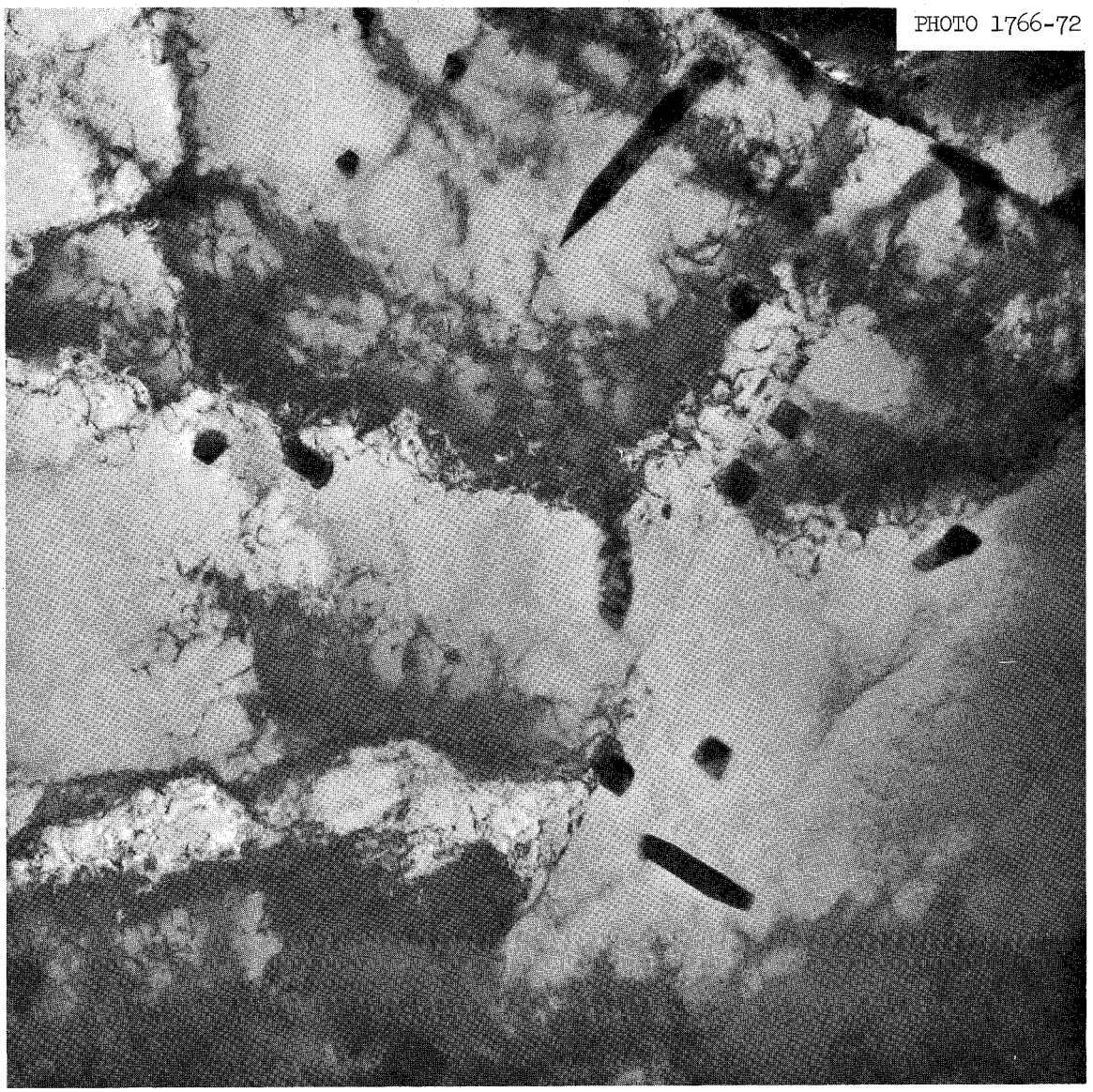

Fig. 6.7. Structure developed in type 304 stainless steel after 7220 hours at 1200°F. The first 5033 hours were at 17,000 psi and the remainder at 20,000 psi. The large particles are $M_{23}C_6$ carbides. Heat 8043813 (specimen P5). Original magnification: 25,000X.

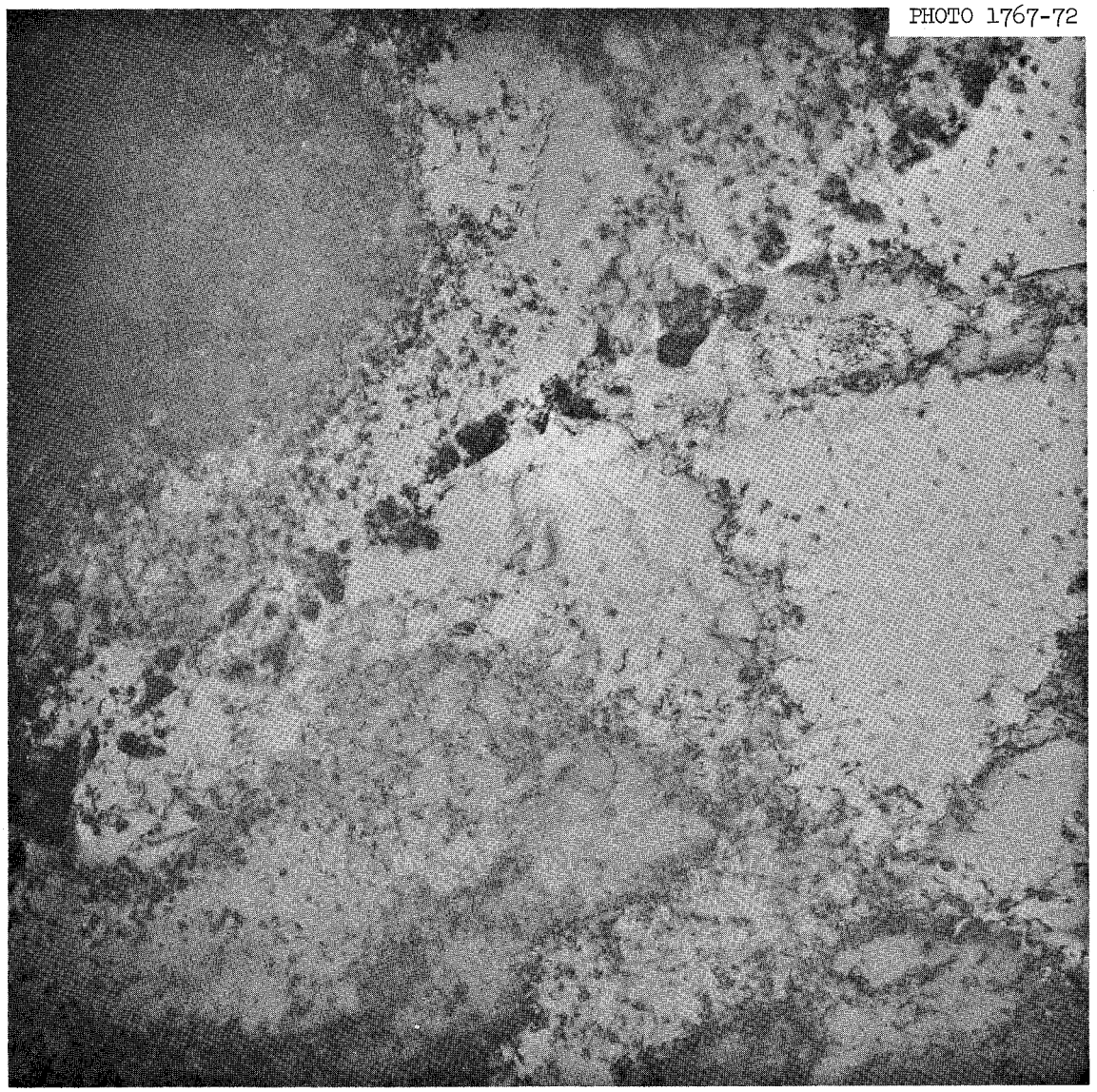

Fig. 6.8. Structure developed in type 304 stainless steel after 3184 hours at 1100°F and 30,000 psi. Heat 8043813 (specimen P9). The fine particles are $M_{23}C_6$ carbides. Original magnification: 25,000X.

6.2. Creep Testing

A complete tabulation of the creep tests performed on the reference heat (9T2796) is given in Tables 6.3, 6.4, and 6.5. The first item to be discussed is the plastic strain that occurred on loading. Up to now we have initially loaded specimens through the use of a step loading method with 1250 psi increments. This technique resulted in reproducible strains and a well-defined initial time. For reasons unknown, possibly either machine momentum or Portevin-Le Chatelier effects,[33] we find the plastic strains to be higher after step loading than we expected from tensile test data. We intend to use a motor drive to lower the weights in future tests and specimen RP-86 listed in Table 6.3 was our first attempt. The strain introduced in this specimen was closer to the value expected from tensile tests. A comparison of plastic strains in tensile and creep tests is made for the RP series specimens in Fig. 6.9.

We found the nature of the strain-time response immediately after loading was dependent on stress. At very high stresses (30 to 40 ksi) an induction period was observed in which the creep rates accelerated and then decelerated toward the minimum. At intermediate stresses (15 to 30 ksi) the initial creep rate seemed to be finite, but decelerated after a short constant period. At lower stresses (7.5 to 15 ksi) the strains were too small to observe the short-time response except at the higher temperatures where often it was not possible to separate plastic strains from creep strains. Data obtained at stresses below the proportional limit (approximately 7 ksi) were too meager to allow generalizations.

The strain-time response immediately after loading could be made compatible with the exponential creep equation either by adding a second exponential as was done by Pugh[34] and Blackburn,[35] or by modifying the exponential creep equation by placing an exponential, β, on time. This method was used by Chuang, Kennedy, and Perry.[36] Thus, we could develop one of the following equations:

$$\epsilon_{prim} = A_1 \left(1 - e^{-r_1 t}\right) + A_2 \left(1 - e^{-r_2 t}\right)$$

or

Table 6.3. Summary of creep and stress rupture tests performed on type 304 stainless steel plate annealed at 2000°F (heat 9T2796)

Specimen no.	Temperature (°F)	Stress (ksi)	Plastic[a] strain on loading (%)	Minimum creep rate (%/hr)	Time to[b] tertiary creep (hr)	Intercept[c] creep strain (%)	Test[d] time (hr)	Fracture[e] elongation (%)	Reduction in area (%)
RP6[f]	1000	45.0	18.6	~0.03			60.1R	29	28.4
RP8	1000	40.0	14.3	0.021	130	0.1	162.8R	22	21.9
RP9	1000	35.0	11.0	0.004	510	0.3	594.8R	18	
RP24	1000	30.0	8.3	≤0.00064		≥0.5	1171.2D		
RP78	1000	25.0	5.5	≤0.00015		≥0.4	2000.0I		
RP26[g]	1000	20.0	3.3	≤0.000005		≥0.29	5057.0D		
RP75	1000	15.0	1.21				113.0D		
RP73	1000	15.0	1.18	≤0.00002		≥0.16	3000.0I		
RP31	1000	10.0	<0.05	≤0.000002		≥0.035	5035.0D		
RP86	1100	35.0	9.2	0.23	24	0.6	29.6R	20	27.0
RP4	1100	35.0	11.7	0.34	20	0.2	25.1R	27	35.8
RP5	1100	30.0	8.3	0.046	80	0.85	110.8R	19	
RP7	1100	25.0	5.8	0.011	280	0.7	440.1R	16	
RP54	1100	25.0	5.5	0.010	310	0.7	402.5D		
RP32	1100	22.5	4.6	0.0035	550	0.6	878.1R	15	11.2
RP23[h]	1100	20.0	3.3	≤0.00085		≥0.45	1000.0D		
RP58	1100	20.0	2.8	0.00065	4700	1.95	5060.5D		
RP40	1100	17.5	2.8	≤0.00023		≥1.3	5100.0D		
RP25[i]	1100	15.0	1.6	≤0.00033		≥0.2	1006.1D		
RP74[j]	1100	15.0	1.55	≤0.0003		≥0.25	986.6R		
RP79	1100	15.0	1.6	≤0.00018		≥0.33	2000.0I		
RP62	1100	12.5	0.65	≤0.000025		≥0.63	5660.1D		
RP28[k]	1100	10.0	0.16	≤0.00004		≥0.07	5000.0D		
RP76	1100	10.0	0.11	≤0.000015		≥0.037	1000.0D		
RP71	1100	7.5	0.004				500.0D		
RP1	1200	25.5	5.5	0.46	18	0.95	27.7R	25	30.2
RP2	1200	20.0	3.3	0.087	50	0.6	111.2R	25	28.9
RP85	1200	17.5	2.4	0.05	70	0.53	250.0R	27	30.0
RP3	1200	15.0	1.35	0.015	150	0.3	730.0R	21	
RP61	1200	12.5	0.76	≤0.005		≥0.2	260.0D		
RP22	1200	10.0	0.06	≤0.0009		≥0.3	1002.0D		
RP100	1200	7.5	0.003				100.0I		
RP27	1300	15.0	1.8	0.33	20	0.4	46.9R	27	
RP102	1300	12.5	0.65	0.067	130	0.25	244.4R	48	42.0
RP29	1300	10.0	0.18	≤0.038		≥0.1	73.9D		
RP83	1400	12.5	0.62	1.43	12	0.5	19.9R	42	36.6
RP30	1400	10.0	<0.25	0.43	30	0.3	45.7R	26	
RP41	1400	7.5	<0.05	≤0.105		≥0.08	20.0D		
RP84	1400	7.5	<0.05	0.044	500	3.46	697.7R	47	39.0
RP81	1500	10.0	0.17	3.6	5	0.6	8.4R	53	25.4
RP80	1500	7.5	<0.05	0.38	50	2.0	77.7R	42	40.3
RP59	1500	5.0	<0.05	≤0.028		≥2.2	166.0D		

[a]All specimens except RP86 were step loaded at 1.25 ksi increments. RP36 was loaded smoothly.

[b]Time to tertiary creep was based on the 0.2% offset from the minimum rate line.

[c]Intercept creep strain does not include the elastic and initial plastic components.

[d]R = rupture; D = discontinued; I = in test.

[e]Elongation over approximately 9X diameter.

[f]Approximately 1.6% strain introduced at 20 hr.

[g]Approximately 0.05% strain introduced at 570 hr.

[h]Approximately 0.66% strain introduced at 47 hr.

[i]Approximately 0.27% strain introduced at 700 hr.

[j]Temperature excursion to 1600°F at 986.6 hr.

[k]Approximately 0.08% strain introduced at 2200 hr.

Table 6.4. Summary of creep and stress rupture tests performed on type 304 stainless steel 5/8-in. bar (hot rolled) annealed at 2000°F (heat 9T2796)

Specimen no.	Temperature (°F)	Stress (ksi)	Plastic[a] strain on loading (%)	Minimum creep rate (%/hr)	Time to[b] tertiary creep (hr)	Intercept[c] creep strain (%)	Test[d] time (hr)	Fracture[e] elongation (%)	Reduction in area (%)
RR37	1100	35	10.0	0.49	19	0.65	23.0R	27	30
RR36	1100	30	6.7	0.088	75	1.0	101.0R	20	24
RR35	1100	25	4.5	0.015	300	0.8	430.0R	16	18
RR47	1100	15	0.85				0.0D		
RR49	1100	15	0.6				100.0D		
RR50	1100	15	1.1				1000.0D		
RR33	1150	20	2.6	0.014	190	0.6	464.0R	16	17
RR66	1200	25	6.0	0.75	15	0.75	27.5R	38	34
RR38	1200	20	2.6	0.11	50	0.8	114.0R	24	25
RR41	1200	15	1.4	0.018	150	0.5	649.5R	22	22
RR32	1250	20	2.8	0.62	15	0.8	28.8R	29	33
RR42	1250	15	1.3	0.11	70	0.5	135.3R	24	30
RR45	1250	10	<0.05	≤0.0029		≥1.1	1261.6D		
RR40	1300	15	1.1	0.36	30	0.7	54.5R	29	28
RR44	1300	10	<0.05	0.0225	660	1.6	993.1R	31	32
RR46	1400	10	<0.05	0.32	60	1.2	82.4R	36	34
RR39	1500	10	0.29	3.3		1.5	12.0R	38	36

[a]All specimens step loaded at 1.25 ksi increments.

[b]Time to tertiary creep based on the 0.2% offset from the minimum rate line.

[c]Intercept creep strain does not include the elastic and plastic components.

[d]R = rupture; D = discontinued.

[e]Elongation over approximately 9X diameter.

Table 6.5. The influence of thermo-mechanical variables on the short-time creep rupture of type 304 stainless steel (heat 9T2796)

Specimen no.	Product form	Condition	Temperature (°F)	Stress (ksi)	Plastic strain on loading (%)	Minimum creep rate (%/hr)	Rupture life (hr)
RP86	Plate	2000°F annealed	1100	35.0	9.2	0.23	29.6
RP4	Plate	2000°F annealed	1100	35.0	11.7	0.34	25.1
RR37	5/8-in. bar	2000°F annealed	1100	35.0	10.0	0.49	23.0
796-9	5/8-in. bar	1950°F annealed	1100	35.0	8.5	0.33	43.7
RR43	5/8-in. bar	A479 (hot rolled)	1100	35.0	5.0	0.38	37.6
FRP7	Plate	2000°F annealed plus 10 cycles at 2% $\Delta\epsilon$	1100	35.0	0.75	0.29	34.8
RP5	Plate	2000°F annealed	1100	30.0	8.3	0.046	110.8
RR36	5/8-in. bar	2000°F annealed	1100	30.0	6.7	0.088	101.0
796-8	5/8-in. bar	1950°F annealed	1100	30.0	1.0	0.06	168.8
796-2	5/8-in. bar	A479 (hot rolled)	1100	30.0	2.0		274.2
796-7	5/8-in. bar	A479 (hot rolled)	1100	30.0	2.5	0.044	281.4
RP1	Plate	2000°F annealed	1200	25.0	5.5	0.46	27.7
RR9	1-in. bar	2000°F annealed	1200	25.0	6.7	0.7	25.5
RR10	1-in. bar	2000°F annealed	1200	25.0	5.1	0.8	22.4
RR11	1-in. bar	2000°F annealed	1200	25.0	4.4	0.78	25.0
RR12	1-in. bar	2000°F annealed	1200	25.0	5.3	0.85	19.5
RR66	5/8-in. bar	2000°F annealed	1200	25.0	6.0	0.75	27.5
796-10	5/8-in. bar	A479 (hot rolled)	1200	25.0	2.0	0.34	62.7

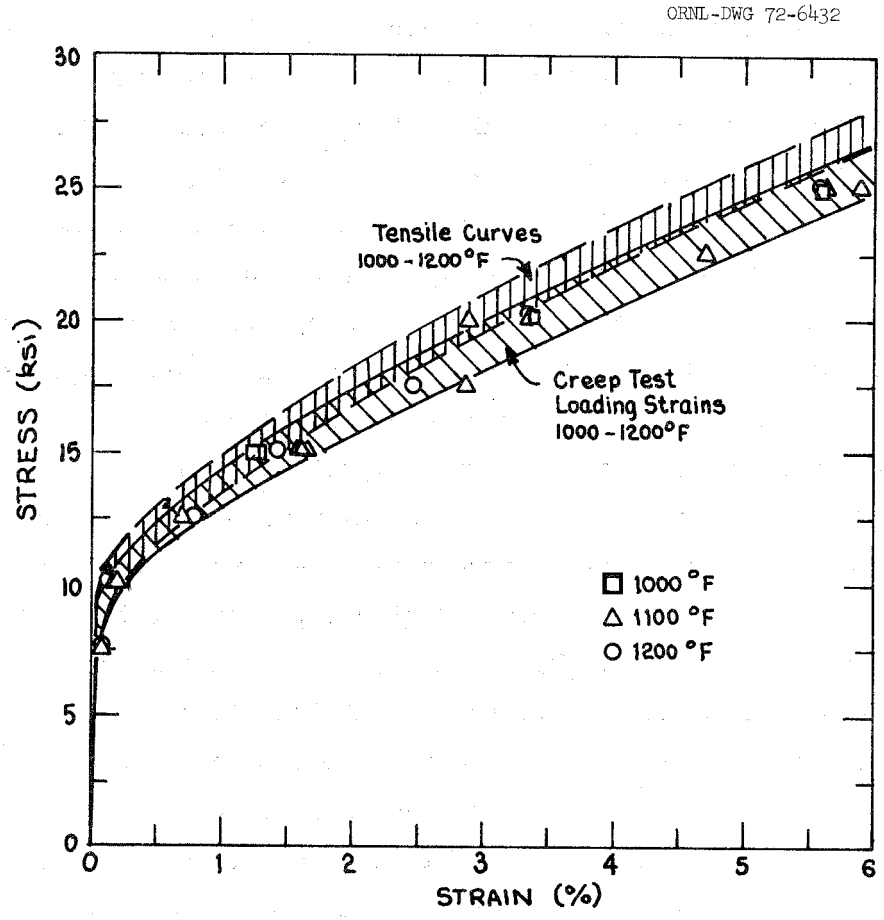

Fig. 6.9. Comparison of tensile curves for type 304 stainless steel with the strains obtained by loading creep test in the temperature range 1000 to 1200°F (heat 9T2796 plate annealed at 2000°F).

$$\epsilon_{prim} = A\left(1 - e^{-rt^{\beta}}\right),$$

where ϵ_{prim} is the primary creep, t is time, and everything else is a material constant which is stress and temperature dependent. If we consider something other than an exponential creep equation, there are many alternatives. Before taking this approach, additional and detailed work is needed to sort out the relationship between the methods of loading creep tests and the short-time strain response. Several years ago we found, when testing type 316 stainless steel, that the shape of the initial creep curve could be drastically altered by varying the loading conditions.[37]

The minimum creep rates, intercept creep strains, times to tertiary creep (defined by 0.2% offset from the minimum slope), rupture lives, elongations, and reductions in area are all contained in Tables 6.3, 6.4, and 6.5. Although such data are very important from an engineering viewpoint, they do not provide a very clear picture of strain-time behavior. Figure 6.10 shows a plot of a high-stress creep test, RP9, at 35,000 psi and 1000°F. The slight acceleration of creep rate out to 50 hr and subsequent deceleration to 300 hr are details which are lost by restricting descriptive creep parameters to those contained in the tables. Specimen RP7, at 25,000 psi and 1100°F, produced a creep curve which is more conventional (see Fig. 6.11), but specimen RP58, at 20,000 psi and 1100°F, exhibited unexpected behavior and this is shown in Fig. 6.12. Notice that the creep rate was almost constant between 500 and 1000 hr. We expected this test to go into tertiary creep around 1500 hr and perhaps fail around 2500 hr. Instead, a new period of decelerating creep developed. Such behavior profoundly affected the value of the intercept creep strain. Indeed we found many of the longer time tests, for both product forms, had high intercept creep strains. We do not know, just yet, whether these effects were due to experimental factors or resulted from real and reproducible metallurgical phenomena.

Several short-time creep tests were performed at 35,000 psi and 1100°F to investigate the influence of the thermo-mechanical condition on the deformation behavior. The results are summarized by Fig. 6.13. There was about a factor of 2 or less between the extremes of behavior. The weakest condition corresponded to the 5/8-in.-diam bar specimen which was annealed

ORNL-DWG 72-6433

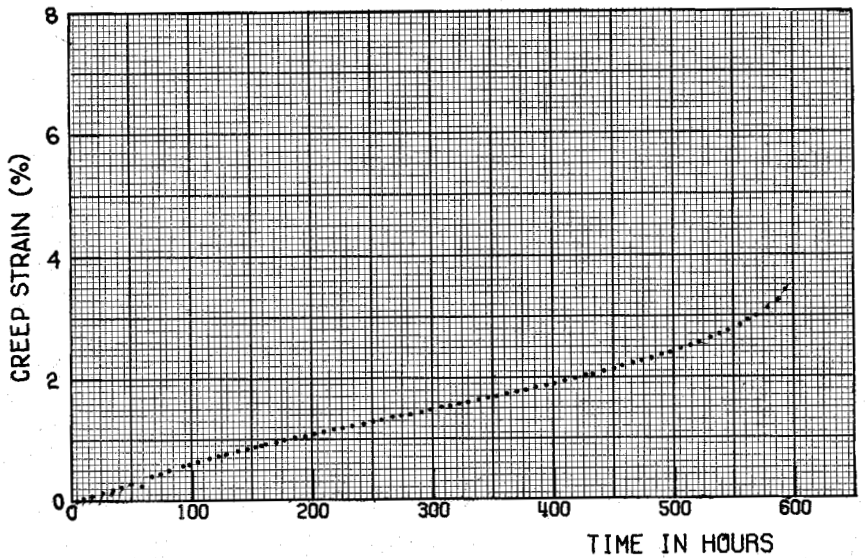

Fig. 6.10. Creep curve for type 304 stainless steel at 1000°F and 35,000 psi (heat 9T2796 plate annealed at 2000°F).

ORNL-DWG 72-6434

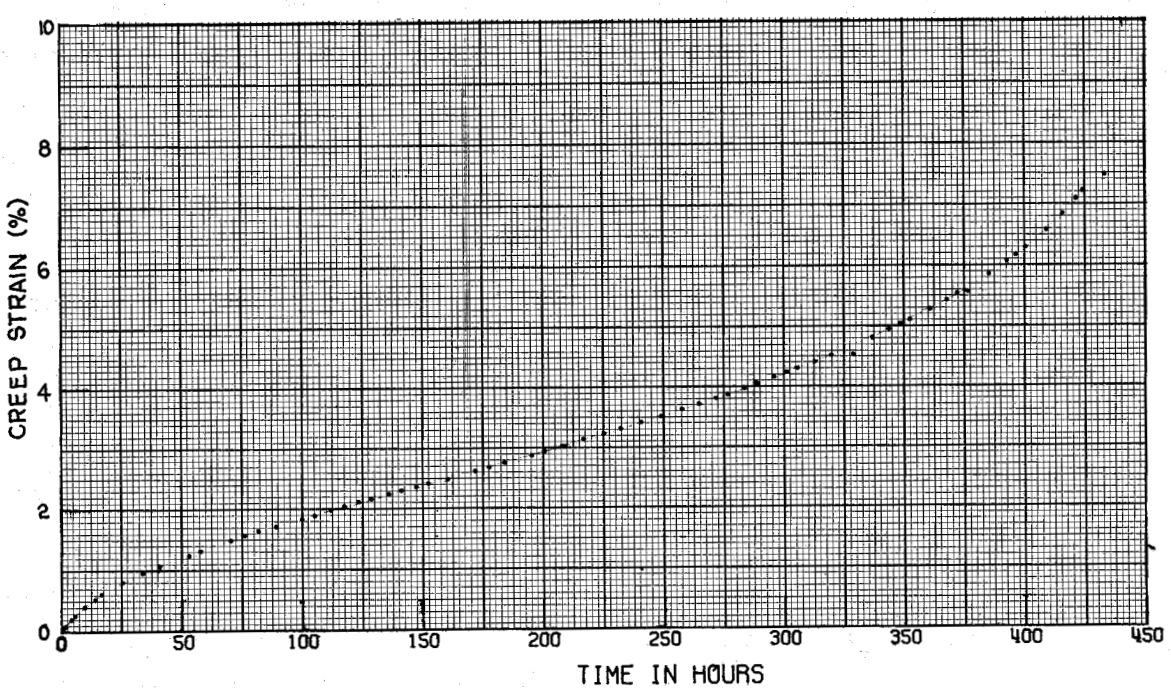

Fig. 6.11. Creep curve for type 304 stainless steel at 1100°F and 25,000 psi (heat 9T2796 plate annealed at 2000°F).

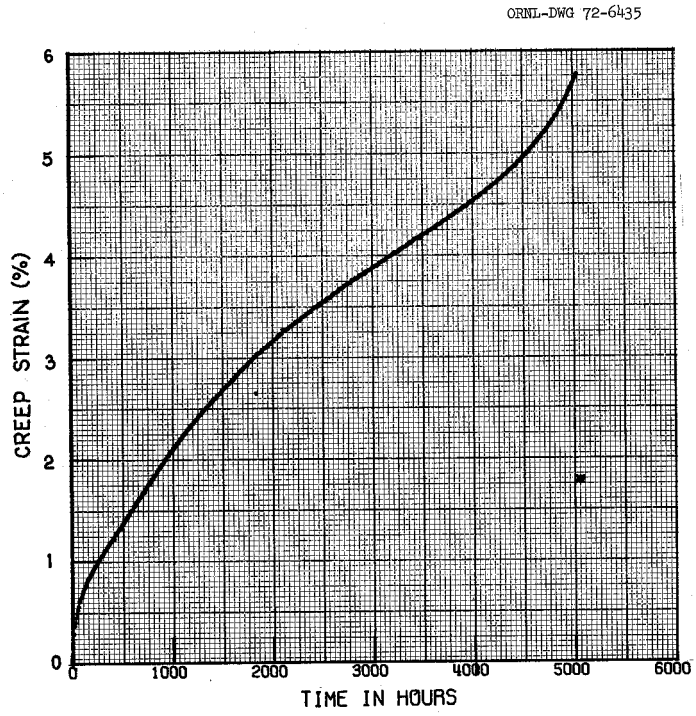

Fig. 6.12. Creep curve for type 304 stainless steel at 1100°F and 20,000 psi (heat 9T2796 plate annealed at 2000°F).

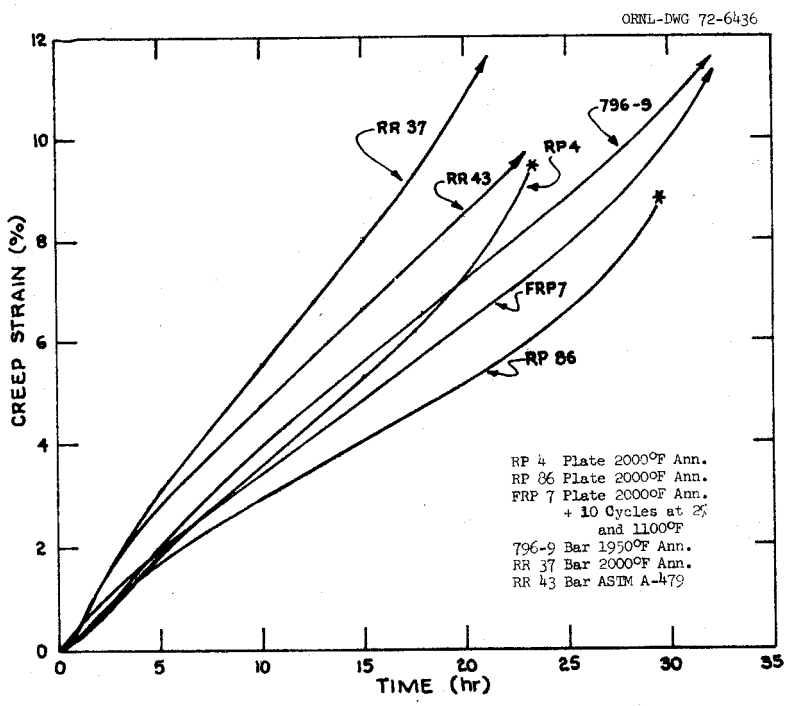

Fig. 6.13. Comparison of the effect of thermo-mechanical treatment on creep for type 304 stainless steel (heat 9T2796) at 1100°F and 35,000 psi.

at 2000°F (specimen RR37). The strongest was taken from 1-in. plate and annealed at 2000°F (specimen RP86). In between we find bar material in the A-479 condition (specimen RR43) and plate material reannealed at 1950°F (specimen 794-9). Also included are two other specimens taken from plate. One was annealed at 2000°F (specimen RP4), and the other annealed at 2000°F was then strain cycled ten times at 1100°F and ±1% strain amplitude (FRP7).

A group of test results obtained at 15,000 psi and 1100°F are compared in Fig. 6.14. Included are three tests performed on specimens machined from plates (RP25, RP74, and RP79), two tests on bar material (RR49 and RR50), and a compression test on a tubular specimen machined from 1-in. plate. All specimens were reannealed at 2000°F prior to testing. With the exceptions of specimen RR50, the data grouped together fairly well. It appeared that the compression test was beginning to deviate at 250 hr, and we suspect this may continue as the diametric restraint, exerted by extensometer and specimen shoulders, becomes more pronounced.

A comparison of two-step load creep tests performed at 1100°F with constant-load creep data is shown in Fig. 6.15. Total strains rather than creep strains have been plotted in order to show an increase in the plastic flow stress which developed as a consequence of creep exposure. When we compared only the creep components of strain, we found results which were quite similar to those reported[38] for the preliminary heat (8043813). At low stresses it was hard to distinguish whether the time- or the strain-hardening rule looked the best. At higher stresses the strain-hardening rule is superior.

We have had difficulty performing tests on type 304 stainless steel at 1100°F because the creep rates were low and stresses had to be high relative to the plastic yield stress. Bumping of the creep machines often introduced more plastic strain. At very high stresses (more than 30,000 psi) we found that accidental plastic strains, introduced during creep, produced temporary hardening effects. Just as for the first loading, creep rates were low at first and then accelerated. However, we found at intermediate stresses (15,000 psi) a temporary acceleration in creep rate after a plastic strain pulse. Possibly, new dislocations generated or unlocked by the plastic strain participated in the creep processes until

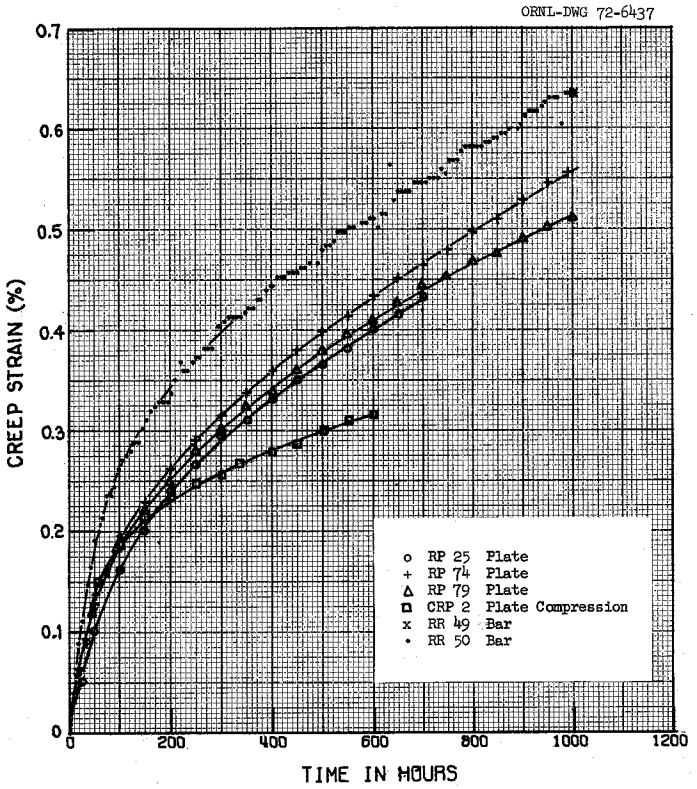

Fig. 6.14. Comparison of several creep tests performed on type 304 stainless steel (heat 9T2796 annealed) at 1100°F and 15,000 psi.

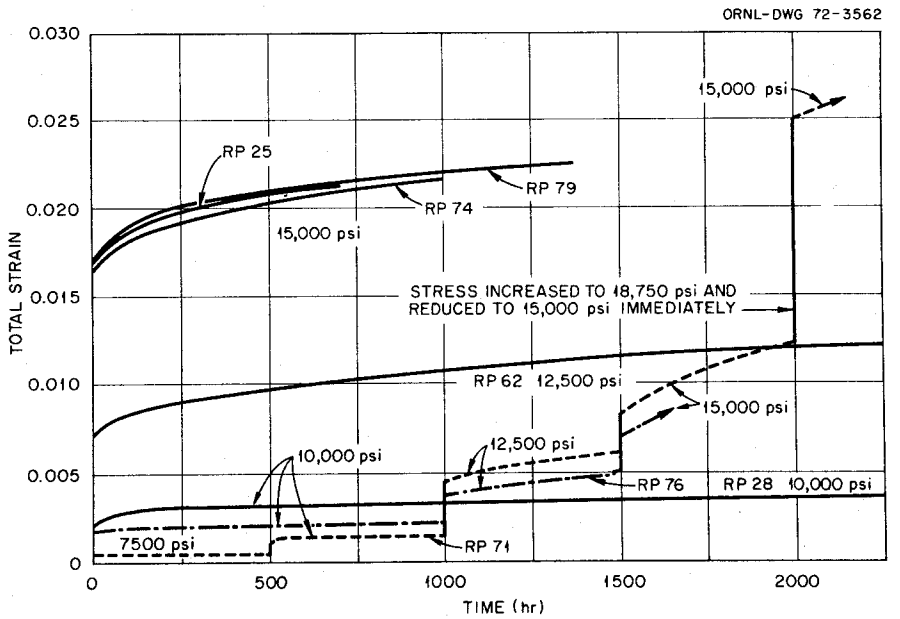

Fig. 6.15. Comparison of constant load and step load strain-time response for type 304 stainless steel at 1100°F (heat 9T2796 annealed).

they were immobilized once again. If this is true, then the concept of a limiting transient creep strain, uniquely associated with a stress, may not be a completely realistic model.

6.3. Relaxation Testing

Relaxation testing was resumed toward the end of this reporting quarter. Two more tests, at 1050 and 1150°F, were performed, and these are included in the summary plot shown in Fig. 6.16. The pneumatic-hydraulic machine was placed in operation this quarter and relaxation tests to 1000 hr should begin soon.

6.4. Cyclic Testing

A few cyclic tests were performed this quarter at room temperature, 800, and 1100°F. The tensile stress amplitudes obtained from several of these tests are compared at two strain amplitude levels in Table 6.6. The results were consistent with our expectations and revealed rapid work hardening at elevated temperatures and relatively high strain amplitude.

7. ANALYTIC RATCHETTING STUDIES

T. R. Branca
J. L. McLean

Teledyne Materials Research Co.

During this reporting period, Teledyne's initial analytic ratchetting studies were completed and a final report was published (Teledyne Technical Report E-1414). The results of this study are far too extensive to present in a complete package as a progress report. Thus the following presentation outlines only the basic approach taken and the more significant results obtained.

The ANSYS program was used in the parametric ratchet study to solve all the cases involved. The general capability of ANSYS and the problems encountered in setting it up on the NYU CDC-6600 computer have been discussed previously.[39] A multilinear stress-strain curve, temperature-

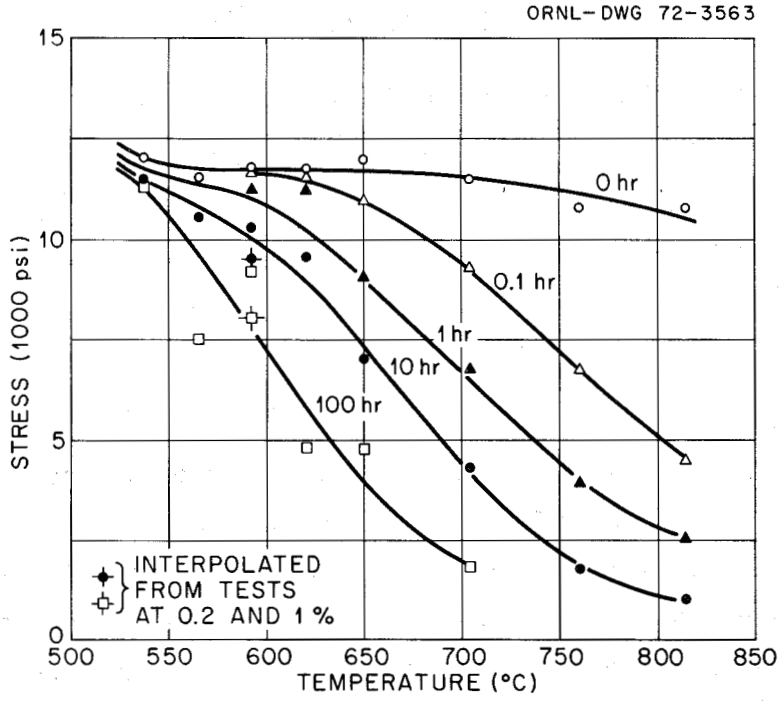

Fig. 6.16. Relaxation stresses at several temperatures and times for type 304 stainless steel (heat 9T2796). Tests were held at 0.5% total strain.

Table 6.6. Summary of several strain-cycling tests performed on type 304 stainless steel (heat 9T2796 reannealed at 2000°F)

Specimen no.	Temperature (°F)	Tensile[a] strain amplitude (in./in.)	Tensile stress amplitude at indicated cycle number (ksi)			
			1/4	1 1/4	2 1/4	10 1/4
FRP2	Room	0.0045	27.0	29.2	30.2	33.2
FRP4	800	0.0045	15.5	17.7	19.2	25.0
FRP9	1100	0.0045	12.2	15.5	17.5	24.5
FRP3	Room	0.0092	29.5	34.5	36.8	42.2
FRP5	800	0.0095	16.5	21.5	25.5	40.0
FRP6	1100	0.0097	12.8	18.8	23.5	40.2

[a]Axial control over 0.5-in. gage length at 0.05 per minute strain rate.

dependent properties, kinematic hardening, and strain-hardening creep were considered in these studies. However, due to the limitations of ANSYS and of computer run time, cases were still limited to long, axisymmetrical, cylindrical geometries with axisymmetric loadings.

In order to make the results of this study more applicable to FFTF and SPTF component and piping design, the parameters of the ratchet cases considered were selected to cover the range of interest in the two liquid-metal programs. For example, the material considered was 304 stainless steel, and the selection of the thermal transients and pressure conditions was based on design specifications for FFTF and SPTF components.

The form of the temperature history considered was similar to that used by Minami and Roberts;[40] it consists of a severe down-transient from the normal operating temperature followed by a short hold time at the lower temperature of approximately one-half hour. The fluid temperature is then slowly raised to the upper temperature and held there for 500 hours with an internal pressure loading. For the 26 ratchet cases of this study the pressure was held constant through the entire thermal cycle. Down-transients of 40°F/sec, 30°F/sec, 10°F/sec, and 2°F/sec were considered with temperature drops during the transients of 400°F and 300°F. The normal operating temperatures investigated were 1000°F, 1100°F, and 1200°F. Pipe wall thicknesses of 0.375 in. to 1.35 in. were considered. A summary of the input parameters used for each case is given in Table 7.1.

7.1. Analysis

7.1.1. Finite element model

With the nodal coupling options available in ANSYS, a long axisymmetric cylinder was idealized as shown in Fig. 7.1. For all ratchet cases considered, there were 16 equal quadrilateral axisymmetric ring elements taken through the wall thickness as shown. The nodes on one lateral face of the model were free to move only in the radial direction; on the other lateral face, the nodes were constrained to move uniformly in the axial direction while being free in the radial direction. This set of constraints simulates the long pipe by placing the axisymmetric model in a state of generalized plane strain. The nodes of the same radius were also forced

Table 7.1. Ratchet-run input parameters

Run no.	Operating temperature (°F)	Thermal transient (°F/sec)	ΔT (°F)	Wall thickness (in.)	Internal pressure (psi)
1	1000	−40	400	0.851	635
2					423
3					211
4		−30	300	1.35	992
5					496
6		−10	300	0.531	400
7					266
8		−2	300	1.06	787
9				0.531	400
10	1100	−40	400	0.851	300
11		−30	300	1.35	624
12					208
13				0.851	300
14				0.375	134
15		−10	300	0.700	331
16					220
17				0.531	189
18		−2	300	0.851	400
19	1200	−40	400	0.851	195
20		−30	300	1.35	457
21					220
22		−10	300	0.700	243
23					81
24				0.531	185
25					123
26		−2	300	0.851	293

ORNL-DWG 72-6438

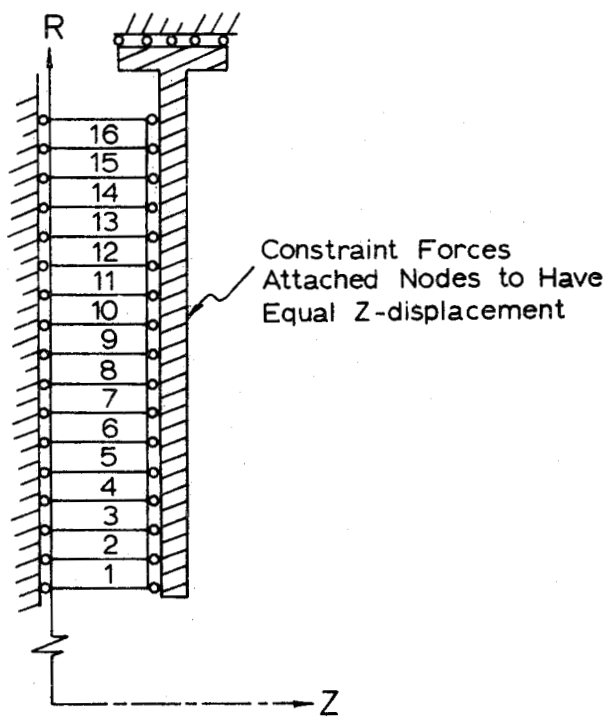

Fig. 7.1. Sixteen element model showing boundary conditions used to simulate a long straight pipe.

to move equally in the radial direction. The nodal coupling in the two directions reduces the number of displacement unknowns from 34 to just 18.

The same model geometry was used for the solution of the associated thermal problem. In the thermal solution, nodes at equal radii were temperature-coupled.

7.1.2. Plasticity solution technique

The ANSYS program uses the initial strain approach for the plastic and creep strains in the formulation of the finite element system of equations. In this technique, for small displacement analysis, only the right-hand side of the equation is modified for each change in the loading or inelastic strains. However, in the ratchet cycle there are large temperature changes; thus, it was necessary to modify the stiffness matrix, which is a function of the temperature-dependent elastic properties, for each iteration that involved a temperature change. For subsequent iterations of the elastic-plastic solution at a given input temperature distribution, the current stiffness matrix was saved. Approximately 35 temperature distributions were used in the elastic-plastic solution for each ratchet cycle, and at each of these temperature steps, six iterations were taken to converge the solution.

The plasticity subroutine of ANSYS requires the stress-strain curves to be input in the form of multilinear curves of five segments for each temperature of interest. The stress-strain curves used in this study represent average properties of 304 stainless steel and were given in tabular and graphical form in Ref. 39. The bilinear stress-strain curve could have been used as a special case of the multilinear representation. However, it was decided that the bilinear representation would not be helpful since the plasticity logic in ANSYS was not developed from a consistent theory that requires the bilinear curves.

In this study no attempt was made to include the effects of cyclic changes of the stress-strain curve. Thus, the monotonic stress-strain curves were used throughout the cyclic loading. The nonisothermal conditions are accounted for by linear interpolation between input temperature-dependent stress-strain curves and physical properties at each iteration.

The ANSYS plasticity subroutine that was used for this study considers the input stress-strain curves as generalized stress-strain curves for both isotropic and kinematic hardening. Within the ANSYS kinematic hardening option for the monotonic portion of a cyclic loading, the plastic strain increments are calculated by a method of isotropic hardening. The multiaxial plastic stress-strain relation used is the "modified total strain" version of the Prandtl-Reuss equation as described by Mendelson.[41] If used directly for reversed loading cases, the Mendelson approach is one of isotropic hardening. However, in the ANSYS kinematic scheme that was used, when the largest elastic strain component changes sign relative to its corresponding plastic strain component during a load reversal, the required kinematic shift in the origin of the yield surface takes place. During this shift the initial size of the yield surface is resumed.

It is clear that the ANSYS kinematic hardening scheme used for this study is not an analytically consistent hardening theory.* However, for the particular case under consideration, that is, the thermal ratchet of a straight pipe, the ANSYS inconsistencies do not appear to lead to serious problems. The reason is that the loading on the pipe is predominantly thermal. Thus, in stress space, the loading is approximately radial with σ_1 equal to σ_2. In the region of the yield surface near this radial loading line, the yield surfaces from the ANSYS development and a more analytically consistent theory are not significantly different. Therefore, for the pipe ratchetting study the analytical development of the ANSYS kinematic hardening subroutine was considered to be adequate.

7.1.3. Creep solution technique

The specific creep equation used together with background information have been covered previously.[39] The multiaxial creep relations of ANSYS are the Prandtl-Reuss equations for creep-strain increments as given in Mendelson.[41] These equations are of the isotropic hardening type. The particular ratchet program under consideration is an intermittent creep problem and not a creep reversal problem. Therefore, the ANSYS creep approach is an adequate strain-hardening formulation.

---

*A more general and consistent kinematic hardening option was added to ANSYS after this study was completed.

7.1.4. Post-run analysis: evaluation of the finite element results

To summarize the numerical results, the ratchet growth (cumulative strain) was plotted as a function of the elastic thermal stress and the pressure stress. For the present study the value plotted as the abscissa is the primary stress intensity, P_m. On the ordinate the value plotted is the equivalent linear elastic secondary stress intensity, Q_{EL}. The following formulas were used to calculate these two quantities:

$$P_m = \frac{1}{a}\int_o^a \sigma_\theta dr - \frac{1}{a}\int_o^a \sigma_r dr \ , \tag{7.1}$$

$$Q_{EL} = \frac{6}{a^2}\int_{-a/2}^{a/2} \sigma_\theta r dr - \sigma_{ri} \ , \tag{7.2}$$

where

a = pipe wall thickness,

σ_θ = hoop stress from elastic calculation,

r = radius,

σ_r = radial stress from elastic calculation,

σ_{ri} = radial stress at inside diameter.

To obtain the elastic results necessary to compute P_m and Q_{EL}, an elastic-only finite element solution was obtained. This solution used the same temperature input as used in the corresponding cyclic elastic-plastic-creep solution.

7.1.5. Input parameters and computer run times for the ratchet cases

The input parameters for the ratchet cases used in this study were presented in Table 7.1. The heat transfer coefficient at the wetted surface for each case was 50 Btu/hr-in.^{2}-°F. In an attempt to avoid the complicating influence of thick cylinder effects, an inside diameter of 30 in. was used for all cases. A 500-hr hold time was considered for all runs.

This 500-hr hold time represents an "arbitrary average" of the estimates of the hold times for SPTF and FFTF components. The 500-hr hold time was also easily manageable in a computer solution.

The internal pressure of the runs was limited by the requirement of existing criteria[42] that $P_m \leq \overline{S}_m$. The $\overline{S}_m$ values used are:

$$\overline{S}_m = 11{,}500 \text{ psi at } 1000^\circ\text{F} ,$$

$$\overline{S}_m = 7{,}250 \text{ psi at } 1100^\circ\text{F} ,$$

$$\overline{S}_m = 4{,}400 \text{ psi at } 1200^\circ\text{F} .$$

The ratchet cases each required approximately 3000 central processor seconds on the CDC 6600. The iteration schemes used were probably conservative in that more load-time steps were taken than are required for an accurate solution. However, even if the number of steps were cut in half and an accurate solution resulted, the implications are that ratchetting analysis on any but the simplest geometry will be very expensive. The form of the solutions obtained is indicated by Figs. 4.3 and 4.4, Section 4.3, of this report, which are typical hoop stress vs hoop strain results obtained by TMR for the ORNL pipe thermal ratchetting problem.

7.2. Results

7.2.1. Cumulative strain

The values for the incremental strain growth are based on differences between the hoop strain at the inner surface from cycle to cycle, the hoop strain being the maximum positive principal strain. The inelastic ratchet calculations were done for five cycles. The incremental growth did not in every case settle to a steady value by the fifth cycle. Therefore, it was necessary to make some approximation concerning the steady-state growth per cycle. At one point we considered using an extrapolation procedure to determine the steady-state growth value. However, due to present uncertainties of inelastic and creep analyses, it was decided to adopt a more conservative approach and consider the incremental strain growth between the fourth and fifth cycles as the steady-state incremental strain growth. The total strain growth after n+5 ratchet cycles was thus calculated by

$$\epsilon_\theta = \epsilon_{\theta_5} + n\delta_{\theta_{4-5}} , \qquad (7.3)$$

where

ϵ_θ = the final total hoop strain (minus hoop thermal strain), maximum value of cycle for inside surface,

ϵ_{θ_5} = the total hoop strain (minus hoop thermal strain), maximum value of fifth cycle for inside surface,

$\delta_{\theta_{4-5}}$ = incremental strain growth from fourth to fifth cycle, $\epsilon_{\theta_5} - \epsilon_{\theta_4}$.

The maximum hoop strain for the cycle as opposed to the strain during the thermal-transient-free state was used in the cumulative strain calculations to present a conservative value for the hoop strain increase. Using Eq. (7.3), 100-cycle cumulative strain results were calculated and are presented in the Bree-type diagrams, Figs. 7.2, 7.3, and 7.4. In these figures approximate contours were drawn between the data points.

7.2.2. Comparison of results to FRA-152, Rev. 3

In the comparison of the results of this study to the ratchetting rules of FRA-152, Rev. 3, considerable liberty has been taken. First of all, FRA-152, Rev. 3, states that the maximum absolute accumulated inelastic strain be used in the deformation limit evaluation. The maximum positive principal strain was considered as opposed to the maximum absolute principal strain in the cumulative strain calculations. Secondly, in paragraph 4.2.4.2(b)2, FRA-152, Rev. 3, states that thermal stresses from all sources be less than $2\sigma_{y_{min}}$. The peak stress was not considered in the evaluation of this paragraph; therefore, the requirements of the paragraph were relaxed to limiting Q_{EL} to be less than or equal to $2\sigma_{y_{min}}$.

There are essentially three ratchetting rules in FRA-152, Rev. 3. The first ratchetting rule, paragraph 4.2.4.2(a), requires $(P_m + Q_{EL})_{range} \leq \sigma_y$. Examination of Figs. 7.2, 7.3, and 7.4 shows this limit to be very conservative when compared to the 100-cycle cumulative strains of this study. Note, however, that this rule applies for any operational life. If, from Figs. 7.2, 7.3, and 7.4, an estimate is made of the cumulative strain at 350 cycles (approximately equal to 20 years operational life), the rule of paragraph 4.2.4.2(a) would still be quite conservative, especially for the 1000°F curves.

ORNL-DWG 72-6439

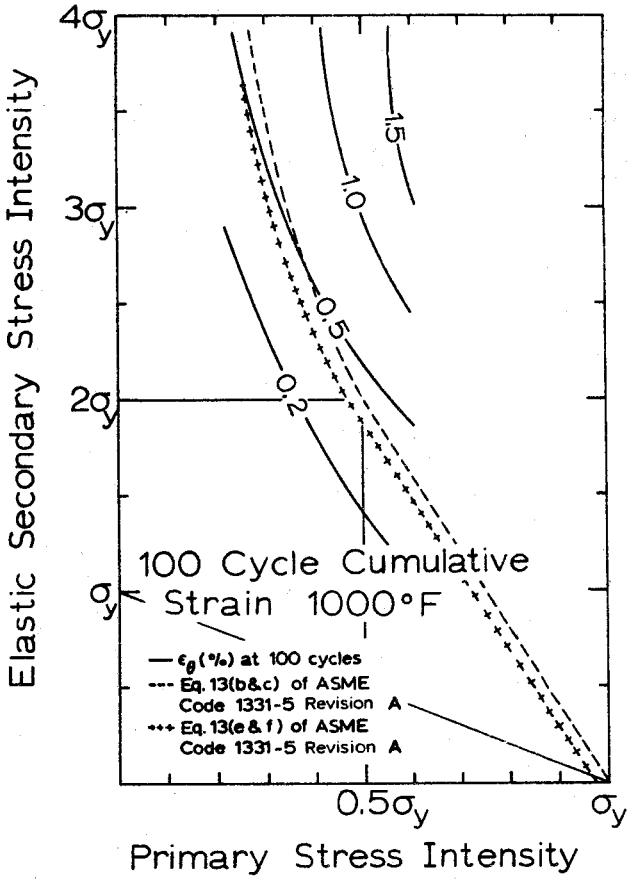

Fig. 7.2. Comparison of the cumulative hoop strain after 100 ratchet cycles at an operating temperature of 1000°F to the limit lines of existing and proposed ratchet rules.

ORNL-DWG 72-6440

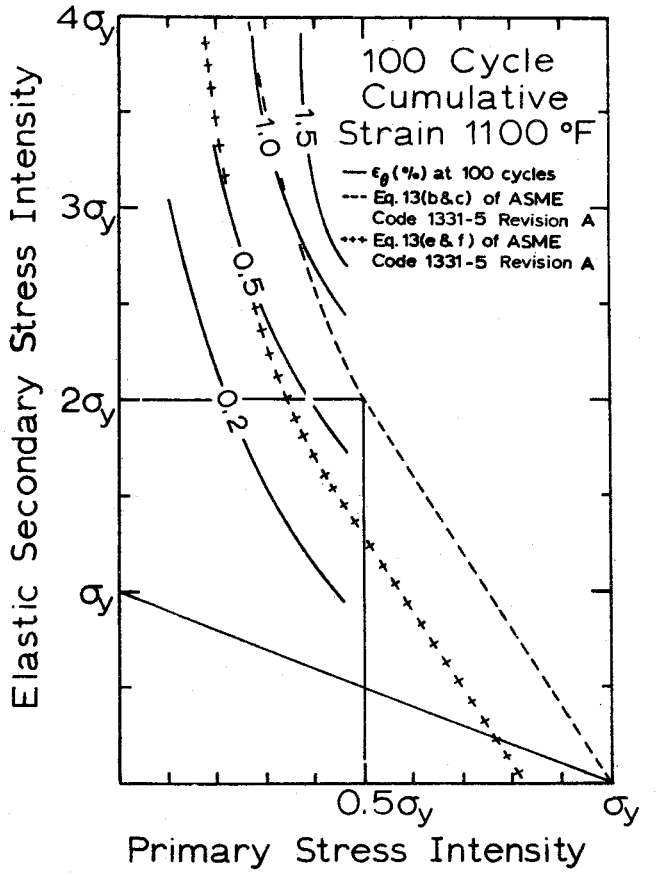

Fig. 7.3. Comparison of the cumulative hoop strain after 100 ratchet cycles at an operating temperature of 1100°F to the limit lines of existing and proposed ratchet rules.

ORNL-DWG 72-6441

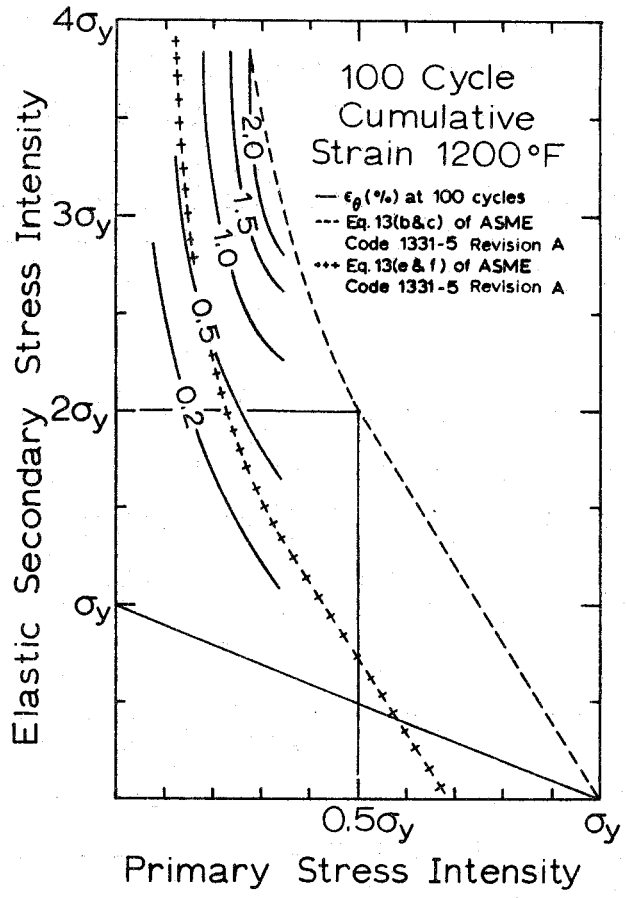

Fig. 7.4. Comparison of the cumulative hoop strain after 100 ratchet cycles at an operating temperature of 1200°F to the limit lines of existing and proposed ratchet rules.

The second and third rules of FRA-152, Rev. 3, for ratchetting are each made up of three sections. The first and second sections of the two rules are identical. And for the cycle of the ratchet study, the third sections of the rules, that is, paragraph 4.2.4.2(b)3 and paragraph 4.2.4.2(c), are equally restrictive. Using the isochronous stress-strain curves given in FRA-152, Rev. 3, rules 4.2.4.2(b) and 4.2.4.2(c) can only be invoked if the life in hours is less than the values shown below.

Applicability of Paragraphs 4.2.4.2(b)3 and (c) of FRA-152, Rev. 3, for 304 Stainless Steel

Temperature, °F	1000	1100	1200
Life, hr	10^4	$<10^3$	0

Thus the 100-cycle life investigated in Figs. 7.2, 7.3, and 7.4 is too long to be considered by the second and third rules of FRA-152, Rev. 3. However, for completeness, the limit lines (modified for this study) of paragraphs 4.2.4.2(b)1 and 2, that is, $Q_{EL} \leq 2\sigma_{y_{min}}$ and $P_m \leq 0.5\sigma_{y_{min}}$, are shown.

7.2.3. Comparison of results to the ratchetting rules of the LMEC Proposed "Appendix A, Supplement to Code Case 1331-5"

The ASME Code Case 1331-5 requires that ratchetting deformation be considered in high-temperature design, but the analytical procedures and materials properties as included are nonmandatory.[43] However, provision is made in this code case for alternate criteria to be used by the Manufacturer subject to the Owner's approval. The LMEC, as an Owner, has proposed such alternate ratchetting criteria to supplement Code Case 1331-5 for use in design of LMEC facilities. It is intended that the supplement will be made a part of the Design Specification for all Class I Nuclear Components for which LMEC has the technical management responsibility.[44] It was felt that a thorough evaluation of ratchetting criteria should consider the rules of this supplement, Ref. 44, henceforth referred to as Appendix A.

For the simple straight pipe model used for the ratchet cases, the rule A.2.1.2(1) of Appendix A is approximately the $(P_m + Q_{EL})_{range} \leq \sigma_y$ rule discussed for FRA-152, Rev. 3, and the same comments apply. The

ratchet limit curve given in Appendix A, A.2.1.2(2a) is shown in each of Figs. 7.2, 7.3, and 7.4.* However, this limit curve is not applicable to 100-cycle lives because of the second part of this rule, paragraph (2b). From the isochronous stress-strain curves of the code, paragraph (2b) limits the design life for 304 stainless steel to the following:

Applicability of Rule A.2.1.2(2b) of Appendix A for 304 Stainless Steel

Temperature, °F	1000	1100	1200
Life, hr	10^4	<500	<50

Paragraph (2c) is satisfied for all the ratchet cases of this study.

For the cycle used in this study, the limits set by rule A.2.1.2(3) are approximately as restrictive as the limits set by rule A.2.1.2(2a, b, and c).

The limits set by rule A.2.1.2(4a) are specified by two equations, Eqs. 13(e) and 13(f) of the Appendix A. Equations 13(e) and 13(f) were calculated for each of the temperatures considered. The resulting curves are plotted in Figs. 7.2, 7.3, and 7.4.

From these figures it is seen that the present analysis indicates that rule A.2.1.2(4) is conservative with respect to the 2% surface strain limit of the code. However, because of the uncertainties of the present analysis and the unknowns that may enter due to more complex temperature and pressure cycles and more complex geometries, we do not think that the present analysis indicates that the rule is excessively conservative.

7.3. Conclusions

Although there is some question about the particular kinematic hardening scheme available in ANSYS at this time, the results presented in this study indicate that the program can produce reasonable solutions that show the essential features of a more consistently developed hardening scheme.

---

*In Figs. 7.2, 7.3, and 7.4, the term Revision A should read Appendix A as discussed above.

The results presented in Figs. 7.2, 7.3, and 7.4 are useful in that they indicate the analytically predicted growth as a function of elastic primary and secondary stress intensities. The growth curves were generated for a 500-hr hold time, but should also apply conservatively to a loading sequence where hold times are less than 500 hr. These results may not be overly optimistic for hold times in excess of 500 hr, since most of the stress relaxation has occurred before the end of the 500 hr. However, it should be noted that experimental pipe ratchet results and further analytical solutions are necessary to completely evaluate the results of the present study.

The present analysis indicates that the ratchetting rules presented in both FRA-152, Rev. 3, and in the LMEC proposed supplement to ASME Code Case 1331-5 for loadings with long hold times are very conservative, with one exception. That exception is rule A.2.1.2(4) of the proposed supplement to the ASME code. When compared to the results of this analysis, the rule A.2.1.2(4) is consistently and reasonably conservative for all loadings and temperatures studied.

The analysis indicates that a complete ratchetting study of any complex structure will be an expensive undertaking due to the large computer run times necessary. Therefore, it is our opinion that an important area of study in the near future, in addition to the ratchetting experiments, will be in the development of standard techniques to construct simplified finite element models from large complex finite element idealizations. The simpler models must be manageable from a computer-run-time point of view, and also must realistically represent the boundary conditions imposed by the larger parent model.

8. HIGH-TEMPERATURE CREEP COLLAPSE TESTS OF PIPING ELBOWS

R. I. Jetter
J. Moldenhauer

Atomics International

8.1. Test Conditions

In order to obtain fundamental information on the high-temperature behavior of piping systems, a series of creep collapse tests is to be performed on thin-walled, long-radius piping elbows fabricated to close tolerances from 304 type stainless steel. The test elbows will be 16 in. in diameter, and will have the same characteristics as those incorporated in the FFTF design.*

The test specimen will be "L" shaped, consisting of two straight pipe extensions welded to the ends of a 90° elbow, with one end of the test specimen fixed. During the tests the elbows are to be maintained at a uniform constant temperature of 1100°F within a tolerance band of about ±1/2%. A suitable constant load will be applied at the free end to produce creep collapse in about 200 hours.

Altogether three tests are to be performed. The first and second tests will be on elbows with a 3/8-in. wall with the loads applied in-plane and out-of-plane, respectively. The last test will be on a 1/4-in. wall elbow with the load applied in-plane or, if such an elbow cannot be manufactured at a reasonable cost, a 3/8-in. wall elbow may be tested with an applied in-plane displacement. In the latter case, the objective will be to measure the relaxation characteristics of the elbow and to determine if creep collapse is possible under such conditions.

8.2. Test Data

During the tests, two types of data will be recorded as a function of time. Temperatures along the elbow surface will be recorded by means

*Efforts are currently underway by ORNL to obtain elbows for these tests identical to those to be manufactured for the FFTF piping system.

of six calibrated thermocouples, while the gross displacements of the test specimen will be measured with dial gages, and continuously monitored by means of variable resistance potentiometers actuated by the motions of the test specimen.

Before and after each test, measurements will be taken across the diameter of the test specimen at various circumferential and axial positions. A grid of shallow blunt indentations are to be placed on the elbows surface, prior to testing, in order to insure that both sets of measurements will be made at the same locations.

8.3. Test Assembly Design

Conceptual design of the heating system has been completed. Internal heating of the sodium-filled test specimen was selected as the most practical means of obtaining and maintaining a uniform temperature distribution, while at the same time being able to provide for the relatively large displacements anticipated under collapse conditions. In the final design, provisions are being made for a maximum angular displacement of about 9 degrees.

Two alternate heating methods were also given serious consideration: (1) a clamshell oven lined with electrical resistance heaters, and (2) a clamshell enclosure through which air, heated by a duct heater, would be recirculated by a high-temperature fan. Both of these external oven concepts had to be abandoned, however, primarily because a practical method of providing for adequate thermal closure, while still allowing for large displacements of the test assembly, could not be found.

Design work on the reference sodium concept, which is shown in Fig. 8.1, is now about 30% complete.

The test assembly is mounted off a large reinforced concrete slab with the horizontal leg at an initial angle of 9 degrees with respect to the true horizontal. The test load will be placed on the end of the horizontal leg causing it to displace towards the ground. A restraint structure prevents the assembly from rotating past the horizontal position; thus, most of the sodium can be drained from the system when the test is finished.

ORNL-DWG 72-6442

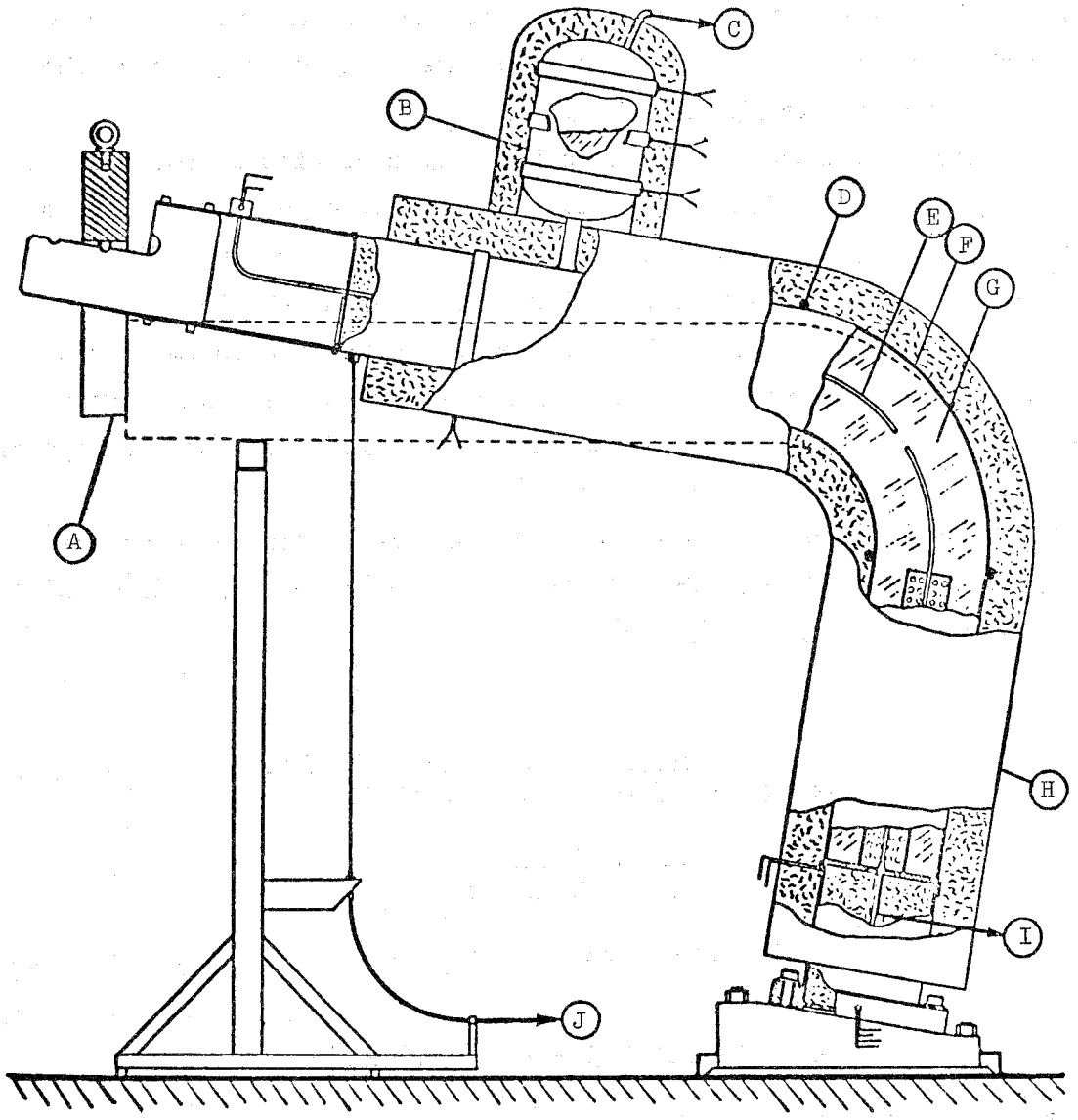

A	Steel weight	F	Test elbow (16-in.-diam sch. 30)
B	Expansion tank	G	Liquid sodium
C	To vent, vacuum, and argon supply	H	Insulation (6-in. thick)
D	Calibrated thermocouple (6 each)	I	To sodium fill line
E	Immersion heater	J	To displacement transducers

Fig. 8.1. Test assembly for high-temperature elbow creep test (in-plane configuration shown).

The primary heating system consists of a pair of tubular immersion heaters. These heaters project axially towards the center of the elbow from bulkheads located in the horizontal and vertical leg and are bent to conform to the axis of the elbow portion of the test assembly. Porous tubular shrouds, cantilevered from the bulkheads, serve to support the heaters over their straight length.

In order to achieve an adiabatic boundary condition at the ends of the test specimen, auxiliary band heaters are mounted on the outside of the test specimen at the bulkhead locations. Thermal output of the auxiliary heaters, though adjustable, will be fixed during the test.

Temperature control is to be achieved by means of a thermocouple sensor mounted at the end of one of the heater support shrouds. Power to the primary heaters will be automatically regulated to hold the system temperature at the set point.

As a result of safety considerations, all tests are to be enclosed in a sealed metal enclosure filled with an argon cover gas. Design of the enclosure is now in progress.

9. DEVELOPMENT OF A SIMPLIFIED INELASTIC DESIGN ANALYSIS FOR PIPING SYSTEMS

G. H. Workman
E. C. Rodabaugh

Battelle-Columbus Laboratories

9.1. Progress During January 1972

The research effort was initiated this month. The research project will follow that outlined in the previous progress report,[45] with the following exception. Upon the request, Battelle will furnish at the end of Phase I a copy of the digital computer program generated by this effort, a user's manual, program listing, and sample problems. This program will be operational on the CDC 6400 computing system at Battelle-Columbus.

During the first month Battelle developed a two-dimensional straight pipe element. The element has a circular cross section and assumes the presence of a linearly varying bending moment along the length (constant

shear force element). The formulation, at this stage, assumes that, at any time, the curvature of the beam element has two components. One is an elastic component, which is recoverable. The other is a creep component, whose behavior is characterized by the following equation:

$$\dot{\epsilon} = K \left(\frac{\sigma}{\sigma_o}\right)^n ,$$

where

$\dot{\epsilon}$ = strain rate,

σ = stress,

K, σ_o, n = material and temperature-dependent coefficients.

Assuming plane sections remain plane during bending, the above equation can be integrated over the beam's circular cross section to obtain a moment-curvature relation for the creep component of beam bending.

Using standard finite element techniques, namely the method of initial strains, the beam element stiffness matrix and associate creep and temperature initial force vectors were obtained. This numerical formulation was then inserted in a digital computer program and simple problems with known closed-form solutions have been solved. The basic solution technique utilizes an iterative procedure within each time step. Excellent agreement between computed and "exact" solutions has been obtained for both creep and relaxation problems.

The results of two problems are illustrated in Figs. 9.1 and 9.2. Figure 9.1 is the resulting maximum bending stress and strain for a cantilever beam with a constant end displacement. Figure 9.2 is the resulting end displacement and maximum bending strain for a cantilever beam with a constant end shear. In both cases, for the scale used, there were no plottable differences between the computed and theoretical[46] solutions.

9.2. Progress During February 1972

During this month's effort the basic two-dimensional straight-uniform beam element was expanded to a full three-dimensional straight-uniform beam element. The two perpendicular bending components, the axial component, and the torsional component are all decoupled in this element. This

ORNL-DWG 72-6443

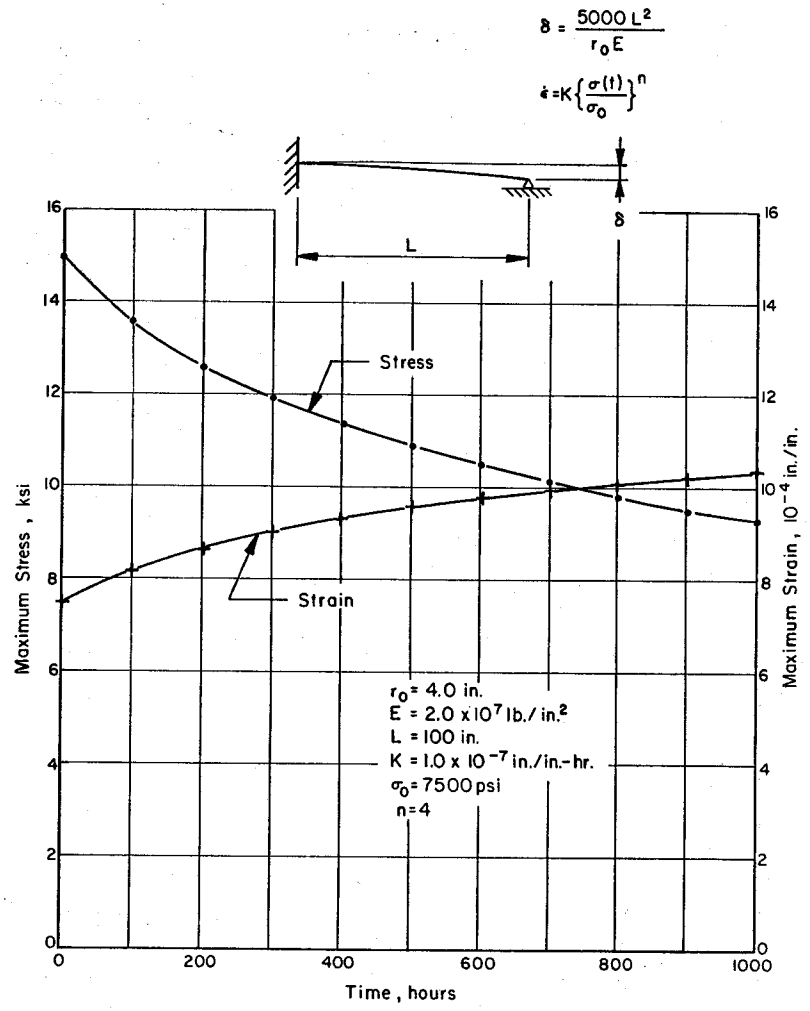

Fig. 9.1. Relaxation analysis of cantilever beam with constant end displacement. The curves represent analytical predictions and the points, finite element predictions.

ORNL-DWG 72-6444

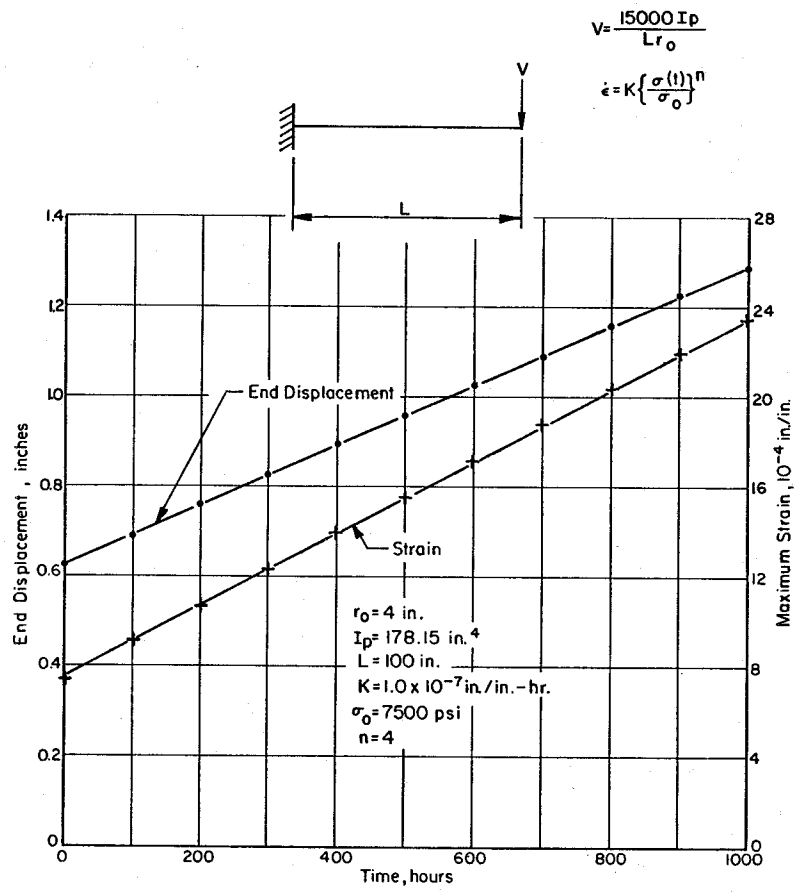

Fig. 9.2. Creep analysis of cantilever beam with constant end shear. The curves represent analytical predictions and the points, finite element predictions.

element has been tested against closed-form solutions for simple example problems, but no fully three-dimensional piping system has been analyzed by this element.

The generation of the three-dimensional finite element computer program was initiated, and the program progressed to the point where a three-dimensional piping analysis of a system with given end displacements could be attempted.

9.3. Progress During March 1972

During this month's effort the formulation of the coupled three-dimensional straight-uniform pipe element was initiated. This element utilizes the same basic assumptions as reported above except that the bending, axial, and torsional creep strains are coupled together. The development of this element has progressed to the point where extensive numerical integration will have to be employed to obtain a solution within the framework of the present digital computer program. Therefore, the generation of the element was deferred until the formulation of the basic uncoupled circularly curved pipe element has been completed. This will insure that a working program as outlined in the proposal will be completed within the predicted cost and time estimates. Once the basic uncoupled program is generated this fully coupled element will be pursued.

An example three-dimensional problem was analyzed. The basic model of this simple piping system is given in Fig. 9.3. The curved portion was modeled by a number of straight pipe elements, nodes 6-16. The straight portions were divided into a number of short elements so the distributed weight of the system could be lumped at a number of points. The pipe was 1 1/4-in. schedule 80, and the material was Incoloy 800. The basic creep law for this material at 1600°F was assumed to be:

$$\frac{d\epsilon}{dt} = 1.065 \times 10^{-30}\ \sigma^{7.057} .$$

The basic loadings (end displacements, distributed load, and thermal loads) are shown in Fig. 9.3.

ORNL DWG 72-6445

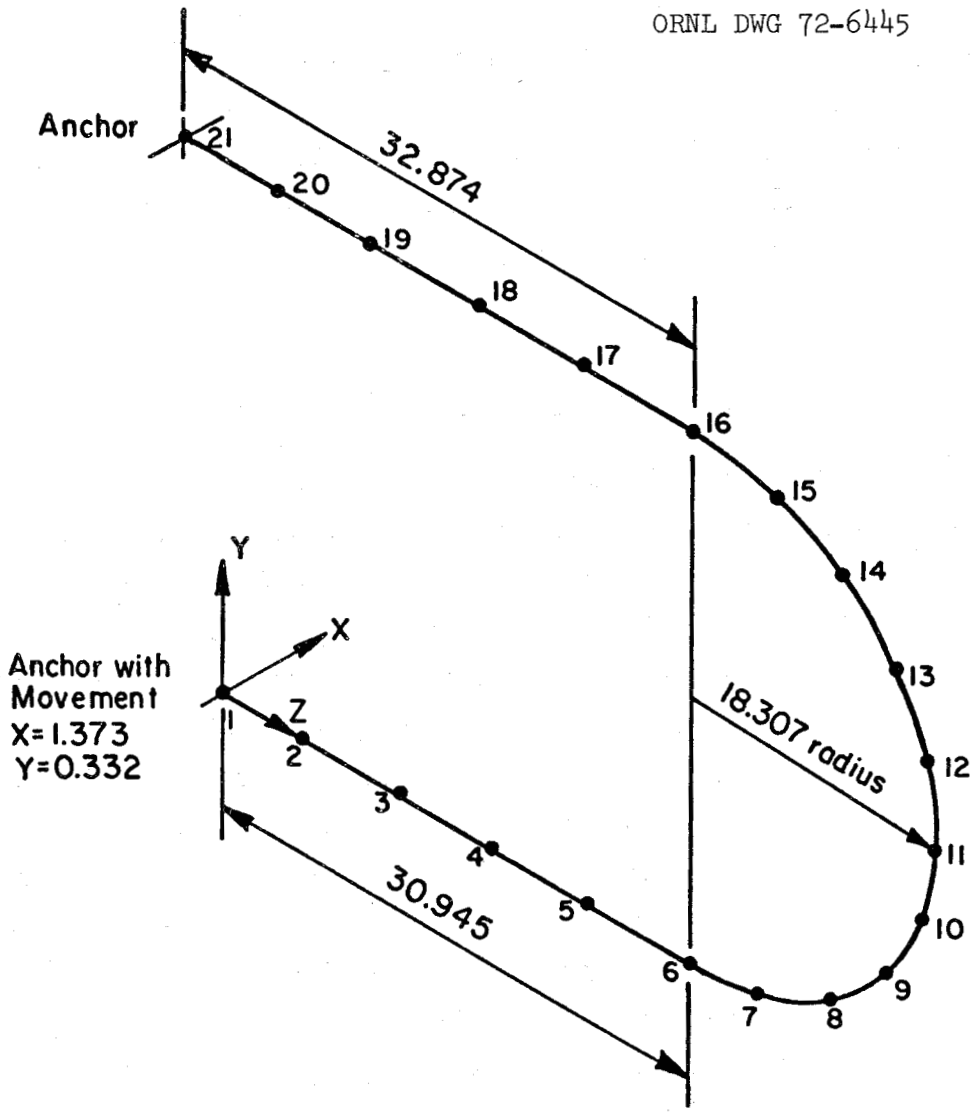

Temperature: 70° to 1560°F
Material: Incoloy 800 – 1.25" Sch. 80
E_C = 28.50 psi x 10^6
E_H = 19.20 psi x 10^6
α 70°–1600°F = 0.0153 in./in.
Insulation weight = 1.8 lb./ft.
Pipe weight = 3.0 lb./ft.
4.8 lb./ft.

Fig. 9.3. Computer model of example piping system.

The maximum initial strains due to the thermal loads occurred in the plane of the piping. Figure 9.4 shows the resulting bending moment along the length of the piping system in the plane of the piping. The moment diagram with thermal load is approximately symmetrical. Figure 9.5 shows the bending strains along the length of the piping system. The high strain concentration at the anchor, node 1, is quite evident. The 1000-hr strain is approximately five times the initial strain at the anchor, node 1.

Figure 9.6 shows the initial maximum bending stress and strain for the first 0.1 hour of operation. Figure 9.7 shows a semi-log plot of the same maximum bending stress and strain from 0.01 hour through 1000 hours. The piping system exhibited relaxation in bending and torsion due to the out-of-plane displacements; however, this was not as great as for the thermal loads and no plots of these data are given herein.

Next month the generation of the uncoupled circularly curved pipe element with a flexibility factor will be initiated. It is anticipated that three or four months will be required to complete the formulation of this element.

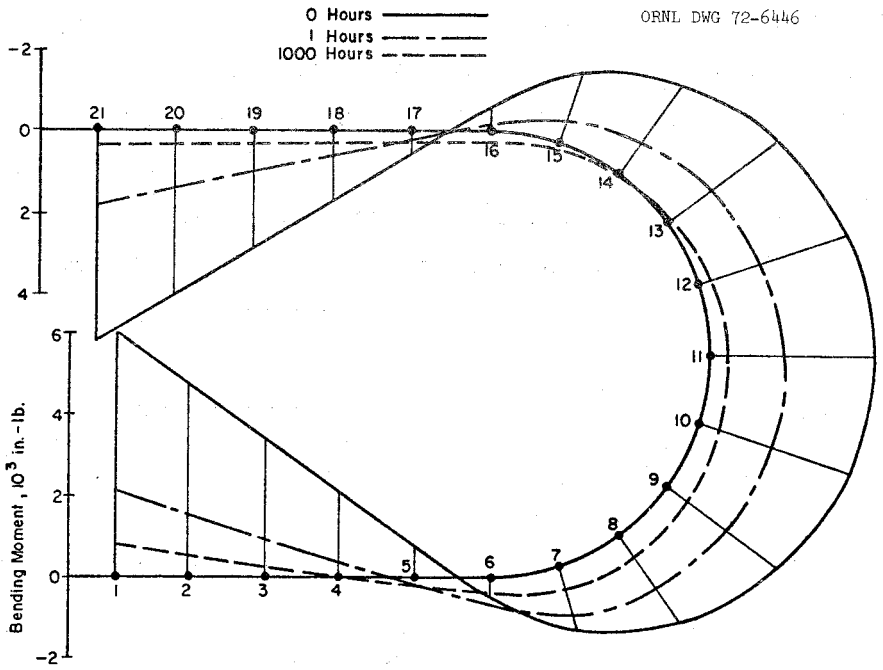

Fig. 9.4. In-plane bending moment along length of piping system.

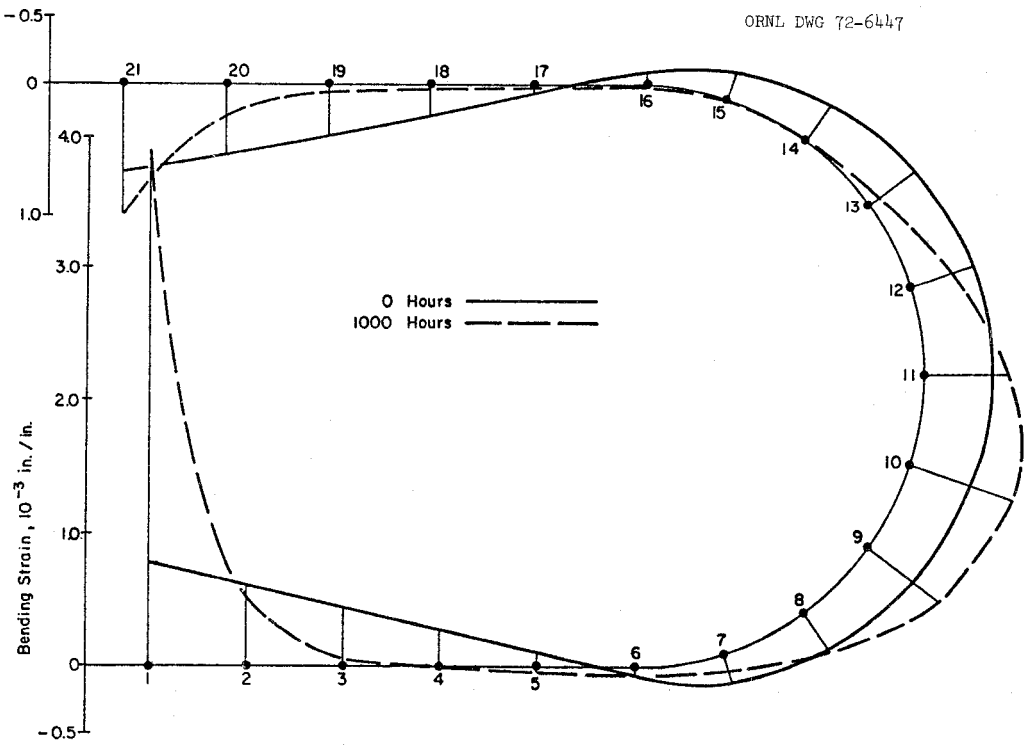

Fig. 9.5. In-plane bending strain along length of piping system.

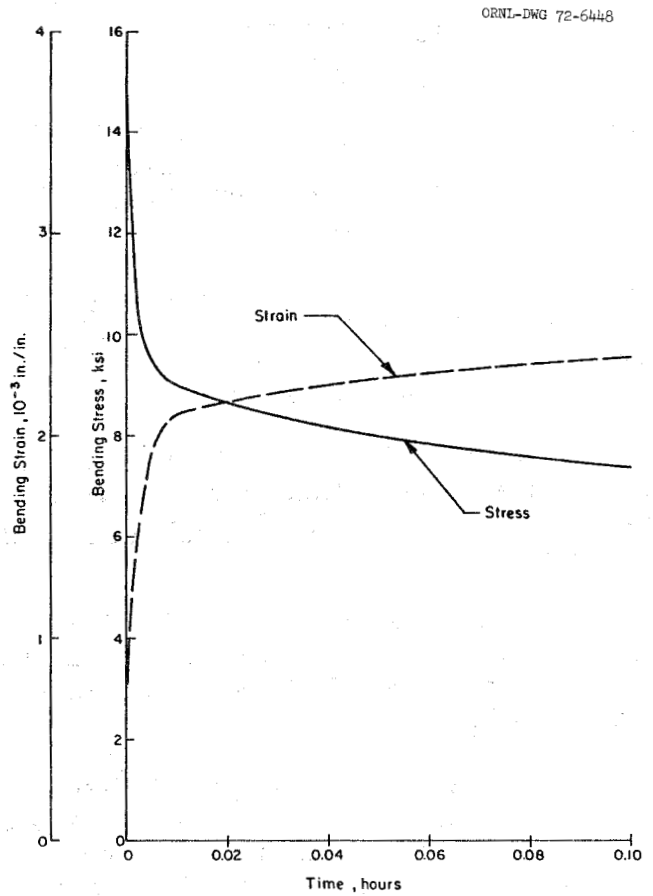

Fig. 9.6. Maximum in-plane bending stress and strain for time 0.0 to 0.10 hr.

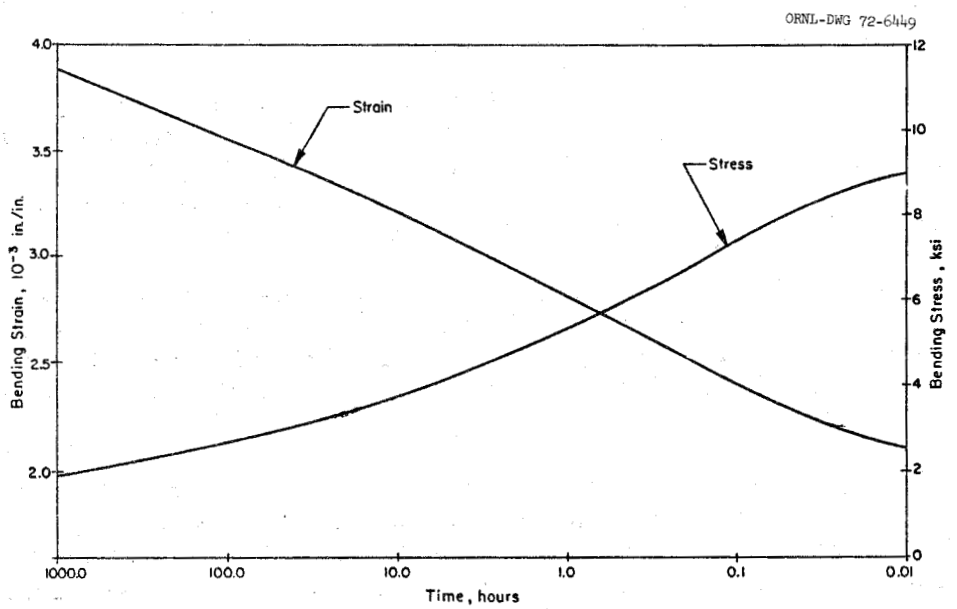

Fig. 9.7. Maximum in-plane bending stress and strain for time 0.01 to 1000 hr.

10. REFERENCES

1. W. L. Greenstreet, J. M. Corum, and C. E. Pugh, "Informal Progress Reports on Structural Design Methods for LMFBR Components for Period Ending May 31, 1970," USAEC Report ORNL-CF-70-6-14, Oak Ridge National Laboratory, June 1, 1970.

2. K. C. Liu, Elastic-Plastic Behavior Studies, pp. 22-32 in "High-Temperature Structural Design Methods for LMFBR Components Quarterly Progress Report for Period Ending December 31, 1971," USAEC Report ORNL-TM-3736, Oak Ridge National Laboratory, March 1972.

3. J. Bree, "Elastic-Plastic Behavior of Thin Tubes Subjected to Internal Pressure and Intermittent High-Heat Fluxes with Application to Fast-Nuclear-Reactor Fuel Elements," J. Strain Analysis, 2(3): 226-238 (1967).

4. J. M. Corum, Summary and Status, pp. 5-8 in "Informal Progress Reports on Structural Design Methods for LMFBR Components for June and July 1971," USAEC Report ORNL-CF-71-8-54, Oak Ridge National Laboratory, August 1, 1971.

5. Teledyne Materials Research Co., Analytical Ratchetting Studies, pp. 159-171 in "High-Temperature Structural Design Methods for LMFBR Components Quarterly Progress Report for Period Ending December 31, 1971," USAEC Report ORNL-TM-3736, Oak Ridge National Laboratory, March 1972.

6. R. W. Swindeman, Creep Testing, pp. 115-117 in "High-Temperature Structural Design Methods for LMFBR Components Quarterly Progress Report for Period Ending December 31, 1971," USAEC Report ORNL-TM-3736, Oak Ridge National Laboratory, March 1972.

7. C. E. Pugh, Creep Law Development for the ORNL Preliminary Heat of Type 304 Stainless Steel, pp. 55-56 in "High-Temperature Structural Design Methods for LMFBR Components Quarterly Progress Report for Period Ending December 31, 1971," USAEC Report ORNL-TM-3736, Oak Ridge National Laboratory, March 1972.

8. C. E. Pugh, Specifications of Materials Properties Data Needs, pp. 122-131 in "High-Temperature Structural Design Methods for LMFBR Components Quarterly Progress Report for Period Ending December 31, 1971," USAEC Report ORNL-TM-3736, Oak Ridge National Laboratory, March 1972.

9. C. E. Pugh, Some Comparisons of Variable Stress Creep Data with Predictions of Recommended Interim Constitutive Equations, pp. 56-60 in "High-Temperature Structural Design Methods for LMFBR Components Quarterly Progress Report for Period Ending December 31, 1971," USAEC Report ORNL-TM-3736, Oak Ridge National Laboratory, March 1972.

10. C. E. Pugh, Time-Dependent Behavior Studies, pp. 14-18 in "Informal Progress Reports on Structural Design Methods for LMFBR Components for April and May 1971," USAEC Report ORNL-CF-71-6-57, Oak Ridge National Laboratory, June 1, 1971.

11. C. E. Pugh et al., Currently Recommended Constitutive Equations for Inelastic Design Analysis of FFTF Components, pp. 2-22 in "High-Temperature Structural Design Methods for LMFBR Components Quarterly Progress Report for Period Ending December 31, 1971," USAEC Report ORNL-TM-3736, Oak Ridge National Laboratory, March 1972.

12. J. M. Corum and M. Richardson, Elastic-Plastic-Creep Beam Tests, pp. 72-90 in "High-Temperature Structural Design Methods for LMFBR Components Quarterly Progress Report for Period Ending December 31, 1971," USAEC Report ORNL-TM-3736, Oak Ridge National Laboratory, March 1972.

13. C. E. Pugh, Creep Law Development for the ORNL Preliminary Heat of Type 304 Stainless Steel, pp. 55-56 in "High-Temperature Structural Design Methods for LMFBR Components Quarterly Progress Report for Period Ending December 31, 1971," USAEC Report ORNL-TM-3736, Oak Ridge National Laboratory, March 1972.

14. W. L. Greenstreet, J. M. Corum, and C. E. Pugh, "Informal Progress Reports on Structural Design Methods for LMFBR Components for June and July 1971," USAEC Report ORNL-CF-71-8-54, Oak Ridge National Laboratory, August 1, 1971.

15. D. R. Miller, "Thermal-Stress Ratchet Mechanism in Pressure Vessels," ASME Paper No. 58-A-129, 1958.

16. Letter from W. F. Anderson (LMEC) to the PVRC Subcommittee on Plastic Fatigue Strength, February 23, 1972, Subject: Tentative Recommendations of Test Requirements for Mar-Test Proposed Test.

17. C. E. Pugh, J. M. Corum, K. C. Liu, and W. L. Greenstreet, "Currently Recommended Constitutive Equations for Inelastic Design Analysis of FFTF Components," USAEC Report ORNL-TM-3602, Oak Ridge National Laboratory (to be issued).

18. C. E. Pugh et al., Currently Recommended Constitutive Equations for Inelastic Design Analysis of FFTF Components, pp. 2-22 in "High-Temperature Structural Design Methods for LMFBR Components Quarterly Progress Report for Period Ending December 31, 1971," USAEC Report ORNL-TM-3736, Oak Ridge National Laboratory, March 1972.

19. Liquid Metal Fast Breeder Reactor Materials Handbook, HEDL-71-32, Hanford Engineering Development Laboratory, June 1971.

20. J. M. Corum and M. Richardson, Elastic-Plastic-Creep Beam Tests, pp. 72-90 in "High-Temperature Structural Design Methods for LMFBR Components Quarterly Progress Report for Period Ending December 31, 1971," USAEC Report ORNL-TM-3736, Oak Ridge National Laboratory, March 1972.

21. C. E. Pugh et al., Currently Recommended Constitutive Equations for Inelastic Design Analysis of FFTF Components, pp. 2-22 in "High-Temperature Structural Design Methods for LMFBR Components Quarterly Progress Report for Period Ending December 31, 1971," USAEC Report ORNL-TM-3736, Oak Ridge National Laboratory, March 1972.

22. H. C. Young, "Quality Assurance Program Plan for the Thermal Transient Tests," USAEC Report ORNL-CF-72-3-8, Oak Ridge National Laboratory, March 6, 1972.

23. J. M. Corum, H. C. Young, and A. G. Grindell, Pipe Thermal Ratchetting Tests, pp. 93-100 in "High-Temperature Structural Design Methods for LMFBR Components Quarterly Progress Report for Period Ending December 31, 1971," USAEC Report ORNL-TM-3736, Oak Ridge National Laboratory, March 1972.

24. J. M. Corum et al., "Conceptual System Design Description for the Thermal Transient Tests," USAEC Report ORNL-CF-71-11-40, Oak Ridge National Laboratory, November 30, 1971.

25. J. M. Corum, H. C. Young, and A. G. Grindell, Pipe Thermal Ratchetting Tests, pp. 93-100 in "High-Temperature Structural Design Methods for LMFBR Components Quarterly Progress Report for Period Ending December 31, 1971," USAEC Report ORNL-TM-3736, Oak Ridge National Laboratory, March 1972.

26. W. J. McAfee and M. Richardson, Weldment Creep-Rupture Studies, pp. 100-106 in "High-Temperature Structural Design Methods for LMFBR Components Quarterly Progress Report for Period Ending December 31, 1971," USAEC Report ORNL-TM-3736, Oak Ridge National Laboratory, March 1972.

27. R. W. Swindeman, Material Characterization, pp. 110-111 in "High-Temperature Structural Design Methods for LMFBR Components Quarterly Progress Report for Period Ending December 31, 1971," USAEC Report ORNL-TM-3736, Oak Ridge National Laboratory, March 1972.

28. R. W. Swindeman, Tensile Testing, pp. 111-115 in "High-Temperature Structural Design Methods for LMFBR Components Quarterly Progress Report for Period Ending December 31, 1971," USAEC Report ORNL-TM-3736, Oak Ridge National Laboratory, March 1972.

29. R. W. Swindeman and R. D. Waddell, Jr., Mechanical Properties of Type 304 Stainless Steels, pp. 188-206 in "Fuels and Materials Development Program Quarterly Progress Report for Period Ending December 31, 1971," USAEC Report ORNL-TM-3703, Oak Ridge National Laboratory, March 1972.

30. J. Moteff, "Correlation of Substructure with Mechanical Properties of Plastically Deformed AISI 304 and 316 Stainless Steel," USAEC contract no. AT(11-1)-2107, University of Cincinnati.

31. J. T. Barnby, "Effect of Strain Aging on Creep of an AISI 316 Austenitic Stainless Steel," J. Iron and Steel Inst., 204: 23 (January 1966).

32. L. M. T. Hopkins and L. H. Taylor, "Creep Properties of Cr-Ni-Mo Austenitic Steel in Relation to Structure," J. Iron and Steel Inst., 205: 17 (January 1961).

33. A. Portevin and F. Le Chatelier, C.R. Acad. Sci. (Paris), 176: 507 (1923).

34. C. E. Pugh, Time-Dependent Behavior Studies, pp. 14-18 in "Informal Progress Reports on Structural Design Methods for LMFBR Components for April and May 1971," USAEC Report ORNL-CF-71-6-57, Oak Ridge National Laboratory, June 1, 1971.

35. L. D. Blackburn, (equations developed for use in the) Liquid Metal Fast Breeder Reactor Materials Handbook, HEDL-TME-71-32, Hanford Engineering Development Laboratory, 1972.

36. J. W. Chuang, T. W. Kennedy, and E. S. Perry, "An Approach to Estimating Long-Term Multiaxial Creep Behavior from Short-Term Uniaxial Creep Results," University of Texas at Austin, Research Report 2864-3, June 1970.

37. Unpublished work in support of the LMFBR Fuel Element Design and Model Development Program at ORNL.

38. C. E. Pugh, ORNL Studies of Time-Dependent Behavior, pp. 15-19 in "Informal Progress Reports on Structural Design Methods for LMFBR Components for February and March 1971," USAEC Report ORNL-CF-71-4-58, Oak Ridge National Laboratory, April 1, 1971.

39. Teledyne Materials Research Co., Analytical Ratchetting Studies, pp. 159-171 in "High-Temperature Structural Design Methods for LMFBR Components Quarterly Progress Report for Period Ending December 31, 1971," USAEC Report ORNL-TM-3736, Oak Ridge National Laboratory, March 1972.

40. H. M. Minami and G. O. Roberts, "Elastic-Plastic-Creep Ratchetting Study," enclosure to 71-LMEC-281, February 1971.

41. A. Mendelson, Plasticity: Theory and Application, MacMillan, New York, 1968.

42. "Interim Supplementary Structural Design Criteria for Elevated Temperatures," FRA-152, Revision 3, November 6, 1970.

43. "Code Case 1331-5: Nuclear Vessels in High-Temperature Service," Section III ASME Boiler and Pressure Vessel Code, August 4, 1971.

44. Letter from W. F. Anderson (LMEC) to Distribution, January 21, 1972, Subject: Supplements to ASME Code Case 1331-5, Enclosure 2, "Appendix A, Supplement to Code Case 1331-5."

45. E. C. Rodabaugh and J. E. Sorenson, Development of a Simplified Inelastic Design Procedure for Piping Systems, pp. 171-176 in "High-Temperature Structural Design Methods for LMFBR Components Quarterly Progress Report for Period Ending December 31, 1971," USAEC Report ORNL-TM-3736, Oak Ridge National Laboratory, March 1972.

46. E. L. Robinson, "Steam-Piping Design to Minimize Creep Concentrations," ASME Transactions, 1955.

Internal Distribution

1. S. E. Beall
2. H. W. Behrman
3. E. E. Bloom
4. S. E. Bolt
5. J. W. Bryson
6. J. P. Callahan
7. H. P. Carter
8. S. J. Chang
9. R. D. Cheverton
10. C. J. Claffey
11. C. W. Collins
12-21. J. M. Corum
22. W. B. Cottrell
23. J. S. Crowell
24. F. L. Culler
25. W. G. Dodge
26. A. P. Fraas
27. W. R. Gall
28-30. W. L. Greenstreet
31. A. G. Grindell
32. R. C. Gwaltney
33. W. O. Harms
34. H. W. Hoffman
35. P. R. Kasten
36. K. C. Liu
37. M. I. Lundin
38. T. S. Lundy
39. R. N. Lyon
40. R. E. MacPherson
41. W. R. Martin
42. W. J. McAfee
43. H. E. McCoy
44-46. H. C. McCurdy
47. J. G. Merkle
48. A. J. Miller
49. S. E. Moore
50. H. A. Nelms
51. P. Patriarca
52. A. M. Perry
53. T. W. Pickel
54-63. C. E. Pugh
64. M. Richardson
65. M. W. Rosenthal
66. W. K. Sartory
67. Myrtleen Sheldon
68. M. J. Skinner
69. G. M. Slaughter
70. J. E. Smith
71. I. Spiewak
72. D. A. Sundberg
73. R. W. Swindeman
74. D. B. Trauger
75. R. S. Valachovic
76. R. D. Waddell, Jr.
77. J. R. Weir
78. G. D. Whitman
79. G. T. Yahr
80. H. C. Young
81-82. Central Research Library
83. Y-12 Document Reference Section
84-87. Laboratory Records Department
88. Laboratory Records (RC)

External Distribution

89. L. E. Alsager, U.S. Atomic Energy Commission, Washington, D.C.
90. W. F. Anderson, Liquid Metal Engineering Center, Canoga Park, Calif.
91. D. L. Becker, Westinghouse Hanford Co., Richland, Wash.
92. I. Berman, Foster Wheeler Corp., Livingston, N. J.
93. C. C. Bigelow, U.S. Atomic Energy Commission, Washington, D.C.
94. E. C. Bishop, Westinghouse Electric Corp., Madison, Penna.
95. L. D. Blackburn, Westinghouse Hanford Co., Richland, Wash.
96. M. Booth, U.S. Atomic Energy Commission, Washington, D.C.
97. T. R. Branca, Teledyne Materials Research Co., Waltham, Mass.
98. C. R. Brinkman, Aerojet Nuclear Co., Idaho Falls, Idaho
99. J. P. Burn, Westinghouse Hanford Co., Richland, Wash.
100. D. R. Campbell, Liquid Metal Engineering Center, Canoga Park, Calif.

101. A. E. Carden, Univ. of Connecticut, Storrs, Conn.
102-103. E. G. Cass, Director, Division of Reactor Standards, U.S. Atomic Energy Commission, Washington, D.C.
104. A. K. Chakraborty, General Electric Co., San Jose, Calif.
105. S. K. Chan, Westinghouse Research Laboratory, Pittsburgh, Penna.
106. T. Y. Chang, Univ. of Akron, Akron, Ohio
107. F. L. Cho, Sargent and Lundy, Chicago, Ill.
108. R. L. Citerley, Anamet Laboratories, San Carlos, Calif.
109. T. T. Claudson, Westinghouse Hanford Co., Richland, Wash.
110. J. C. Cochran, Liquid Metal Engineering Center, Canoga Park, Calif.
111-112. Combustion Engineering, Inc., Chattanooga, Tenn., Attention: Librarian MR & D
113. J. B. Conway, Mar-Test, Inc., Cincinnati, Ohio
114. W. E. Cooper, Teledyne Materials Research Co., Waltham, Mass.
115. R. F. Detman, C. F. Braun and Co., Alhambra, Calif.
116. G. S. Dhaliwal, Valcor Engineering Corp., Kenilworth, N. J.
117. R. J. Dohrmann, Babcock and Wilcox Co., Alliance, Ohio
118. W. D. Doty, U.S. Steel Corp., Monroeville, Penna.
119. J. J. Droher, Liquid Metal Engineering Center, Canoga Park, Calif.
120. J. M. Duke, Westinghouse Electric Corp., Tampa, Florida
121. A. J. Durelli, Catholic Univ. of America, Washington, D.C.
122. A. F. Eckert, Babcock and Wilcox Co., Lynchburg, Va.
123. E. P. Esztergar, 7993 Prospect St., La Jolla, Calif.
124. N. J. Ettenson, Westinghouse Electric Corp., Madison, Penna.
125. L. F. Fidrych, General Electric Co., Sunnyvale, Calif.
126. W. N. Findley, Brown Univ., Providence, R. I.
127. R. H. Gallagher, Cornell Univ., Ithaca, N. Y.
128. J. C. Gerdeen, Michigan Technology Univ., Houghton, Mich.
129. R. G. Gilliland, Univ. of Wisconsin, Milwaukee, Wis.
130. G. A. Greenbaum, Mechanics Research, Inc., Los Angeles, Calif.
131. Nicholas Grossman, U.S. Atomic Energy Commission, Washington, D.C.
132. O. Hagen, Westinghouse Electric Corp., Cheswick, Penna.
133. J. Hagstrom, Chicago Bridge and Iron Co., Oak Brook, Ill.
134. G. R. Halford, NASA Lewis Research Center, Cleveland, Ohio
135. E. E. Hamer, Argonne National Laboratory, Argonne, Ill.
136. D. G. Harman, Westinghouse Electric Corp., Tampa, Florida
137. D. R. Harting, Boeing Co. Aerospace Group, Seattle, Wash.
138. K. Hayashi, Esso Research and Engineering Co., Florham Park, N.J.
139. D. B. Heilig, Bechtel Corp., San Francisco, Calif.
140. K. Hikido, General Electric Co., Sunnyvale, Calif.
141. F. P. Hill, Combustion Engineering, Inc., Chattanooga, Tenn.
142. J. P. Houstrup, Combustion Engineering, Inc., Chattanooga, Tenn.
143. J. R. Hunter, U.S. Atomic Energy Commission, Washington, D.C.
144. M. T. Jakub, Westinghouse Hanford Co., Richland, Wash.
145. C. E. Jaske, Battelle-Columbus Laboratories, Columbus, Ohio
146. R. I. Jetter, Atomics International, Canoga Park, Calif.
147. H. B. Ketchum, Westinghouse Electric Corp., Madison, Penna.
148. W. C. Kinsel, Westinghouse Hanford Co., Richland, Wash.
149. E. E. Kintner, U.S. Atomic Energy Commission, Washington, D.C.
150. R. E. Kosiba, U.S. Atomic Energy Commission, Washington, D.C.
151. Harry Kraus, Rensselaer Polytechnic Inst. of Connecticut, Hartford, Conn.

152. E. Krempl, Rensselaer Polytechnic Inst., Troy, N.Y.
153. Y. S. Lai, Chicago Bridge and Iron Co., Oak Brook, Ill.
154. C. F. Larson, Welding Research Council, New York, N.Y.
155. C. W. Lawton, Combustion Engineering, Inc., Windsor, Conn.
156. M. M. Lemcoe, Battelle-Columbus Laboratories, Columbus, Ohio
157. Josef Maatuk, Crane Co., Chicago, Ill.
158. R. H. Mallett, Westinghouse Electric Corp., Madison, Penna.
159. J. R. Maloney, Westinghouse Electric Corp., Cheswick, Penna.
160. M. J. Manjoine, Westinghouse Electric Corp., Pittsburgh, Penna.
161. P. V. Marcal, Brown Univ., Providence, R.I.
162. J. L. McLean, Teledyne Materials Research Co., Waltham, Mass.
163. R. Mello, Westinghouse Electric Corp., Madison, Penna.
164. J. L. Mershon, U.S. Atomic Energy Commission, Washington, D.C.
165. W. R. Mikesell, CBI Nuclear Co., Memphis, Tenn.
166. R. A. Moen, Westinghouse Hanford Co., Richland, Wash.
167. W. I. Morita, Bechtel Corp., San Francisco, Calif.
168-170. P. A. Morris, Director, Division of Reactor Licensing, U.S. Atomic Energy Commission, Washington, D.C.
171. E. C. Norman, U.S. Atomic Energy Commission, Washington, D.C.
172. E. T. Onat, Yale Univ., New Haven, Conn.
173. W. J. O'Donnell, O'Donnell and Associates, Pittsburgh, Penna.
174. D. H. Pai, Foster Wheeler Corp., Livingston, N.J.
175. C. S. Parker, General Electric Co., San Jose, Calif.
176. W. Pennell, Westinghouse Electric Corp., Madison, Penna.
177. A. G. Pickett, Southwest Research Institute, San Antonio, Texas
178. G. H. Powell, Univ. of California, Berkeley, Calif.
179. F. C. Rally, General Electric Co., Sunnyvale, Calif.
180. Y. R. Rashid, General Electric Co., San Jose, Calif.
181. B. T. Resnick, U.S. Atomic Energy Commission, Washington, D.C.
182. D. R. Riley, U.S. Atomic Energy Commission, Washington, D.C.
183. E. C. Rodabaugh, Battelle-Columbus Laboratories, Columbus, Ohio
184. M. A. Rosen, U.S. Atomic Energy Commission, Washington, D.C.
185. F. A. Ross, U.S. Atomic Energy Commission, Washington, D.C.
186. Robert Rung, Applied Technology Associates, Ramsey, N.J.
187. P. H. Sager, Gulf General Atomic, San Diego, Calif.
188. R. I. Sann, Gulf United Nuclear Fuel Corp., Elmsford, N.Y.
189. A. O. Schaefer, Metals Properties Council, New York, N.Y.
190. J. J. Schreiber, U.S. Atomic Energy Commission, Washington, D.C.
191. C. C. Schultz, Babcock and Wilcox Co., Alliance, Ohio
192. F. Sebring, C. F. Braun and Co., Alhambra, Calif.
193. R. A. Selbey, Westinghouse Hanford Co., Richland, Wash.
194. L. K. Severud, Westinghouse Hanford Co., Richland, Wash.
195. M. Shaw, U.S. Atomic Energy Commission, Washington, D.C.
196. P. G. Shewman, Argonne National Laboratory, Argonne, Ill.
197. Sidney Siegel, Atomics International, Canoga Park, Calif.
198. J. M. Simmons, U.S. Atomic Energy Commission, Washington, D.C.
199. E. E. Sinclair, U.S. Atomic Energy Commission, Washington, D.C.
200. R. J. Slember, Westinghouse Electric Corp., Madison, Penna.
201. G. V. Smith, 104 Berkshire Road, Ithaca, N.Y.
202. A. L. Snow, Westinghouse Electric Corp., Madison, Penna.
203. K. O. Stein, Babcock and Wilcox Co., Alliance, Ohio
204. W. H. Sutherland, Westinghouse-Hanford Co., Richland, Wash.

205. J. A. Swanson, 870 Pine View Drive, Elizabeth, Penna.
206. A. N. Tardiff, U.S. Atomic Energy Commission, Washington, D.C.
207. K. Thomas, Westinghouse Electric Corp., Madison, Penna.
208. J. C. Tobin, Westinghouse Hanford Co., Richland, Wash.
209. I. S. Tuba, Basic Technology, Inc., Pittsburgh, Penna.
210. W. H. Tuppeny, Combustion Engineering, Inc., Windsor, Conn.
211. R. A. Valentin, Argonne National Laboratory, Argonne, Ill.
212. W. A. Van Der Sluys, Babcock and Wilcox Co., Alliance, Ohio
213. R. W. Weeks, Argonne National Laboratory, Argonne, Ill.
214. B. C. Wei, U.S. Atomic Energy Commission, Washington, D.C.
215. D. H. White, Westinghouse Electric Corp., Tampa, Florida
216. B. V. Winkel, Idaho Nuclear Corp., Idaho Falls, Idaho
217. B. M. Wundt, 2346 Shirland Road, Schenectady, N.Y.
218. S. Y. Zamrik, Pennsylvania State Univ., Univ. Park, Penna.
219. Zenons Zudans, Franklin Institute Research Lab., Philadelphia, Penna.
220-221. Technical Information Center, AEC
222. Research and Technical Support Division
223-239. Manager, Technical Information Center (TIC), Oak Ridge, Tenn.